PETROGENETIC EVOLUTION OF PRECAMBRIAN BASEMENT ROCKS OF THE AREA AROUND SONAPAHAR, WEST KHASI HILLS DISTRICT, MEGHALAYA

BY

V.VANTHANGLIANA

Ph.D. Regd. No. MZU/Ph.D/100/7.6.2006

THESIS SUBMITTED IN FULFILLMENT FOR THE AWARD OF THE DEGREE

OF

Doctor of Philosophy in Geology

MIZORAM UNIVERSITY

AIZAWL

2011

ACKNOWLEGEMENT

Thank you Dear Lord. I remember Thy giving me the strength to finish this work.

I owe a great debt of gratitude to my supervisor Dr. M. Faruque Hussain, Department of Earth Science, Assam University, Silchar (on lien from Department of Geology, Mizoram University) for the much needed guidance during the entire course of the present study. It was his encouragement and keen interest in the subject, which led to the completion of this study in time.

I wish to thank the Head, Department of Geology, Mizoram University for providing the facilities during the period of this work.

The perseverance required to see this work through to timely completion stem from the constant advice and encouragement I received from Prof. R. P. Tiwari, Department of Geology, Mizoram University. I also have the good fortune to receive timely suggestions and advice from Dr. Shiva Kumar, Associate Professor, Department of Geology, Mizoram University while carrying out this work.

Thanks are extended to University Grant Commission, New Delhi for providing financial assistance in terms of research fellowship for carrying out the present study.

Thanks are due to Dr. S. B. Dwivedi, Reader, Engineering College, Banaras Hindu University for his advice and suggestions during the initial stages of this work and Dr. K. S. Rao and Dr. V. Z. Ralte (Assistant Professors), Department of Geology, Mizoram University for their encouragement and support at various stages during the present study.

Laldinpuia, Jimmy Lalnunmawia, Lalmuankimi Chhakchhuak, J.Malsawma and Paul Lalnuntluanga of the Department of Geology, Mizoram University helped me in a number of ways while carrying out this work. I sincerely acknowledge their cooperation.

All the staff of the Department of Geology, Mizoram University must be acknowledged for their ever cheering and enthusiastic cooperation throughout the course of this work.

Thanks are also due to my friends in the Department of Geology, Pachhunga University College for their supportive role.

It is a pleasure to pay tribute to all faculties and staff of the Department of Earth Science, Silchar, Assam University for their kind hospitality during visits.

I am indebted to my parents who in a number of ways provided me the wherewithal. I recall my father, late Lalhmuaka, who fetch me good words endlessly and my mother, Sangkhumi, who sincerely brought me up with her care and gently love.

Especial thanks are due to all my brothers for their constant encouragement and support while carrying out this work.

Many thanks go to my wife Rinpuii and my kids, Kuri and Puipuia. Their love and support always give me strength to see this work accomplished.

Date: …… 2011. **(V. VANTHANGLIANA)**

CONTENTS

LIST OF FIGURES

LIST OF PLATES

LIST OF TABLES

Chapter- 1

INTRODUCTION

INTRODUCTION

1.1.0 INTRODUCTION

Shillong plateau is a prominent Precambrian Gneissic Complex, occurs in Northeast India. The plateau is bounded and dissected by several E-W and N-S trending faults formed by the Kerguelen plume-related domal up-arching during the Mesozoic (Gupta and Sen, 1988) and uplift related to collision of the Indian and Tibetan plates during the Cenozoic (Johnson and Alam, 1991; Bilham and England, 2001). Towards south, the plateau is bounded by Dauki Fault, towards north by Brahmaputra Fault and towards east the plateau is bounded by Jamuna Fault (Evans, 1964; Nandy, 1980).

The Shillong Plateau covers an area of about 33000 km^2 within $25^0 20'$N - $26^0 30'$N latitude and 90^0E - $93^0 50'$E longitude (Fig. 1.1). The plateau consists predominantly of Precambrian Gneissic Complex forming the basement, the Proterozoic Shillong Group of metasedimentary rocks overlying the basement and the granitic plutons (ca. 881 to 479 Ma old) intrusive into both the gneissic basement and the Shillong group of rocks (Desikachar, 1974; Mazumder, 1976). Sylhet traps which are flows of basalts form small outcrops over the basement in the southern part of the plateau. Deep drilling and geophysical data shows that Precambrian rocks of the Shillong plateau extend for many tens of kilometers Northeast of the plateau, beneath the Brahmaputra alluvium, and also Westward to the Chotanagpur area (Evans, 1964; Desikachar, 1974).

Geological understandings on the gneisses and granulites belonging amphibolite to granulite facies forming the basement of Shillong plateau are very poor. Not much works have been carried out on the basement rocks of the Shillong plateau with modern understandings on geochemistry. Most of the previous studies were confined mainly to the facies analysis and mineral paragenesis. Detailed investigations on the basement gneisses and granulites have not been carried out to elucidate the geodynamic setting and crustal evolution of Shillong plateau. Recent studies envisaged a Pan-African Suture, the Prydz Bay-Denman Glacier Suture, passing through Shillong plateau with the implication that the different Precambrian crustal blocks of the Eastern Gondwana including that of Shillong plateau assembled

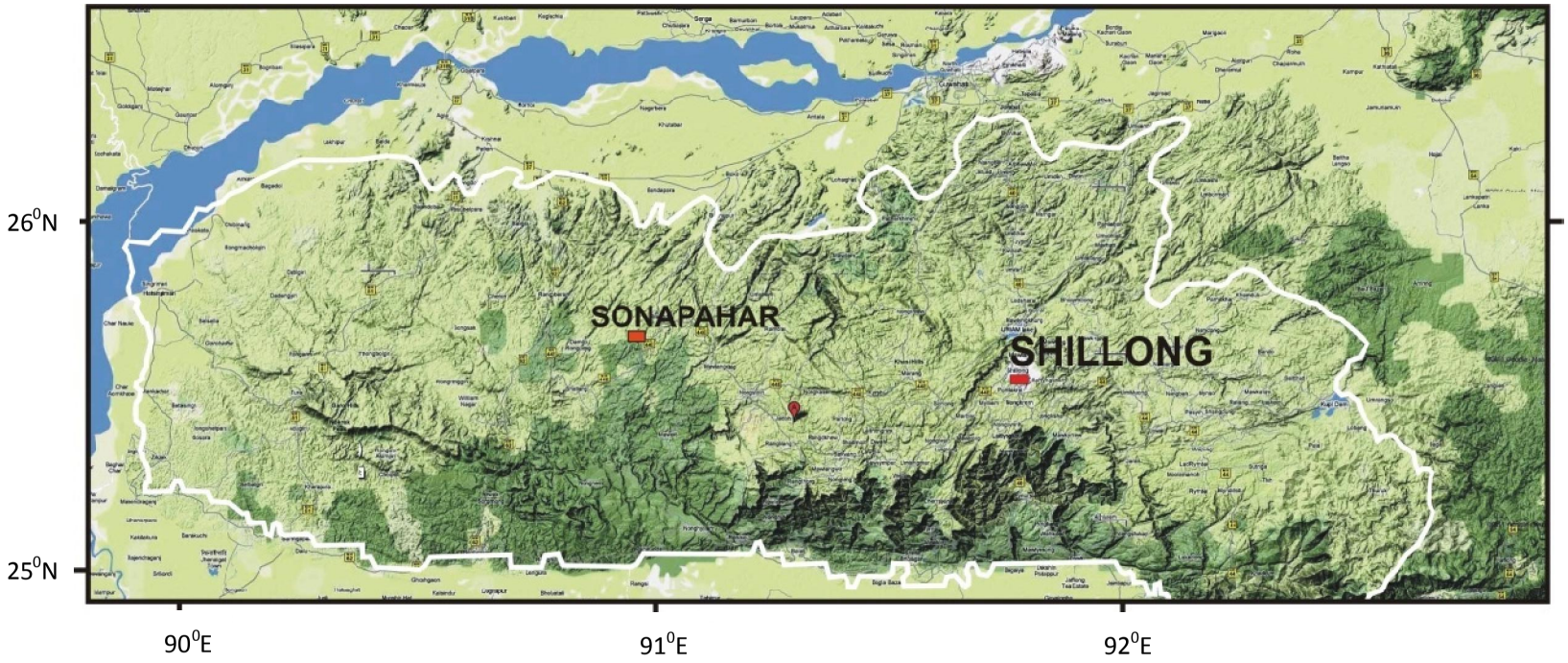

Figure 1.1: Terrain Map of Shillong Plateau showing the location of the study area. *(Source: http://maps.google.co.in/maps?-hl=en&tab=wl*.

at ca. 500 Ma (Zhao *et al*., 1995; Fitzsimons, 2003; Harley, 2003). The Proterozoic granulites gneiss Complexes of the Indian Subcontinent including the Eastern Ghats Belt (EGB); the Chotanagpur Gneissic Complex (CGC) and the central Indian Tectonic Zone (CITZ) occur in Sigmoidal Zone (Fermor, 1936). The available chronological data from the high grade rocks of CITZ (Bhowmik *et al.,* 2005) and CGC (Pandey *et al.,* 1986; Saha, 1987; Harris, 1993; Ray Barman *et al.,* 1994) and the granulites of the EGB (Shaw *et al.,* 1997; Mezver and Cosca 1999; Dobmeier and Raith, 2003) suggest that the domains are largely Proterozoic in age with relict or reworked Archaean components (Ricker *et al.,* 2001; Ramachandra and Roy, 2001) and interspersed Grenvillian domains. Only the EGB exhibits strong Pan-African imprints (Clark and Subbarao, 1971; Shaw *et al.,* 1997; Mezger and Cosca, 1999) at the Cratonic fringe, but it is unclear if the prograde re-heating was an effect of crustal suturing or reactivation at the craton-mobile belt boundary (Mahato and Bhattacharya, 2006).

The SMGC is separated from the main mass of the Indian Peninsular shield by the Tertiary Ganges-Brahmaputra Alluvium, and the Cretaceous Rajmahal volcanics. The Shillong plateau has been described as a detached part of the Indian shield (Evans, 1964) or an extension of the CGC (Desikachar, 1974) or the EGB (Crawford, 1974).

1.2 PHYSIOGRAPHY

The whole of Meghalaya is a plateau (150-1960 m MSL) having western, central and eastern parts, commonly known as Garo, Khasi, and Jaintia Hills. The plateau is marked by great diversities in relief features. It has highly dissected and irregular topography in the northern and western part and steep and regular slopes in the southern part. In the north, the boundary of the plateau is not well defined due to the presence of broken hill ranges (Fig. 1.2).

Garo Hills, which is conglomerate of three districts viz., East Garo Hills, West Garo Hills and South Garo Hills stretches out between $25^0 8'$ N to $26^0 1'$N latitude and $89^0 50'$ E to $90^0 59'$ E longitude. The total area of the three districts is 8167 Sq. Kms. It is bounded in south by Mymensing district and a part of Rangpur district of Bangladesh, by a district of Assam on the North and the West and by the West Khasi Hills District of Meghalaya in the east. The Garo Hills is a highly dissected region

with an average elevation of about 600 m. An interesting feature of Garo Hills is the presence of Tura and Arabella Ranges running parallel in east-west direction. The Tura range (about 50 km long) runs from Siju to Tura and its highest peak is Nokrek (altitude of 1412 m). The Arabella Range runs parallel to the Tura Range on its north. It gradually increases in height and join Tura to the South. The remaining parts of the Garo Hills consist of hill ranges running from north to south with highest points varying in height from 450 to 600 m.

The area is predominantly hilly except for some plain areas in the southern and western parts. The elevation of the hills starts sharply from the southern plain areas and after attaining their highest elevation at Tura and Arbella Ranges, slope downs and merges with the plains of the Brahmaputra in the North. The Tura Range occupies the southern portion stretching across from west to east. Another parallel range is Arbella which runs from West to central part of Garo Hills. A good number of high peaks in the Garo Hills are part of Tura Range. The physical features of Garo Hills are grouped into three regions: (a) The Northern Sub-montane regions (b) The Central Plateau region and (c) The Southern Hills slope region.

To the east of the Garo Hills lie the higher Khasi Hills and the easternmost part of the Meghalaya Plateau is the Jaintia Hills. The Khasi and Jaintia Hills have the following three parts based on their physiographic characteristics:

i) Northern undulating hills,
ii) Central upland zone and
iii) Southern plateau.

The Northern hills (elevation ranging from 170 to 820 m) generally slope towards the Brahmaputra Valley. Above 490 m elevation, most of the hills are flat-topped in appearance. The central upland zone runs from west to east and occupies more than one-third of the central and eastern Meghalaya. The Shillong Peak (1961 m) is its highest point. The southern point of the central and eastern Meghalaya plateau is characterized by steep slopes. The deeply cut valleys divide this section into three parts – the Cherapunjee Platform, the Mawsynram Platform, and the Lynkyrdem Platform. On the Cherapunjee platform there are many small rounded hills made of limestone. These hills have caves with narrow underground tunnels and characteristic

karst features. Towards the plains of Bangladesh, the face of the plateau at many places is characterized by deep precipices caused by abrupt slope and heavy rainfall.

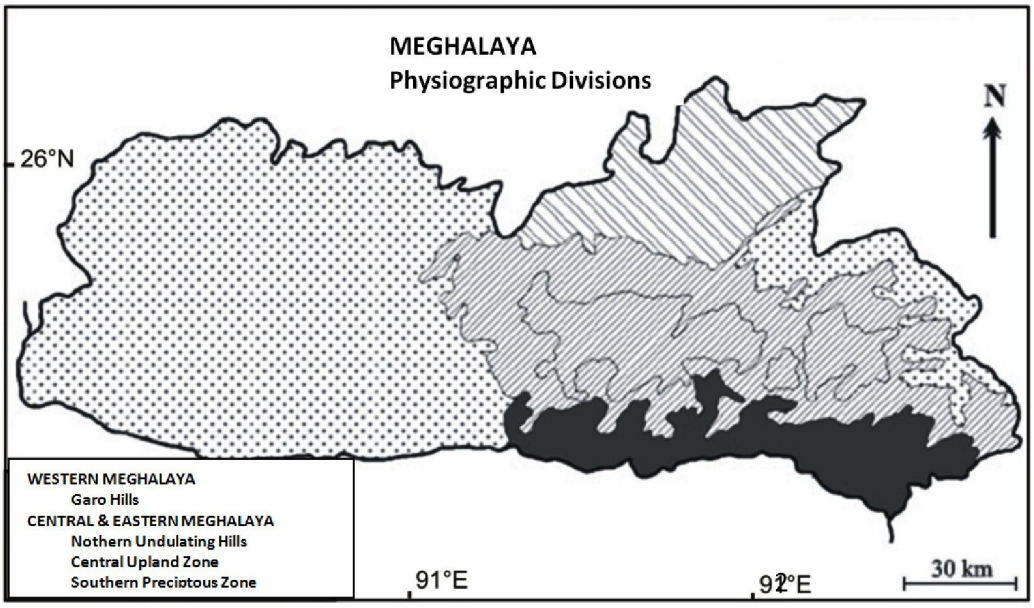

2

Figure 1.2: Physiographic Divisions of Meghalaya.

The Jaintia Hills (eastern plateau) is a contiguous part of the central Meghalaya Plateau but it is relatively lower with an average height of a little more than 1200 m. The Marangksih peak on the Eastern plateau of Jaintia Hills stands majestically at the elevation of 163 m above mean sea level and is the highest peak in the entire district. The main elevation of the district ranges between 1050 m to 1350 m. The three parts of the plateau viz. northern hills, the central upland (Jowai upland) and the southern escarpment coincide with three parts of the Central Meghalaya. The central upland (1500 m) extending from east to west acts as a watershed between the Surma Valley in Bangladesh and the Brahmaputra Valley in Assam. The Jaintia Hills have more low and level lands than the Khasi Hills (Fig. 1.2). In general, the whole district is full of rugged and undulating terrain with the exception of the deep gorges and narrow valley carved out by Umngot, Myntdu, Lukha rivers.

1.3 DRAINAGE SYSTEM

The drainage system of Meghalaya is greatly determined by its geological structure and the physiographic features. The Tura range in Garo Hills and the central uplands in Khasi and Jaintia Hills form watersheds, and from these watersheds the rivers flow down towards the plains of Bangladesh in the south and the Brahmaputra

valley in the north. The important rivers in the Garo Hills (of the northern group from west to east) are the Kalu, Ringgi, Didak, Didram, Krishnai and Dudhnai. Sanda, Bandra, Bhogai, Dareng, Nitai and Simsang are the important rivers of the southern group.

The rivers in Khasi and Jaintia Hills also flow in two reverse directions. The main rivers of the northern groups (Khri, Digaru, Umtrew, Umiew and Myngot) form the boundary of the plateau very irregular. The south bound rivers give rise to deep valleys on the faulted surface of the hills as they leave Meghalaya to enter Bangladesh plains (Fig. 1.3).

1.4 CLIMATE

The climatic conditions of Meghalaya vary according to the altitudinal changes occurring over the north-western part of India and the Bay of Bengal (formation of high pressure) and the warm and moist wind coming from the south or the south-west. Meghalaya receives most of its rainfall from the south-west monsoon winds. Khasi and Jaintia Hills is uniquely pleasant while in Garo Hills the summer is humid and warm, and winter is pleasant. During winters, ground frost is common in the table land of Khasi and Jaintia hills. The monsoon winds from the Bay of Bengal strike against the hill ranges in the southern part of the state experiencing heavy rainfall. The Mawsynram-Sohra belt in this region has the highest rainfall record in the world (1392 cm). More rainfall is at windward slopes and less on the leeward side.

The average annual rainfall in the south-west is about 400 cm, in the central part between 300 - 400 cm and in the north it ranges from 250 to 300 cm. More than 75% of the rainfall is received within 6 months from April to September. Winter months with only 6 cm rainfall are almost dry.

The climate of this region is directly influenced by the Southwest monsoon and the Northeast winds. There are four distinct seasons: (1) Spring from March and April; (2) Summer (Monsoon) May to September; (3) Autumn – October to November and (4) Winter – December to February. Rainfall starts by the 3rd week of May and continue right up to the end of September and sometime well into the middle of October.

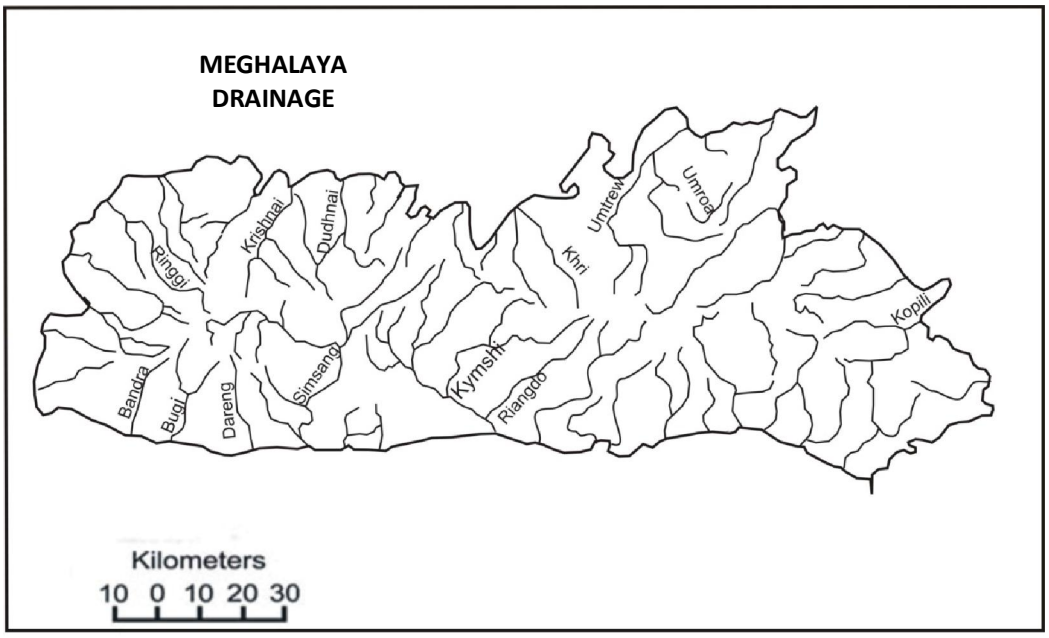

Figure 1.3: Drainage System in Meghalaya.

1.5 PREVIOUS WORK

Oldham (1858) had carried out the pioneering geological work on part of Khasi Hills of the region. The systematic geological mapping of the region was subsequently carried out in details by Medlicott (1869), Godwin Austin (1869), La Touche (1883, 1887) and Mallet (1876). Their contribution gave impetus in the further systematic of different parts of the region by later workers viz. Palmer (1923), Fox (1934-35), Mukerjee (1939), Ghosh (1936-39), Talukdar (1967), Bhattacharya and Barman (2000). Medlicott (1869) reported the occurrence of granitoid massives in the Meghalaya plateau. The Archaean and Precambrian rocks of the plateau have been mapped systematically by Gogoi (1961-73), Munshi (1964-65) and Mazumder (1965-68). Their works led to the delineation of the individual rock units of the Archaean and Precambrian (Shillong group) but also revealed their inter-relationship and also brought interesting structural features of the region. Geological Survey of India (GSI, 1974, 1989) gave the stratigraphic sequence, geology and mineral resources of the region. Since inception of the Assam circle (later Assam-Meghalaya circle/Regional Geology divisions of Meghalaya and Assam) of Geological Survey of India at Shillong in 1961, a programme of systematic geological mapping of Meghalaya Plateau was undertaken this is still continuing. Mazumder (1968, 1976) gave a detail account on the region geology and field relationships of felsic magmatism and

associated litho units of Mylliem, Nongpoh, and Kyrdem and South Khasi region of Meghalaya plateau. Rahman (1991) has thrown light on the emplacement condition of Precambrian felsic plutons of Meghalaya plateau. In series of contributions, the petrology and petrochemistry of Mylliem felsic pluton have also been studied (Rahman, 1972, 1981, 1985, 1987). Ghosh *et al*., (1991, 1994, 2005) made comparative geochronological and geochemical studies of the various granitoids and have inferred that these felsic plutons represent final amalgamation events of the Gondwana Supercontinent.

The geology and geodynamics of the Shillong plateau are reported by Nandy and Das Gupta (1986); Nandy (2001); Srinivasan (2005) and Selvan *et al*., (1995). Chatterjee *et al*., (2007) reported electron microprobe (EPMA) monazite dates and mineral paragenesis of granulite facies metapelites of Shillong Plaeau. Based on the age they reconstructed a Neoproterozoic-Cambrian assembly of the Rodinia supercontinent where in the Shillong plateau was presumed at the leading edge during an oblique collision of India with Australo-Antarctica. Lal *et al*., (1978) discussed the phase petrology of the sapphirine-bearing granulites of the proposed area. While working on the exhumation and uplift of the Shillong plateau, Biswas *et al*., (2007) opined that the exhumation of the plateau began at least 9–15 Ma ago, its surface uplift was chronologically decoupled from its exhumation and started after 3–4 Ma at rates of 0.4–0.53 mm/a, and the long-term horizontal shortening rate accommodated by the plateau is 0.65–2.3 mm/a, which represents only 10–15% of the India-Asia convergence rate. Several works on Seismotectonics of Shillong plateau are carried out, including focal mechanism solutions of earthquake in Shillong plateau (Angelier and Baruah, 2009; Kayal and De Reena 1991; Kayal 2001), the role of major lineaments in the area (Evans, 1964; Mukhopadhyay, 1984; Kayal, 1987), the estimation of b-values (Bhattacharya *et al*., 2002; Bhattacharya and Kayal, 2003; Khan, 2005) and the delineation of crustal as well as upper mantle heterogeneities on the basis of seismic tomography (Kayal and Zhao, 1998).

Although significant progress has been made in the knowledge of this Precambrian Gneissic Complex, yet many of the questions concerning the evolution of the rocks and source characteristics etc. still remains a question. Petrological and geochemical study of these Precambrian rocks had been sporadic and adequate summaries of the results achieved are still meager. In addition, a detailed geochemical

study and a data base on the basement rocks of Shillong plateau are still much warranted. Towards the solution of this problem, the region needs more data for a better understanding of the geodynamic evolution of the Shillong plateau as these rocks represent middle to lower continental crustal rocks of the earth.

1.6 SCOPE OF THE WORK

The principal aim of the work is to generate petrographical and geochemical characteristics of the mafic and felsic granulites of Sonapahar area forming the basement of Shillong plateau and to elucidate the petrogenetic evolution of these basement rocks. Granulites are believed to constitute a major portion of the lower to middle continental crust and thus a better understanding of the petrogenesis of these rocks will enhance our knowledge of geodynamic evolution of deep continental crust. The geochemical study of the Precambrian basement of granulite facies assemblages of Shillong plateau will open further scopes for correlation with other granulite belts found elsewhere in India particularly in Eastern Granulite belt and Southern Granulite terrain. Granulite-facies terranes and granulite xenoliths carried up by volcanic rocks provide windows into the middle and lower crust and have received considerable attention in elucidating crustal evolution history and tectonic processes. The formation mechanisms and exhumation history of granulite facies assemblages from various parts of the world have been topics of many recent investigations (Bingen and Stein., 2003; Blein *et al.,* 2003; Garcia *et al.,* 2003; Owen *et al*., 2003; Santosh and Tsunogae., 2003; Santosh *et al*., 2003a, b; Seth *et al*., 2003; Tsunogae *et al.,* 2003; Yu *et al*., 2003). Thus, study of granulites of the Sonapahar area has important significance for further study of formation and tectonics of deeper crust of the Shillong Plateau. Whole-rock geochemical data are implemented to define compositionally distinct rock types and constrain their possible petrogenetic relations. They also provide important background information for comparison of rock types showing contrasting petrological history of their protolith. The rocks even when metamorphosed to high pressures of the granulite facies retain their geochemical signatures inherited from the source rocks (Cox *et al*., 1995). Thus analysis of major oxides and trace elements including REE could be one of the efficient tools to interpret the composition of the protoliths because the elements with high ionic potential (Ti, Zr, Y, V, Cr, Ni.) and REE are interpreted to have been effectively

immobile during high grade metamorphism (Rollinson and Windley, 1980; Condie 1981; Sheraton, 1980).

The main objective of this research work constitutes:

i) To carry out detailed geological field work and to collect rock samples for laboratory studies.

ii) To carry out detailed petrographic studies of the basement rocks of the Sonapahar area, Shillong Plateau.

iii) To carry out whole rock geochemical analysis of the basement rocks for major, trace including REE and to interpret the data.

(iv) To understand and elucidate the petrogenetic evolution of basement rocks of the Shillong plateau.

Chapter- 2

GEOLOGICAL SETTING

GEOLOGICAL SETTING

2.1 GEOLOGY AND STRATIGRAPHY OF SHILLONG PLATEAU

The geology of the Shillong plateau as a whole is very complex, since the plateau represents a checkered history of evolution with contrasting petrological units of different ages, formulating the stratigraphic sequence as follows:

(a) Archean(?) – Proterozoic Gneissic complex

(b) Proterozoic Basic – Ultrabasic Intrusives

(c) Shillong Group of metasediments of Meso-Proterozoic age

(d) Granite Plutons of Neo-Proterozoic – Lower Paleozoic age

(e) Lower Gondwana sedimentary rocks of Carboniferous – Permian age

(f) Cretaceous Sylhet Traps and Alkaline – Ultramafic- Carbonatite Complexes

(g) Cretaceous – Tertiary Sediments and

(h) Pleistocene to recent fluvial sediments.

The generalized stratigraphic succession of Shillong Plateau is presented in the following table.

Table 2.1: Generalized stratigraphic succession of Shillong Plateau (after GSI, 2009)

Age	Group Name	Formation	Lithology
Holocene	**Newer Alluvium** (Thickness not known)	Unclassified	Sand, silt and clay
Pleistocene	**Older Alluvium** (Thickness not known)	Unclassified	Sand, clay, pebble, boulder and gravel deposit
----------	----------	Unconformity	----------
Mio-Pliocene		**Dupi Tila Formation (1050 m)**	Mottled clay, feldspathic sandstone and conglomerate
----------	----------	Unconformity	----------
Oligo-Miocene	**Garo Group**	**Chengpara Formation (700 m)**	Coarse Sandstone, siltstone, clay and marl.
Oligo-Miocene	**Garo Group**	**Baghmara**	Coarse feldspathic sand-

		Formation (530 m)	stone, pebble, conglomerate, clay, silty clay with a fossiliferous limestone horizon at the top
		Simsang Formation (1150 m)	Siltstone and fine sandstone and alternations of siltstone-mudstone.
Eocene-Oligocene	**Barail Group**	----------	Coarse sandstone, shale, carbonceous shale with streaks and minor lenses of coal.
		Kopili Formation (50 m)	Shale, sandstone, marl and coal.
Palaecene-Eocene	**Jaintia Group**	**Shells Formation (600 m)**	Alternation of sandstone, limestone
		Langpar Formation (100 m)	Calcareous shale, sandstone and limestone.
Upper Cretaceous	**Khasi Group**	**Mahadek Formation (150 m)**	Arkosic sandstone (often glauconitic and uraniferous)
		Conglomerate (25 m)	Conglomerate
		Jadakuta Formation (140 m)	Conglomerate/Sandstone
---------- Unconformity ----------			
Cretaceous	**Alkaline-Ultramafic Carbonatite Complex**	----------	Pyroxenite-serpentinite with abundant development of melilite pyroxene rock, ijolite, syenite and carbonatite.
---------- Unconformity ----------			
Cretaceous	**Sylhet Trap (600 m)**		Basalt, alkali basalt, rhyolite and acid tuffs.
---------- Unconformity ----------			

Carboniferous to Permian	**Lower Gondwana**	**Karharbari Formation**	Very coarse to coarse grained sandstone with conglomerate lense, siltstone, shale, carbonaceous shale and coal.
		Talchir Formation	Basal tillite with sandstone bands, siltstone and shale.
---------- Unconformity ----------			
Neo Proterozoic-Early Paleozoic		**Granite Plutons:** Kyrdem Granite Pluton (479±26 Ma) Nongpoh Granite (550±15Ma) Mylliem Granite (607±13Ma) South Khasi Granite (690±26Ma)	Porphyritic coarse granite, pegmatite, aplite/ quartz vein traversed by epidiorite, dolerite and basalt dykes.
---------- Unconformity ----------			
Proterozoic	**Khasi Basic-Ultra basic intrusives (Khasi Greenstone)**	----------	Epidiorite, dolerite, amphibolite and pyroxenite dykes and sills.
Paleo-Mesozoic Proterozoic	**Shillong Group**	----------	Quartzite, phyllite, quartzsericite schists, conglomerate.
Archean(?)-Proterozoic	**Meghalaya Gneissic Complex**	----------	Biotite gneiss, biotite hornblende gneiss, granite gneiss, mica schist, sillimanite-quartz schist, biotite-granulite-amphibolite, pyroxene granulite, gabbro and diorite.

2.1.1 DESCRIPTION OF VARIOUS LITHO-UNITS OF SHILLONG PLATEAU

The Proterozoic metasedimentary Shillong Group and the basement Gneissic Complex make up most of the plateau. Brief descriptions of various lithounits of Shillong Plateau beginning from the oldest unit are outlined below:

2.1.1.1 **Archean (?) – Proterozoic Gneissic Complex**

The Gneissic Complex is exposed mostly in the central and Nothern parts of the Shillong Plateau covering the districts of West Garo Hills, East Garo Hills, West Khasi Hills and Ri Bhoi (Fig. 2.1). The Archean Gneissic Complex is represented dominantly by para- and ortho-gneisses, migmatites and metasedimentary bands. These are intruded by amphibolites, metadolerites and metapyroxenites. The gneissic rocks and associated gneissic sediments have long been recognized as an extension of Peninsular India (Evans, 1932). According to him, the horizontal movement along the Dauki Fault detached the Shillong Plateau from the main mass of Indian Shield.

The basement gneisses are distinctly older at 1714 Ma and 1150 Ma (Ghosh *et al*., 1991; 1994a; Chimote *et al*., 1988; Selvan *et al*., 1995). Considering the low metamorphic grade of these gneisses it is believed that the Rb-Sr whole-rock ages represent their protolith ages (Ghosh *et al*., 2005). Chatterjee *et al*., (2007) have carried out electron microprobe (EPMA) monazite dating and paragenesis of granulite-facies metapelites from the Shillong plateau that clusters around ca. 1596±15 Ma to ca. 500±14 Ma. Within the basement granite-gneisses are the most abundant rocks with patchy enclaves of amphibolites, banded magnetite quartzite, quartz-dumonterite-tourmaline schist, mica schist, sillimanite-quartz schist, calc granulite, saphirrine cordierite granulite, magnetite granulite etc. The granite- gneisses are mostly medium to coarse grained and composed of quartz, K-feldspar plagioclase, biotite, garnet and a little hornblende with apatite and sphene as accessories. The overall texture of the rock is xenoblastic. The mineral constituents of the amphibolites enclaves are dark green hornblende, plagioclase, and biotite with occational quartz, epidote, sphene and magnetite. The granulites and related mafic- ultramafic rocks are in general medium to very coarse grained, massives and are occasionally associated with carbonate rocks and are composed predominantly of calcite, partially serpentinised olivine, tremolite and spinel. The micaceous schists often occur as narrow strips within the gneisses with gradational boundary. In the basement complex, sillimanite-garnet-K-feldspar-quartz gneisses/schist without muscovite is a common assemblage. In Sonapahar area the sillimanite gneisses contain biotite-cordierite-corundum and chondrodite (?) Proterozoic age. The chondrodite, which indicates a low pressure to intermediate metamorphism, has also been reported in the

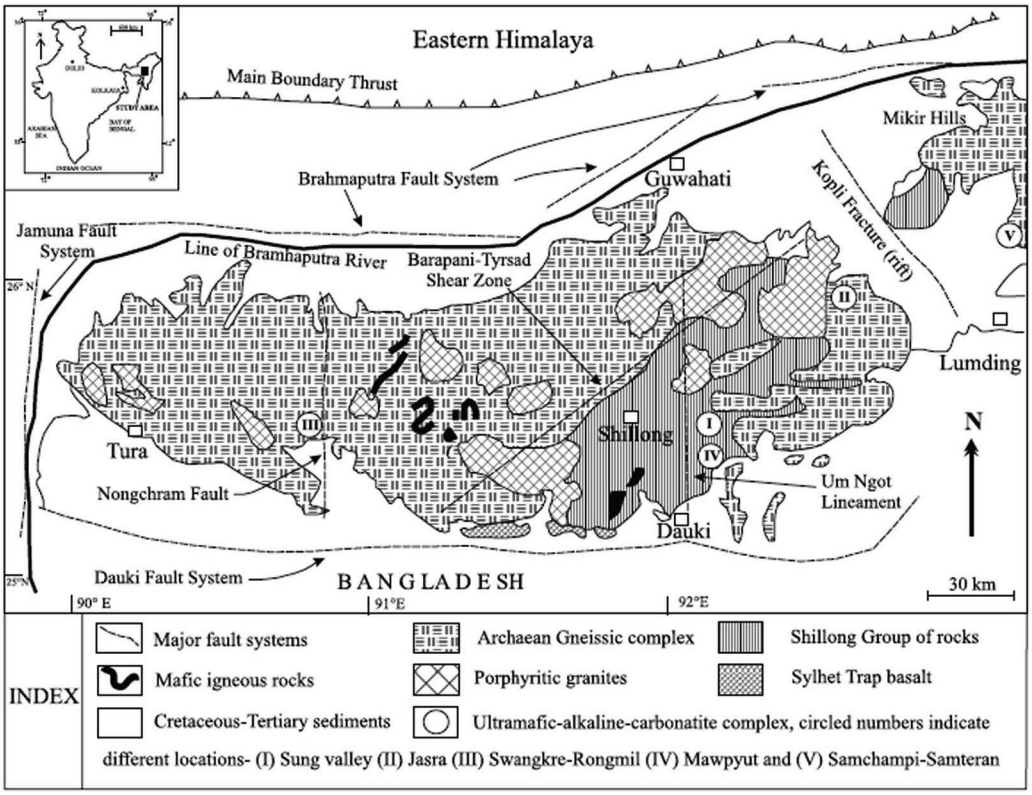

Figure 2.1: Regional geological and tectonic framework of the Shillong Plateau (after Srivastava and Sinha, 2004).

gneisses of Umpirtha areas. The sillimanite bearing rocks represent per aluminous regolith belonging to assemblage of biotite-cordierite occurs south of South Khasi batholith and it represents the metasomatic part of the migmatite. Evidence of retrogression and neocrystallisation have been recorded in garnetiferous schist occurring north of South Khasi Batholith, where micaceous pseudomorphs of aluminosilicate (Andalusite?) are present.

All gradations from augen gneiss to streaky gneiss and banded gneiss indicating different stages of granitisation are noticed in the gneisses. Mazumdar (1976) has recognized relict augen gneisses which are pre-tectonic and belong to an earlier orogeny. In the banded gneisses, quartzo-feldspathic leucosomes alternate with biotite-rich melanosome and the thickness of the gneissis bands varies from place to place. Structures like 'agmatic', 'stromatic' etc, which are typical fabrics in a migmatite terrain, are well displayed at place. Pinching and swelling of the leucosome along the main S-plane and also ptygmatic folding are common features recorded in the migmatite. In the heart of the gneissic terrain homophanous patches of granite-like rocks are recorded, which are developed during the most advanced stage (nebulite) of

the granitisation process. The mobilized rocks are granitic, granodioritic or at places dioritic in composition. In the mobilized rocks, xenoliths of the country rocks are common. The contact between the gneiss and the remobilized granitoids is gradational at many places, while the intrusive relationship has been recorded in some other place. Petrographic characters of some of the granodiorite-granite rocks indicate that they belong to 'plutonic migmatites'.

The basement gneisses have been intruded by acid, basic and ultrabasic intrusive of various dimensions and shapes. The acidic intrusives are dominated by anorogenic granite plutons and veins. The basic/ultrabasic intrusive include ortho-amphibolite, metagabbro and metapyroxenite. Syntectonic intrusive of basic rocks are represented by the Khasi Greenstones, while the other basic bodies and the ultrabasic rocks that had emplaced within the gneisses have scantily been injected by thin sheets of Lamphrophyre (near Rongjeng, Umpirtha etc.) and carbonatite (near Rongeng).

Detailed field works have been carried out in and around Sonapahar area forming the central parts of Archaean Gneissic Complex of Shillong Plateau during the course of this work. A description of rock units in terms of their field occurrences and mutual relationships as observed during the field works are outlined below:

The rock types of the study area consist mainly of medium to coarse grained granitic gneisses, cordierite bearing granulitic gneisses, quartz-sillimanite schist and pyroxene-hornblende granulites in order of abundances along with some minor occurrences of corundum bearing sillimanite (Fig. 2.2). The contact between cordierite gneisses and quartz – sillimanite schist were usually sharp and well defined. Massive corundum bearing sillimanite occur in the cores of folds in the quartz – sillimanite schists and consist predominantly of coarse radiating aggregates of sillimanite with frequent blebs of corundum. Rocks with only sillimanite or corundum also occur. Along fractures and joints in these rocks, coarse veins of sillimanite are common and sometimes coarse biotite segregation intergrowth with sillimanite has been observed.

2.1.1.1a *Granite Gneisses*

Granite gneisses constitute the host rock for other rock unit in the study area. They are largely exposed in and around Sonapahar. Granite gneisses in the study area are basically two types. Rocks exposed along the north-western part of Sonapahar

town were mainly grey in colour with distinct gneissose structure. They are mostly medium to coarse grained, mesocratic rock. The rest are generally leucocratic to

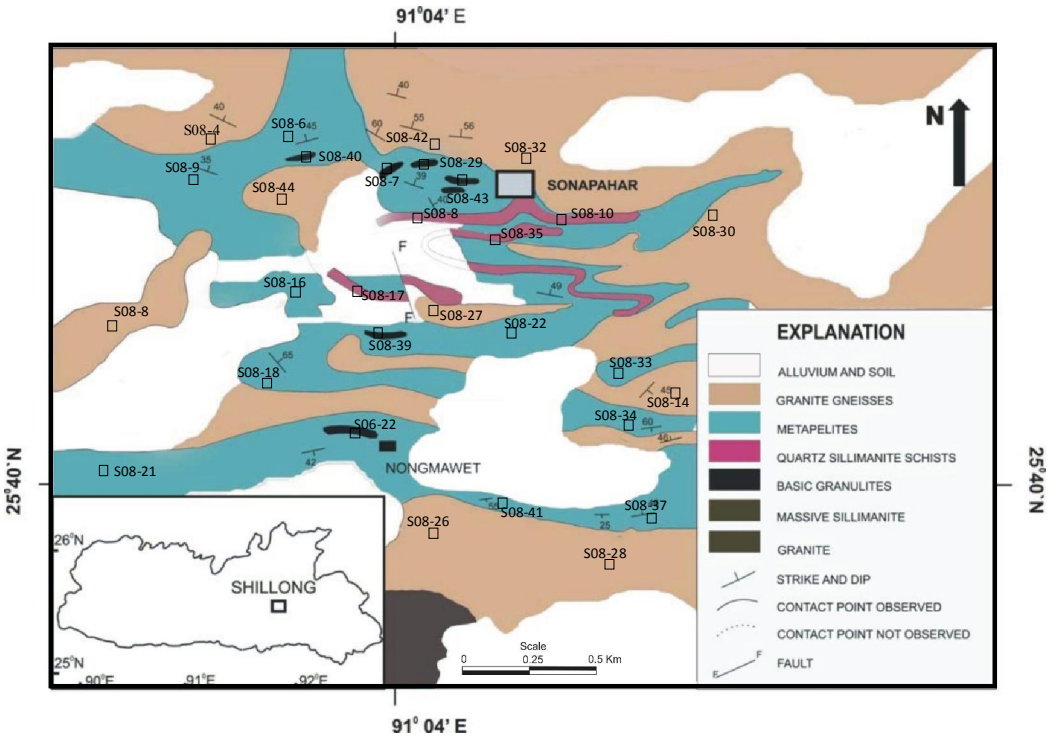

Figure 2.2: Geological and sample location map of the study area

mesocratic with clearly visible alignment of biotite. They are generally medium to coarse grained. These rocks chiefly comprise feldspar, quartz and biotite in varying proportion and with varying grained dimensions resulting into petrological assemblage such as biotite-feldspar gneiss.

2.1.1.1b *Cordierite bearing Granulitic Gneisses*

Cordierite bearing granulitic gneisses is largely exposed in the north-western, western and southern part of Sonapahar. They are intimately associated with granite gneisses. The rocks exposed along the river banks near Sonapahar town, close to large granite gneiss outcrop in the north eastern portion of Sonapahar are highly massive and coarse grained. However, rocks exposed in the north-western area mainly shows schistose character in which parallel alignment of biotite are clearly visible in hand specimen. Rocks exposed along the highway via Nogstoin are generally massive and medium grained without gneissose structure. In general, metapelites of the Sonapahar area are medium to coarse grained, melanocratic rocks. The mineral constituents are

garnet, cordierite, biotite, silimanite, quartz and K- feldspar with plagioclase as minor constituents. Basic granulite occurs as enclaves within cordierite-bearing granulitic gneisses.

2.1.1.1c *Basic Granulites*

These are medium to coarse grained, melanocratic rocks with granulose texture. The observable mutual relationship of these rocks with the metapelitic rocks indicate that these rocks are mostly concordant intrusions but at places, discordant relationships with the cordierite-bearing granulitic gneisses are also observed. These are mainly massive but sometimes foliations are seen due to orientation of hornblende and biotite in hand specimen. The basic granulites show dark to greenish black in colour in which pyroxenes and plagioclase are visible in hand specimens. These rocks are hard and compact. The mineral constituents are orthopyroxenes**,** clinopyroxenes**,** hornblende, plagioclase and quartz with accessory amount of biotite.

2.1.1.1d *Quartz- Sillimanite Schist*

The Precambrian terrain of the Sonapahar area is characterised by the presence of a thin, long, discontinuous band of quartz-sillimanite schist which hosts the massive sillimanite-corundum deposits. The massive sillimanite-corundum occurs as randomly distributed bodies of variable size and shape within the quartz-sillimanite schist. Quartz sillimanite schists are mostly exposed near the Sonapahar town. These rocks exhibit a well developed foliation defined by alternate bands rich in quartz and sillimanite, at places with corundum. The quartz-sillimanite schists are highly crumpled at places, due to intense puckering and incipient axial fractures. They are mainly composed of sillimanite and quartz with accessory biotite.

2.1.1.1e *Corundum bearing Sillimanite*

Individual bodies of corundum bearing sillimanite occur as massive rock types which mostly confined within the sillimanite bearing rocks. These bodies are highly variable in their size. The major constituents of these massive concentrations are mainly sillimanite, corundum with biotite and quartz as minor constituents.

2.1.1.2 **Meso-Proterozoic Shillong Group of Metasediments**

The Shillong Group of metasediments is exposed in the central and eastern part of Meghalaya Plateau. In the western part, south of Sumer, rocks of the Shillong

Group were laid over the Gneissic Complex with an unconformity defined by a basal conglomerate horizon. However, the rocks near the contact between the Gneissic Complex and Shillong Group along Mawshut, Mawlong, Mana, Mawsaw stretch and its extension towards north-east and southwest is transitional and partly migmatised at places. The Shillong Group (earlier termed as 'Shillong Series') was correlated with 'Iron Ore series'. The correlation was based on the presence of magnetite-quartzite and hematite-quartzite in the Shillong Group occurring in the northern part of the plateau. Pascoe (1973) correlated the Shillong Group with the Dharwars, though there exists much difference in their lithology.

The Shillong Group has been broadly classified into a lower dominantly argillaceous unit and an upper arenaceous unit. Metamorphism in the former has reached the 'garnet zone'; while the grade of metamorphism in other part is relatively low and at several localities the rocks are unmetamorphosed. The cover metasediments of the Shillong Group form clastic sequence made up of quartzite and phyllite with subordinate quartz-sericite schists, conglomerate etc. Both basal and intraformational conglomerates have been recorded in the Shillong Group. The lithopackage forms broadly a NE-SW trending belt in the eastern part of Shillong Plateau and is traverse by acidic, basic and ultrabasic intrusives. The acidic intrusive are represented by large bosses of granite with pegmatites and quartz veins. The basic and ultrabasic rocks comprise dolerite, gabbro, pyroxenite etc. belonging to Khasi basic ultrabasic intrusive. The dating of the intrusive indicates a late Proterozoic age (570-900 Ma). It may be inferred that the Shillong Group belongs to Middle Proterozoic age (900-1600 Ma).

The basal conglomerate defining the unconformity is exposed along the part of the western border of the Shillong Group. The base of the Shillong group is represented by a sheared ferruginous quartzite. The basal conglomerate is thickly bedded and sheared. The bedding is well defined at places by pebble layering. Current bedding is preserved occasionally. The clasts are dominated by vein quartz and quartzite set in a quartzofelspathic, micaceous and phyllitic matrix.

The intraformational conglomerate occurs as discontinuous bands/lenses in the quartzites at number of localities (viz; Wah Umiam, Sohiong, Mawphlang, Wah Sohra gorge etc.). Although these conglomerates are disposed along different statigraphic levels, a broad similarity exists in their lithological composition and

structure. The clasts in these conglomerates are subrounded, vary in size from pebble to cobble and even to boulder and are composed of vein quartz and quartzite. It is noteworthy that boulders of metamorphic rocks have been recorded in conglomerate from Wah Sohra gorge. The flattened clasts along the foliation are set in a quartzofelspathic or siliceous matrix. The intensity of flattening varies from place to place. In new Kynsew, the conglomerate contains attenuated pebbles of vein quartz along the strike extension the conglomerate grades into gritty quartzite with smaller clasts of vein quartz.

The quartzite of the Shillong Group varies in colour, composition, grain size and also in degree of recrystallization. Gradation from orho-quartzite arkosic quartzite and to phyllite is a common feature. One dominant variety of medium grained quartzite contains sand size grains in a clayey or argillaceous matrix. The sand grains are of quartz, quartzite and chert, some detrital grains exhibit overgrowth of authigenic quartz and remaining intergranular space are occupied by the matrix material. With increasing recrystallization, aggregates of grains of quartz as well as segregation of layers are produced in a granoblastic mosaic. In the quartzose aggregates, polygonization and development of triple point junction are noticeable. In such varieties, the primary sedimentary fabric is mostly obliterated and the rock resembles an orthoquartzites. The mineral constituents in the quartzites are quartz with variable proportion of feldspar, sericite, biotite, muscovite, garnet, epidote and opaques. The biotite and garnet are only occasionally developed and the grade of metamorphism is relatively high.

Phyllite, siltstone and shale representing the argillaceous components of the Shillong Group often form thick piles in which intercalating bands/lenses of quartzite are common. The pelites are thinly laminated, vary in colour at places are well foliated. Gradation from phyllite to phyllitic quartzite is a common feature. The phyllite is often ferruginous. The rock is composed of very fine grains of quartz, feldspar, chlorite, epidote and sericite with minor amounts of opaques, muscovite and biotite. The opaques are dominantly represented by pyrite and iron oxides. Concentration of opaques along thin layers defining bedding has occasionally been recorded. The foliation is represented by slaty cleavage. The quartzites, which occur as intercalating bands/lenses in phyllite near Tyrsad-Barapani Shear Zone, show evidences of shearing/mylonitisations.

The primary structures (e.g. bedding, current bedding and ripple marks) are very common in metasediments of Shillong Group. The schistosity planes are developed in the proximity to granite plutons. These are in general parallel/sub-parallel to bedding planes and are often transposed in more metamorphosed parts.

2.1.1.3 **Proterozoic Basic – Ultrabasic Intrusives**

The Khasi Basic-Ultrabasic Intrusives comprising basic intrusives like epidiorite, metagabbro, metadolerite etc occur mostly as sills, dykes and rarely as phacoliths in the various subfacies of the Shillong Group. The Khasi Basic-Ultrabasic Intrusives have also intruded the Basement Gneissic Complex in the west central part of the plateau. The basic rocks, which are emplaced predominantly in the Shillong Group, are mostly exposed as tabular bodies, conformable with the beds of the enveloping of the Shillong Group. It has been noticed in several localities (e.g., south of Laitiyngkot, northwest of Sohiong etc.) that the same body is partly concordant, while discordant in other parts. One major exposure of the Khasi Basic-Ultrbasic Intrusives has been recorded at the Um Song gorge, where it persists along the full stretch (910 m) of the gorge. In the areas between Wah Sohra gorge in the east and the Umiew gorge in the west, a number of basic bodies have been emplaced in the fork-like pattern and it is presumed that such sheets might have been originated from a single, concealed body. Detached linear bodies of the Khasi Basic-Ultrabasic Intrusives also occur between Lyniong and Barapani with a width of about 500 m and length upto 7 Km of individual body.

In weathered outcrops, the basic rocks give a reddish brown colour. The rocks are generally dark green, medium to coarse grained and massive. Near the contact with the Shillong Group, The intrusive are at places, finer in grain size. A crude foliation has developed locally. Late magmatic granophyric lenses and pneumatolytic quartz veins occur occasionally in the basic rocks. Secondary quartz-carbonate veins have rarely been noticed.

The Basic-Ultrabasic Intrusives represents an episode of basic magmatism, between the two major phases of granitic activities. The emplacement of basic magma was prior to the onset of metamorphism in the Shillong Group. The disposition of basic bodies is primarily controlled by the regional foliation of the Shillong Group. The Basic-Ultrabasic Intrusives were emplaced in the extension zones of the

extensional regime related to the folding deformation of the enveloping Shillong Group.

2.1.1.4 **Neo-Proterozoic – Lower Paleozoic Granite plutons**

The Meghalaya Plateau is characterized by a number of syn to late tectonic plutons. The granite plutons yield Rb-Sr wholerock ages ranging from 479 Ma to 881 Ma (Ghosh *et al*., 1991; 1994a; Chimote *et al*., 1988; Selvan *et al*., 1995). The Singluli granite exposed in and around Patharkhang area is the only minor post-tectonic granite intrusive so far reported. Some of the granite bosses such as Mylliem Granite are intrusive into the Shillong Group, while several other intrusive bodies at Nongpoh, Hallidayganj, Mawthaliang, Rongjeng, Kyrdem, Kholong etc. have intruded into the basement Gneissic Complex. A large pluton namely the South Khasi Batholith intrudes into Shillong Group.

The Geological Map of the Shillong Plateau (Fig: 2.1) reveals that the plutons are distributed broadly along the NE-SW trending axis close to the western contact between the Shillong Group and the basement Gneissic Complex and also along a NW-SE zone which passes through south of Shillong. Straight margins of some of the plutons (viz; Nongpoh, South Khasi Batholith etc.) might point to some pre existing fractures which might have controlled their emplacement. Apophyses and veins of the granites in the country rocks, presence of discordant xenoliths along with textural features like oscillatory zoning in plagioclase indicate a possible magmatic origin in these granite plutons.

2.1.1.5 **Carboniferous-Permian Lower Gondwana Sedimentary rocks**

The occurrences of Lower Gondwana rocks were first reported by Fox (1934) and later by Femor (1935). Fox reported some fossils and some pieces of vitrinised coal which confirms its Gondwana affinity. Acharyya and Ghosh, (1968a) group the entire sequence into Karharbari Formation. Banerjee *et al*., (1977) on the basis of mega and microflora, assign a lower Barakar age to the fossiliferous carbonaceous shale. The Gondwana rocks are mostly concealed under the thick cover of Brahmaputra alluvium.

2.1.1.6 **Cretaceous Sylhet Traps**

The Sylhet Traps are represented by plateau (flood) basalts exposed in a narrow E-W strip (80 Km long and 4 Km wide) along the southern border of the

Shillong Plateau; the maximum exposed thickness is 550-600 m. These apparently overlie the eroded Precambrian basement and are overlain non-conformably by the Upper Cretaceous-Eocene sediments. This belt is part of Bengal– Sylhet–Rajmahal flood basalt province and is located along the southern margin of the Shillong Plateau having a maximum thickness of 550–650 m (Mazumder, 1986). Baksi (1995) has considered Sylhet Traps to mark the beginning of Kerguelen plume activities beneath the Indian Plate (Nambiar 1988; Baksi 1995; Nandy 2001; Mahoney *et a.,l* 1983; Veena *et a.,l* 1998; Kent *et al.,* 2002) around 117 Ma. The Kerguelen hotspot was situated close to the eastern Indian margin 100–120 Ma ago and was responsible for the extrusion of Rajmahal basalts exposed over the Gondwana Supergroup and Sylhet basalts and related alkaline-carbonatite magmatism of Shillong Plateau (Coffin *et al.,* 2002; Kent *et al.,* 2002). The ultramafic-mafic-alkaline-carbonatite intrusive complexes representing late stage differentiation of Sylhet Trap magmas occur as small, isolated, circular bodies along a NE trending zone in Shillong Plateau (Mamallan *et al.,* 1994; Srivastava and Sinha., 2004, 2007). The sediments and the lavas form a monoclonal flexure and the sediments at the crest of the monocline have subsequently been eroded exposing the traps as inliers at places. The flexure in the Therriaghat-Shella sector with its E-W axis changes along its trace westward to a high angle reverse fault through normal and vertical fault (Dauki fault), which mark the exposed limit of the Sylhet Traps to the south. Then traps to the north at Therriaghat are in contact with the gneisses and granites along the E-W fault, termed the Raibah fault. Immediately south of this fault, the traps dip at 45^0-50^0 to the south. At the southernmost limit, they again dip at 10^0-35^0 along the monocline or at 50^0 against the Dauki fault. The Sylhet Traps comprise predominantly of basalts (nephelene bearing phonolite), rhyolites and acid tuffs. The basaltic flows are 5-7 m in average thickness. Andesites are absent.

Both within the flows, and also in the viscinity of Precambrian rocks to the north, basic dykes are common; within the trap area, the dykes occur as swarms and are younger than lava. The extrusion of Sylhet Traps began with a quiet effusion of thloleiitic flood basalts, accentuated through E-W fissures developed in the peneplained crystallined basement. The Raibah fault was active during and after the volcanism till upper cretaceous. Post eruptive basic dykes and few alkali lamphrophyre dykes intrude along the E-W fractures, especially in the monoclinally

dipping southern portion. Thus the tectonic history of this part of the Shillong Plateau is characterized by relative uplift and down-sinking of different basement blocks like horst and graben along weak zones in the basement.

2.1.1.7 **Alkaline – Ultramafic- Carbonatite Complexes**

A large Alkaline-Ultramafic-Carbonatite Complex occurs as intrusive within the Shillong Group metasediments around Sung. No contact metamorphic effect was noticed near to the vicinity of the intrusive body. However, a narrow zone of fenite and a brecciated admixed zone of fenite and quartzite have developed at places particularly along the contact. The oval shaped complex depicts a partial ring structure with a central serpentinite core surrounded by pyroxenite rim. The dominant rock type of the complex include (i) Peridotite, (ii) serpentinite, (iii) pyroxenite, (iv) uncomphagrite, (v) alkaline rocks, (vi) biotite-alkali feldspar rocks and (vii) carbonatite. Apatite-magnetite rock is also present in significant amount in the complex.

The rocks of the complex are derived from differentiation of primary alkaline magma. MgO shows strong positive correlation with solidification index. Olivine and pyroxene represent the first differentiation products of the primary magma. The rocks are depleted in incompatible elements. However, no systematic variation could be observed among the various rock types.

2.1.1.8 **Cretaceous – Tertiary Sediments**

The Cretaceous-Tertiary sedimentary sequences within Shillong Plateau are represented by the various groups of rocks**.**

The **Khasi Group** is distinct arenaceous facies consisting of the oldest Jadukata Formation, a younger conglomerate unit of 25m thickness occur north of theRaibah fault designated as Basal Conglomerate Formation and the top Mahadek Formation. The Jadukata Formation consists of alternation of conglomerate and sandstone. These rocks nonconformably overlie the Sylhet Trap and their distribution is limited to the south of the Raibah fault. The same formation further to the west in Garo Hills has been termed as the Gumaghat Formation. A younger conglomerate horizon of 25m thickness occurs north of Raibah fault designated as Basal Conglomerate. This is overlain by coarse arkosic sandstone often glauconitic, which is termed as Mahadek Formation.

The Langpar Formation of **Jaintia Group** overlies the Mahadek Formation. The Cretaceous-Tertiary boundary is usually considered at the contact of Mahadek and Langpar Formations. In Cherrapunji and Therriaghat sections, the Langpar Formation comprising of intercaled shale thin limestone bands rests unconformably over the Mahadek Formation. The Mahadek sandstone contains Campanian fauna of Maestrichtian age. The Langpar Formation contains Globigerina pseudobulloides and Globogerina triculinoides of Danian age. The Formation consists of three sandstone and three limestone members beginning with sandstone over the Langpar formation. The six members of the Shella Formation from the base towards the top are as follows:

Lower Sylhet Sandstone (Therria Sandstone), Lower Sylhet Limestone (Lakadong Limestone), Middle Sylhet Limestone (Umlatdoh Limestone), Upper Sylhet Sandstone (Narpuh Sandstone) and upper Sylhet Limestone (Prang Limestone).

The Kopili Formation defines the upper most unit of Eocene sequence of Meghalaya. It comprises alternations of thinly laminated shales with phosphatic nodules, sandstone, limestone and marls. It shows wide variation in thickness from 500 m in Jaintia Hills to 270 m in Shella area.

The **Barail Group** in the Garo Hills was unknown till Bakshi (1966) found definite evidence in support of this. The undivided shelf facies of Barails overlying the Kopili Formation covers a large area over the northern part of North Cachar Hills and the southern part of Mikir Hills. The shelf facies of Barail Group, not exceeding 1000 m in thickness, consists of fairly coarse grained sandstone, shale, carbonaceous shale with streaks and minor seams of coal.

The Supra-Kopili Tertiary sequence of Meghalaya shelf (viz. **Garo Group**) is represented in the Garo Hills by the Simsang Formation which conformably ovelies the Kopili formation without any break in sedimentation. The Simsang Formation consists of cycle of massive festoon cross-bedded sandstone, alternating with siltstone –sandstone units. This Formation can be trace from near $25^0$20`N/$91^0$12`E in the Garo Hills uninterruptedly eastwards upto Shella in the Khasi Hills. Further east, it lies below the alluvium or cut off faults and occurs in isolated patches.

The Dupi Tila Formation consists of alternations of coarse felspathic sandstone with pebbly lenses containing vein quartz and mottled sandy clay. The

sediments of Dupi Tila Formation and the three formations of Garo Group represent mainly deltaic to fluviatile facies.

2.1.1.9 **Pleistocene to Recent Fluvial Sediments**

Outcrops of **Older Alluvium** overlie the Tertiary rocks along the southern and western borders of Garo Hills in isolated areas and along the southern fringes of Khasi Hills. Such outcrops are are also found along the nothern fringes of Garo Hills. These deposits consist of assorted pebble beds with coarse, loose sand and brownish clay. The pebble beds at places occur in irregular repetition. These deposits form spectacular flat-topped low hillocks and mounts with red soil cover.

Recent (Younger) Alluvium occurs in the river valleys on the nothern foot hill region of Garo and Khasi Hills, along the western border of Garo Hills and south foot hill region of Garo and Khasi Hills. The Alluvium consists of fine silty sand light to dark grayish clay with rare pockets and layers of coarse sand and shingles. The fine sand occasionally contains abundant minute flakes of mica and when extremely fine, resembles the weathered loose siltstones.

2.2 TECONIC SETTING

The Meghalaya plateau, elsewhere considered a detached Precambrian block of Indian Peninsula in the northeast India (Evans, 1964) is bounded to the south east by E-W trending Dauki fault, to the north by Brahmaputra fault (Nandy and Dasgupta, 1986) or Oldham fault (Bilham and England, 2001), to the west by the broadly NNE-SSW Indo-Myanmar belt. The plateau is separated from Mikir Hills in the Northeast by the alluvium tract of the Kopili fault system (Dasgupta and Nandy, 1982). The northern reverse fault 'Oldham fault' is stated to be deep-seated fault extending from 9-45 km beneath the surface and so it is not exposed at the surface (Bilham and England, 2001). The rocks of Shillong plateau has suffered intense compressional forces from orthogonal directions from the north and the east because of the two orogenies, the Himalaya and Indo-Myanmar fold belts, respectively (Das *et al.*, 1995).

Newly available SRTM 90-meter resolution digital topography data of the Shillong Plateau show a smooth, regular erosion surface that defines a doubling-plunging, south-vergent anti-cline composed of Proterozoic and Archean basement rocks in the core of the range and dipping Cretaceous to Miocene(?) age sedimentary

rocks on the limbs (Clark and Bilham, 2008). The orientation of these sedimentary rocks generally follows the overall topographic trend of the anticline, except in the south where normal displacements occur locally within the Cenozoic strata (Srinivasan, 2005). Clark and Bilham (2008) interpret the anticlinal folding of sedimentary strata and exposure of the basement core to be the result of a blind or emergent reverse fault system at depth.

The Shillong plateau is also considered to be a basement pop-up structure, uplifted along steep and seismically active reverse faults: the E-W trending Dauki fault in the south, and the inferred WNW-ESE trending Oldham Fault in the north (Bilham and England, 2001; Rajendran *et al*., 2004; Biswas and Grasemann, 2005; Kayal *et al*., 2006). However, Clark and Bilham (2008) argued that Oldham fault is not a bounding structure to the Shillong Plateau, as in a pop-up structure. It does not form the northern topographic boundary of the plateau, but rather forms a small topographic step that is largely within the plateau itself and causes only a minor offset in the largely anticlinal geometry of the plateau.

A number of linear fractures on regional scale are present in the Shillong Plateau. These include tectonic features like persistent pervasive foliation trend, litho-contacts, cleavage and major joints, faults and fractures. The earliest structural trend in the Shillong Plateau seems to have been E-W. Subsequently the trend seems to have been transposed to NE-SW, probably accentuated by the intrusion of porphyritic granite plutons. The disposition of the present day Shillong Plateau is mainly along the E-W trend (Murthy *et al*., 1967). However, some N-S and NW-SE faults and fractures are also reported from the plateau, which have affected the major E-W trending Dauki fault system and are still active.

Plate – 1

A. An outcrop of granite gneisses on top of the hill, north-east of Sonapahar. **B.** Ductlile deformation within granite gneisses evidence from the kinking of aplite veins (Locality: Sonapahar)**.**

Plate- 2

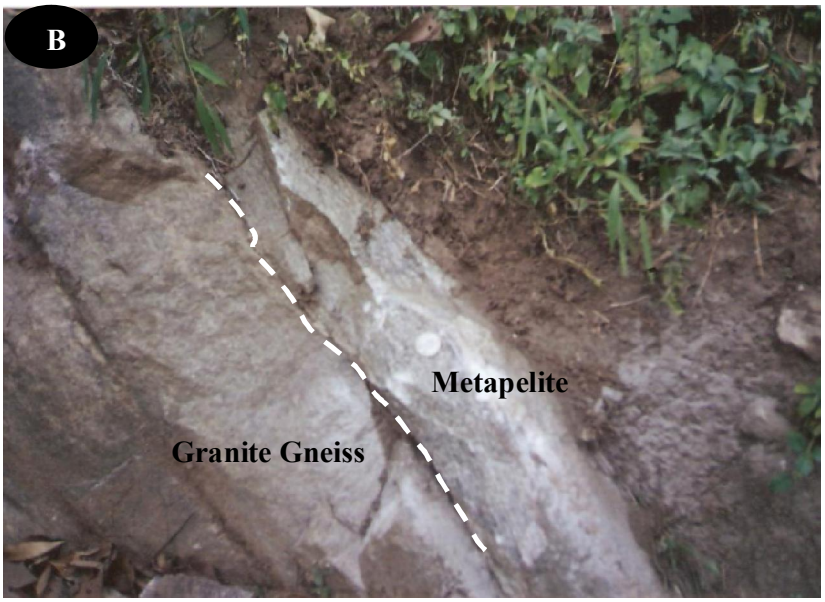

A. An outcrop of cordierite bearing granulitic gneisses (metapelites) along the road side, south west of Sonapahar. **B.** A sharp contact between granite gneisses and cordierite granulitic gneisses exposed along Tura road, north-west of Sonapahar Town.

Plate- 3

Selected sample photograph from the study area. **A - D**: Granite gneisses; **E - H**: Cordierite bearing granulitic gneises.

Plate- 4

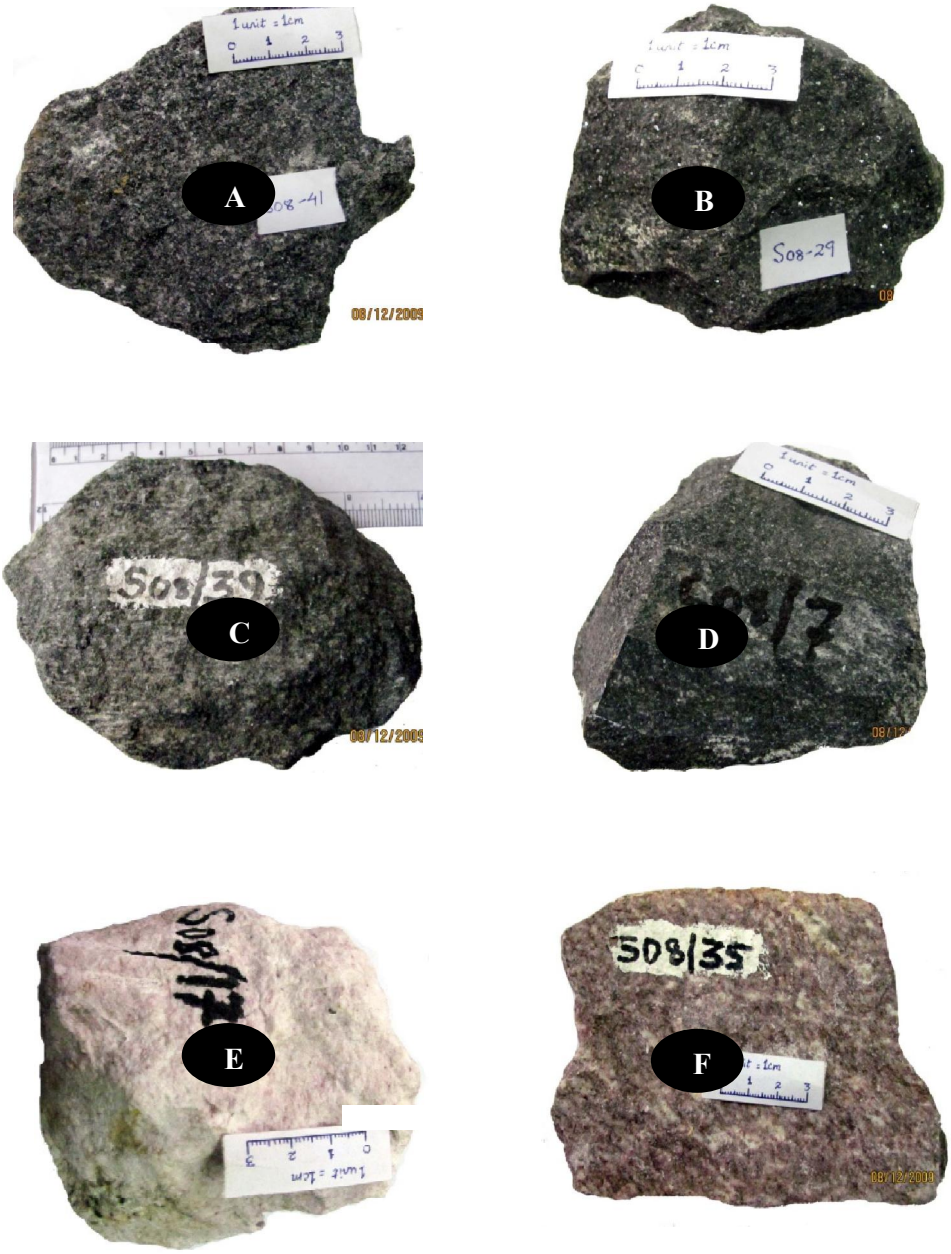

Selected sample photograph from the study area. **A - D**: Basic Granulites; Cordierite bearing granulitic gneises; **E** and **F**: Quartz Sillimanite Schists.

Chapter- 3

PETROGRAPHY

PETROGRAPHY

3.1 INTRODUCTION

In this section, a detailed petrographic account of different rock types of the basement rocks encountered in the study area has been presented. The petrographic description of each lithotype consists of two parts, viz. megascopic characters of rocks in hand specimen and microscopic characters describing textures, structure and optical properties of the constituent minerals.

Petrographically, the basement rocks of the study area are divided into four main types, they are:

i) Cordierite bearing granulitic gneisses (referred to as *metapelites* in this work)
ii) Granite gneiss
iii) Basic granulites
iv) Quartz – sillimanite schists

The rocks of the investigated areas display excellent textural evidences of metamorphic reactions involved in the formation of diverse mineral assemblages documented by different types of reaction coronas and symplectites intergrowth. The megascopic and microscopic characters of the rocks are described below:

3.2 GRANITE GNEISSES

3.2.1 MEGASCOPIC CHARACTERS

These rocks are medium to coarse grained, mesocratic and exhibit typical gneissose structure. The gneissose structures with perfect alternate bands of mica and quartzo-fedspathic minerals are preserved in the granite gneisses (Plate 3). The mafic layer is consists mainly of biotite and the felsic layer is dominated by K-felspar, plagioclase and quartz. The foliations were defined by parallel orientation of biotite flakes. In some samples, hornblendes are common and can be identified in hand specimen.

3.2.2 MICROSCOPIC CHARACTERS

Granite gneisses of the study area are mainly characterized by a medium to coarse grained mosaic of inequigranular, polyonal grains of mesoperthitic K-feldspar, biotite, plagioclase and quartz which show interlocking boundaries. In addition to perthite, myrmekite and graphic intergrowth textures are also developed. The fabric is

typically gneissose. But in some slides, foliation is weakly developed and hardly recognizable.

The dominant fabric (S_2) is well defined by parallel orientation of biotite flakes alternating with granular mosaic of feldspar and quartz. They show porphyroblastic texture with the development of K-feldspar and plagioclase phenocrysts set in a groundmass of quartz and biotite. In general, the granite-gneisses consist mainly of K-feldspar, biotite, quartz and plagioclase with hornblende in subordinate amount. Magnetite and sphene are occurring as accessory minerals. Three prominent mineral associations are identified. These are: a) Quartz – K-feldspar – Plagioclase – Biotite, b) Quartz – Plagioclase – Biotite – K- feldspar – Garnet and c) Quartz – K-feldspar – Plagioclase – Biotite – Hornblende.

3.2.2.1 Biotite

Biotite occurs as flakes, fine to medium grained subhedral crystal. It is the most dominant mineral next to feldspar in these types of rock. Biotites are usually interstitial and commonly intergrowned with quartz and felspar. They are arranging parallel to the foliation (Plate 5A). Biotites occurred in two distinct forms. One as light to deep brown felted mass (Fe-rich biotite) without well defined crystals outline and the other as distinct greenish to brownish sub-idioblastic grains with marginal alteration to chlorite and sericite (Plate 5B).

3.2.2.2 Felspar

Both microcline and orthoclase are present in considerable proportion, but orthoclase is less common. Generally, the crystals are sub-idioblastic but few are idioblastic and xenoblast. Myrmekite and perthitic textures are commonly developed. Occasionally, K-felspar show integrowths with sericitized plagioclase forming a reaction zone at the border area of K-felspars, resulting in the formation of myrmekites (Plate 5C). These crystals with biotite defined the foliation while with plagioclase and quartz show the granoblastic mosaic. It contains fine lamellae of plagioclase in perthite intergrowth. Inclusion of some opaque minerals, biotite, quartz and apatite are present.

3.2.2.3 Plagioclase

Plagioclase occured as medium to coarse grained subhedral crystal. Plagioclase commonly occurred as tabular, usually fractured, elongated and prismatic,

occasionally surrounded by mosaic of quartz crystals. At places it contains inclusion of quartz and biotite. In most of the samples, sericitized plagioclase is developed and these sericitized plagioclase grains contain inclusion of quartz and iron oxides (Plate 5C). Because of seritization, plagioclase crystals show clouded nature. Myrmekitic intergrowth with quartz are commonly noticed (Plate 6A). Plagioclase showing tabular habit is perhaps the earliest mineral to crystallize, whereas anhedral K-feldspar phenocrysts, which contain abundant inclusions of other phases, occurred later. Albite twinning is commonly seen and some twinnings are deformed. Anorthite content in plagioclase is ($An_{35-39.85}$).

3.2.2.4 Quartz

Quartz garins are highly variable and irregular in shape. It is usually anhedral to sub hedral. Quartz is generally interstitial in most of the samples, but also commonly occurs as rounded inclusions in plagioclase, K-feldspar and biotite, thus indicating an early crystallization. Strained quartz is commonly observed (Plate 5B). The occurrence of quartz in the form of interstitial and inclusion indicate the occurrences of different generations of quartz. Occurrence of ribbon quartz with undulating extinction, bending in biotite, bending and cracks in plagioclase which are invaded by plastically mobilized quartz, etc. are some of the features indicative of ductile shearing of the rocks.

3.2.2.5 Garnet

Garnets occur as medium grained xenoblastic crystal. The grains are devoid of rational faces. At places, garnet grains are consuming biotite marking the transition from uppermost amphibolite to lower granulite facies (Plate 6B). They are not very common and constitute additional phases in granite gneisses. It is generally inclusion free but occasionally rimmed by plagioclase (Plate 6B). At places, garnets are highly fractured and are partially wrapped by flakes of biotite.

3.2.2.6 Hornblende

Hornblendes are commonly occuring as medium grained xenoblastic crystals. Two sets of cleavage are frequently seen, but one set is more common (Plate 6C). They are strongly pleochroic and the pleochroic scheme of hornblende is X = light green; Y = green and Z = dark green.

Plate – 5

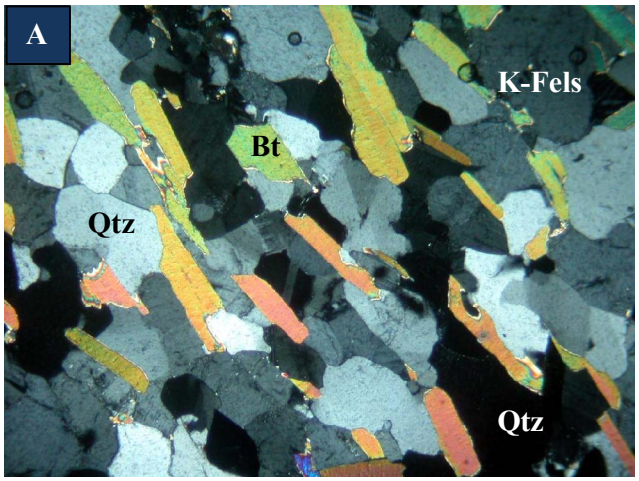

5-A: Flakes of biotite (Bt) defining schistosity in granite gneisses in a ground mass of K-felspar and quartz (Qtz) (Under crossed nicols).

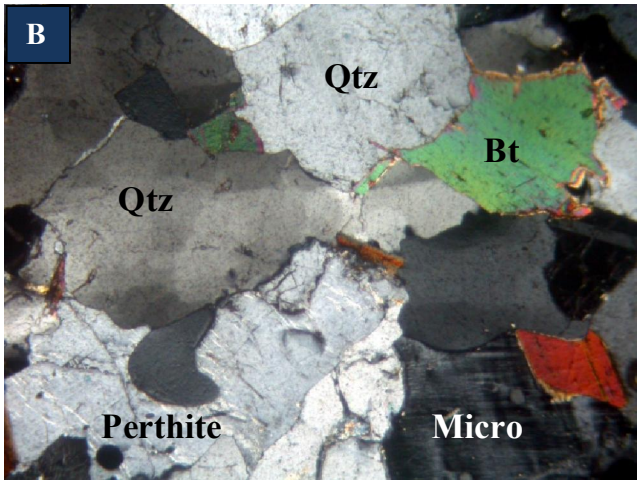

5-B: Mineral associations of strained quartz (Qtz), corroded biotite (Bt) and perthite in granite gneisses (Under crossed nicols).

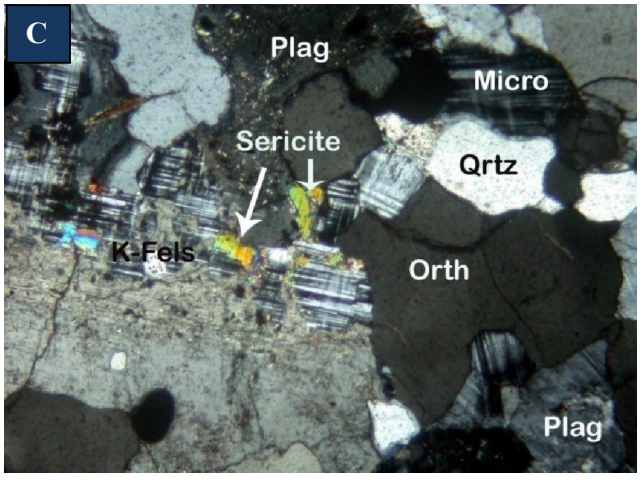

5-C: Microcline and albite inter-growth.The microcl-ine has tar-tan twinning, while the albite is the globular gray areas. This was probably a solid solution that cooled; the two minerals separated and formed a perthitic interg-rowth (Under crossed nicols).

Plate - 6

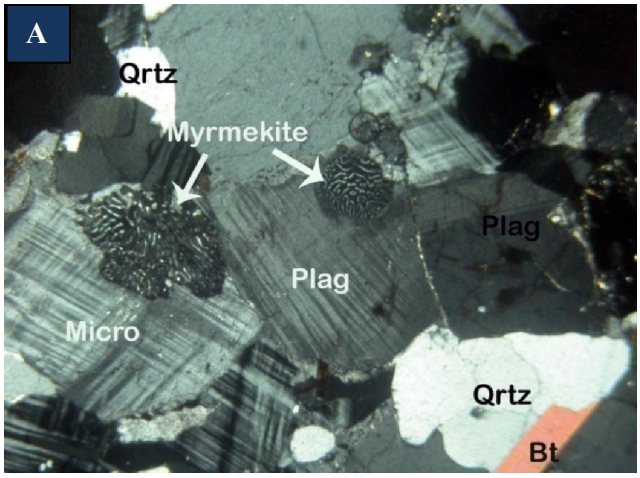

6-A: Irregular, wormy penetra-tion by quartz in plagioclase feldspar (myr-mekite) which occur after the rock crystallizes by replacement of the plagio-clase during hydro-thermal alteration (Under crossed nicols).

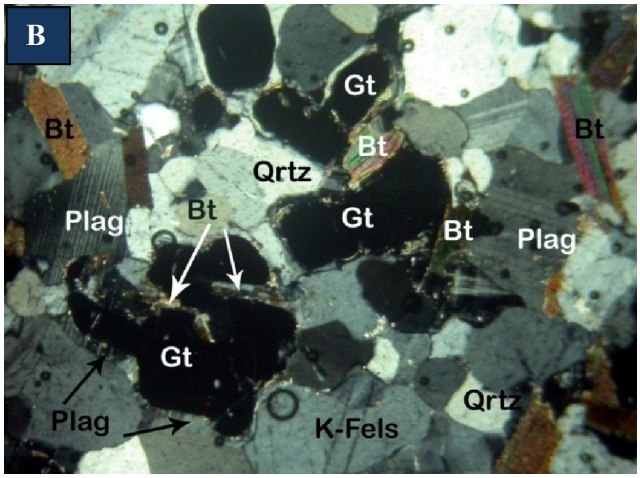

6-B: Inclusion-free garnet (Gt) consumes biotite (Bt) in granite gneisses, marking the transition from upper-most amphibolite to lower granulite facies (Under crossed nicols).

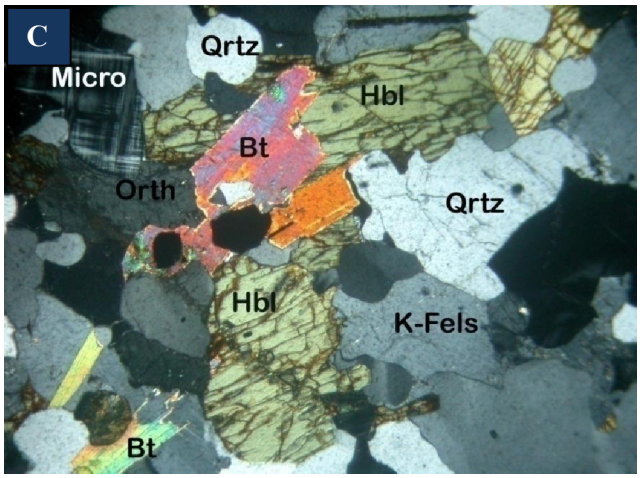

6-C: Biotite (Bt) partially rimmed by hornblende (Hbl) within a mosaic of K-felspar and quartz (Qtz) (Under crossed nicols).

3.1 CORDIERITE BEARING GRANULITIC GNEISSSES

3.1.1 MEGASCOPIC CHARACTERS

They are medium to fine grained with gneissose structure having garnet as one of their constituent minerals. Few samples are massive and showing no trace of foliation. At places, porphyroblast cordierite is clearly visible in hand specimen. The rocks are melanocratic. The dark color is mainly imparted by the presence of biotite. The foliation is well defined by parallel orientation of biotite flakes. Other identified minerals are cordierite, sillimanite and quartz (Plate 3).

3.1.2 MICROSCOPIC CHARACTERS

Metapelites of the study area are mainly characterized a medium to fine grained mosaic of equant, polyonal, strain free grains of mesoperthitic K-felspar (Kf), quartz (Qtz), biotite (Bt), cordierite (Crd), sillimanite (Sill), plagioclase (Plag) and garnet (Gt). The dominant fabric (S_2) is defined by quartz ribbons and preferred alignment of biotite and to a lesser extent sillimanite. Four mineral associations are distinguished, which include: a) Garnet – Cordierite – Biotite – Sillimanite – Quartz – K-feldspar ± Plagioclase, b) Cordierite – Biotite - Sillimanite – K-feldspar – Quartz ± Plagioclase (± spinel), c) Cordierite – Biotite – Sillimanite – Quartz and d) Garnet – Cordierite – Biotite – Sillimanite - Quartz (± spinel).

3.1.2.1: Garnet

Garnet occurs as coarse xenoblasts and is poikiloblastic containing biotite. The grains are devoid of rational faces. At places, garnet grains appear to be replaced by the intergrowth of biotite and plagioclase. They are not very common in some samples and constitute additional phases in metapelites. Inclusions of sillimanite, biotite and k-felspar in garnet are common. However, cordierite is not seen included in garnet. The external schistosity (S_2) does not demonstrably wrap around, but neither does the schistosity passed through the garnet grains. It is likely that garnet formed prior to the S_2 schistosity. A spectacular example of synkinematic prophyroblast growth is provided by the so-called snowball garnets, which have spiral trails of biotite inclusions (Plate 7A) that indicate rotation of either the garnet or the matrix foliation during garnet growth. Some of the garnet grains neighbouring S_2 sillimanite are thinly mantled by cordierite grains. At places, fibrous sillimanite occur

at garnet grain boundaries replacing garnet at grain edges within cordierite crystal (Plate 7B).

3.1.2.2 Cordierite

Cordierite occurs as coarse xenoblasts crystal or in coarse granular aggregates which overprints the fabric of the matrix. Some cordierite grains show characteristic pleochroic halos (Plate 7C). At some places, cordierite rims the xenoblasts of garnet and needles of sillimanite. Polysynthetic lamellar twinning is commonly observed in some larger grains of cordierite. Garnet inclusions within cordierite are frequently observed (Plate 8A). Inclusion of quartz with rounded shapes and of biotite in a large grain of cordierite is common. The inclusions show evidence of adjustment of their boundaries towards low energy configurations.

In some cases, aggregates of S_2 biotite grains weakly wrapped around the cordierite grains, but cordierite hosted inclusion trails (S_1) biotite-sillimanite defined foliation (Plate 8B). These textural relations suggest biotite + sillimanite recrystallization broadly syn-tectonic with respect to the S_2 fabric. Occasionally, the cordierite grains contain inclusions of quartz and spinel (Plate 8C). This textural relation may be explained by the cordierite forming reactions:

Spinel + quartz = cordierite …….. (1)

Spinel + magnetite + sillimanite + quartz = cordierite + O_2 …….. (2)

Cordierite grains never occur as inclusion within garnet. At places, cordierite is wrapped by needles of sillimanite and flakes of biotite. Inclusion of sillimanite, biotite, quartz and magnetite are commonly seen within cordierite.

3.1.2.3 Sillimanite

Sillimanite occurs as coarse prismatic crystals and sometimes fibrous, usually colorless. Both textural type of sillimanite define the S_2 fabric. In places, fibrolite occur at garnet grain boundaries replacing garnet at grain edges (Plate 7B). In few samples, needle sillimanite are enveloped by growth of cordierite grains. It also occurs as inclusion but still defining S_2 fabric (Plate 8B). It is completely and sometimes partially flank by biotite and garnet at places. It also occurs as inclusion within biotite, cordierite and garnet. It has commonly intergrown with biotite and at places with garnet and cordierite. The common occurrences of garnet rimmed by

sillimanite and quartz within coarse grains of cordierite strongly suggest the following reaction:

Garnet + Sillimanite + Quartz = Cordierite …….. (3)

3.1.2.4 Biotite

Biotite commonly occurs as small flakes. It is the most dominant minerals next to cordierite and quartz. Biotite are oriented parallel to foliation and the alignment defined the dominant fabric S_2. Two generations of biotite were identified, primary biotites that exist before garnet mostly occurs as inclusion in the latter. Secondary biotite defines S_2 fabric. At places, biotites are almost totally consumed by garnet (Plate 7B) suggesting the following retrograde reaction:

Garnet + K-Felspar = Biotite + quartz …… (4)

Inclusion of quartz, feldspar and sillimanite are commonly seen. Biotites are pleochroic from pale yellow (X) to dark brown (Y). The absorbtion scheme is X < Y = Z. In some slides, biotite is commonly rimmed by quartz, sillimanite and cordierite. These textural relations suggest the following reaction:

Biotite + Sillimanite + Quartz = Cordierite + K-Feldspar …….. (5)

3.1.2.5 K-feldspar

Both microcline and orthoclase are present, but orthoclases are less common and mostly occur as medium grained. Generally, the crystals are sub-idioblastic but few are idioblastic and xenoblasts. These crystals with biotite defined the foliation while with plagioclase and quartz show the granoblastic mosaic (Plate 8A). It contains fine lamellae of plagioclase in perthite intergrowth. Inclusions of some opaque minerals, biotite, quartz, and apatite are present. K-Felspars also show undulose extinction suggesting post crystalline deformation.

3.1.2.6 Plagioclase

Plagioclase is less dominant in comparison to K-felspar. They are medium to fine grained, sub-idioblastic to idioblastic. The anorthite content in Plagioclase is An_{20-31}. Plagioclase is sericitised and it shows polysynthetic twinning at places. Myrmekitic intergrowth with quartz is noticed in some samples. Plagioclases are commonly occurring as tabular, elongated and prismatic usually surrounded by mosaic of quartz crystals.

3.1.2.7 Quartz

Quartz occurs as equant and inequant grains arrange in the direction of the foliation. In some slides, quartz occurs as polycrystalline aggregates. It shows wavy extinction suggesting post crystalline deformation. Quartz occurs as inclusion within garnet, cordierite etc. (Plates 7A and 8A). Quartz symplectite is seen in some slides. At some places, it occurs as coarse xenoblasts which documents evidence of crystallization of quartz after all the deformation ceased.

3.1.2.8 Spinel

Spinels are commonly xenoblastic to idioblastic with small grain size. They typically occur as inclusions within cordierite grains (Plate 8C), and often in association with inclusion trails of biotite and sillimanite. Spinel grains are mostly co-exists with cordierite.

Plate- 7

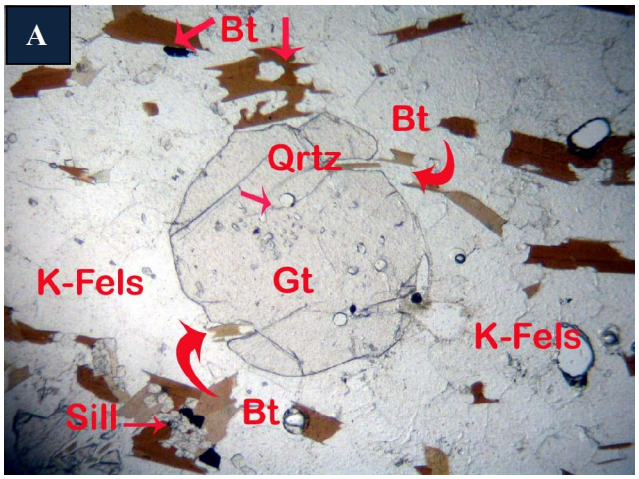

7-A: Garnet (Gt) porphyroblasts with inclusions of biotite (Bt) suggesting the syn-kynematic crystallization (under plane polarized light).

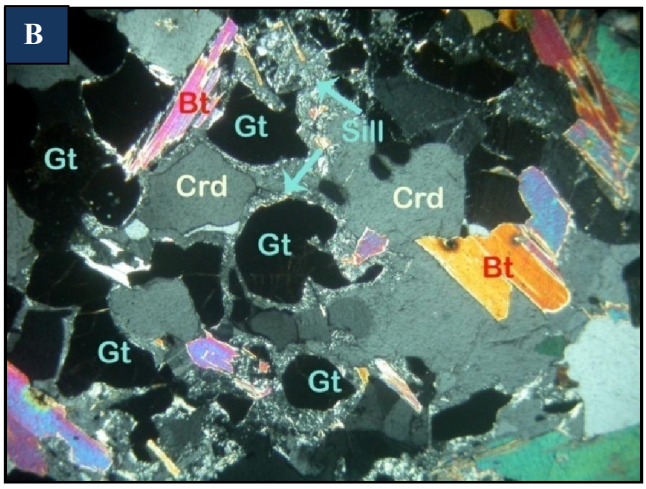

7-B: Fibrous sillimanite (Sill) occur at garnet grain boundaries replacing garnet (Gt) at grain edges within cordierite (Crd) (under cross nicols).

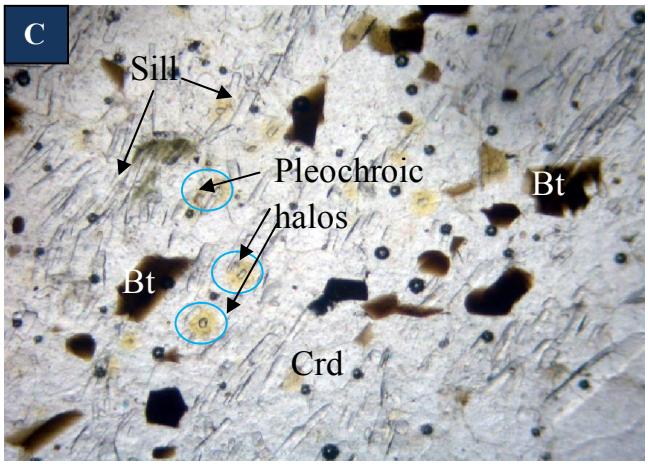

7-C: Cordierite (Crd) porphyro-blast showing pleochroic halos (under plane polarized light)

Plate - 8

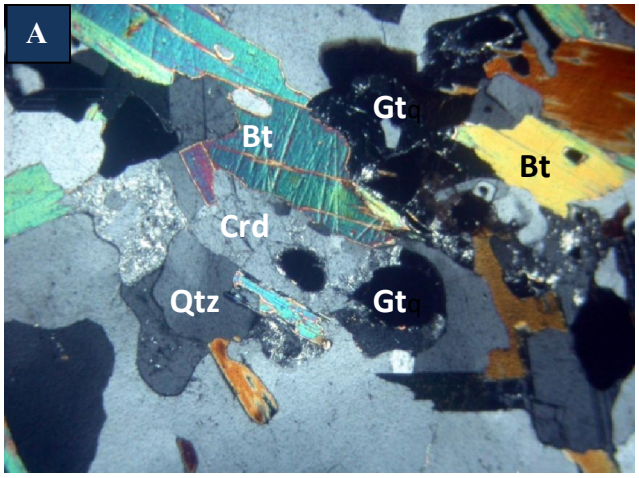

8-A: Inclusion of garnet (Gt) within cordierite (Crd). Cordierite is partia-lly rimmed by bio-tite (Bt). (Under crossed nicols).

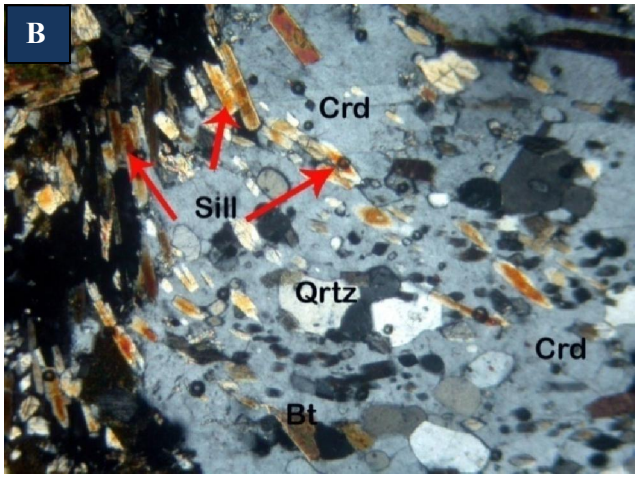

8-B: Porphyroblast cordie-rite (Crd) crystal with numerous inclusions of needle sillimanite, quartz and biotite (Bt) (under cross nicols). Note that sillimanite inclusions de-fine S_1 schistosity.

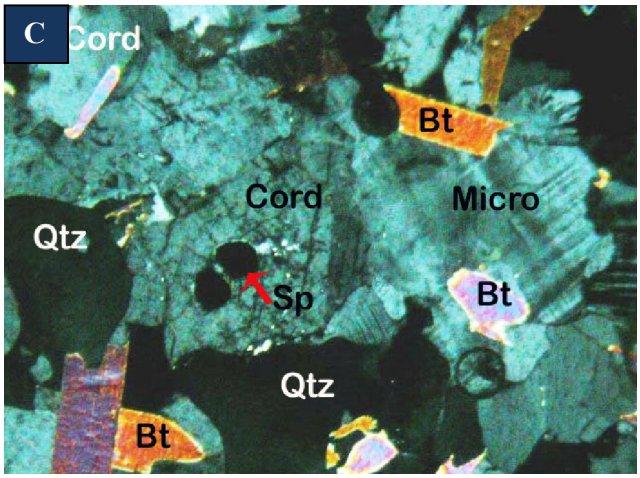

8-C: Inclusions of quartz and spinel (Sp) in cordierite (Crd) grains partially rim-ed by biotite (Bt) (Under crossed nicols).

3.3 BASIC GRANULITES

3.3.1 **Megascopic characters**

The basic granulites are medium to coarse grained rocks with granulitic textures. They are mainly massive but sometimes foliation is seen due to orientation of hornblende and biotite in hand specimens. The basic granulites show dark to greenish black in colour (Plate 4). Basic granulites are characterized by foliation (S_2) defined by the parallel alignment of the prism of hornblende and flakes of biotite rarely diopside and hypersthene. In majority of the samples, basic granulites display medium to coarse compositional banding with alternate layer of hornblende–biotite showing preferred orientation defining the prominent foliation S_2 and fabric containing predominantly of the pyroxenes and plagioclase.

3.3.2 **Microscopic characters**

Basic granulites of the study area are characterized by granulose texture and grain sizes vary from medium to coarse. They commonly exhibit subidioblastic to xenoblastic crystals. The basic granulites of the study area mainly consist of orthopyroxene, clinopyroxene, hornblende, biotite and plagioclase as major constituents. Two prominent mineral associations are identified, which are: a) Hornblende - Clinopyroxene - Orthopyroxene - Plagioclase - Biotite – Quartz and b) Hornblende - Orthopyroxene - Plagioclase – Biotite - Quartz.

3.3.2.1 Hornblende

It occurs as medium to coarse xenoblasts to prismatic crystals. They are highly pleochroic, green, yellowish green, bluish-green, dark green and greenish brown. In some samples, the xenoblasts of hornblende are oriented parallel to the foliation S_2 and defining nematoblastic texture. Some samples shows gneissose texture in which the foliation is defined by biotite and hornblende. Inclusion of quartz, orthopyroxene and biotite within hornblende are frequently observed (Plate 9A). They are commonly associated with biotite.

3.3.2.2 Orthopyroxene

Orthopyroxene includes hypersthenes. It occurs as sub-idioblastic to xenoblastic crystals. It is highly pleochroic from pale yellowish to pink. In most of the samples, hypersthene occurs as medium grained aggregates and closely associated

with hornblende and diopsite (Plate 9B). At places, it occurs as coarse porphyroblast crystal containing inclusion of biotite, hornblende, plagioclase and quartz (Plate 9C). The occurrence of hornblende and quartz within hypersthenes (Plate 10A) suggested the following prograde reaction:

Hornblende + Quartz ↔ Orthopyrxene + Clinopyroxene + Plagioclase + H_2O ….. (6)

At places, orthopyroxenes are partially rimmed by hornblende which suggests the reversal reaction (4) (Plate 10B).

3.3.2.3 Clinopyroxene

Clinopyroxene occurs as subidioblastic and is colourless with inclined extinction. It is mainly diopside (Plate 9B) and contains inclusion of hornblende and plagioclase, which also provides evidence of the reaction:

Hornblende + Quartz ↔ Hypersthene + Clinopyroxene + Plagioclase + H_2O…… (7)

3.3.2.4 Plagioclase

Plagioclase occurs as medium to coarse aggregate and anorthite content varies from An_{21} to An_{37}. At times it also occurs as large crystal with numerous inclusions of hypersthene, biotite, magnetite etc. Plagioclase also shows anti perthitic intergrowth in many samples and also shows deformed twin lamellae which give evidence of post crystalline deformation (Plate 10C).

3.3.2.5 Biotite

Biotite occurs as flakes and prismatic crystal and also occured as idioblastic to sub-idioblastic aggregates. Biotite shows pleochroism X= pale greenish yellow; Y=Z=dark brownish green. X<Y<Z. It is commonly associated with hornblende and plagioclase which defines the foliation S_2 (Plate 10A). It also occurs as inclusion within hornblende and plagioclase.

3.3.2.6 Quartz

Quartz occurs as xenoblasts in association with plagioclase and along the intergranular space between the prisms of pyroxenes. It also occurs as inclusion within hornblende and pyroxenes (Plates 9A, B; 10A).

Plate - 9

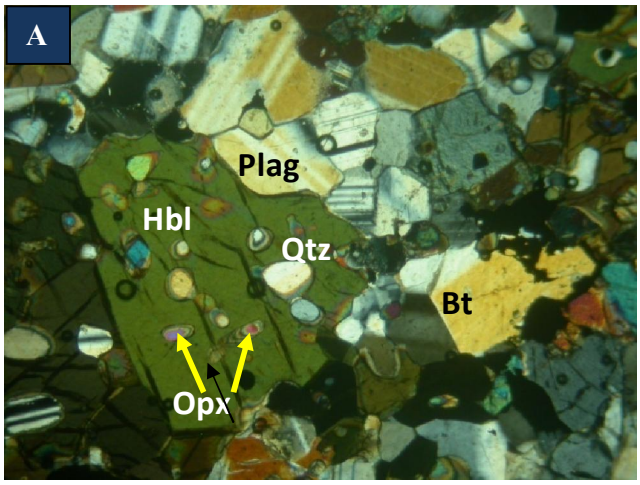

9-A: Inclusion of quartz (Qtz) and armoured relicts of ortho-pyroxenes (Opx) within large grain of hornblende (Hbl) (Under crossed nicols).

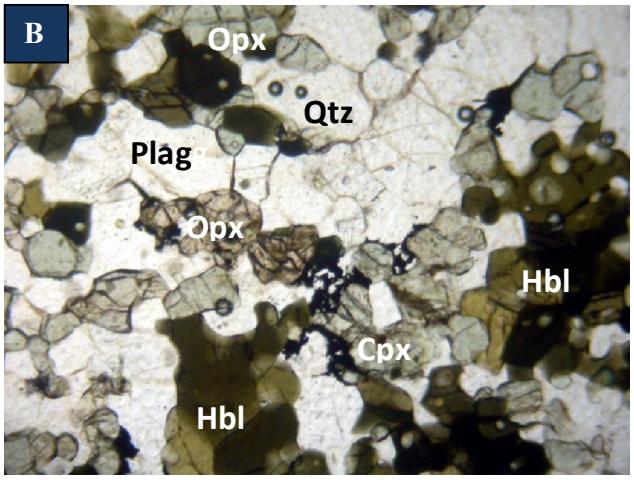

9-B: Aggregates of orthopyroxene (Opx) grains closely associated with hornblende (Hbl), clinopyroxene (Cpx) and quartz (Qtz) (Under plane polarized light).

.

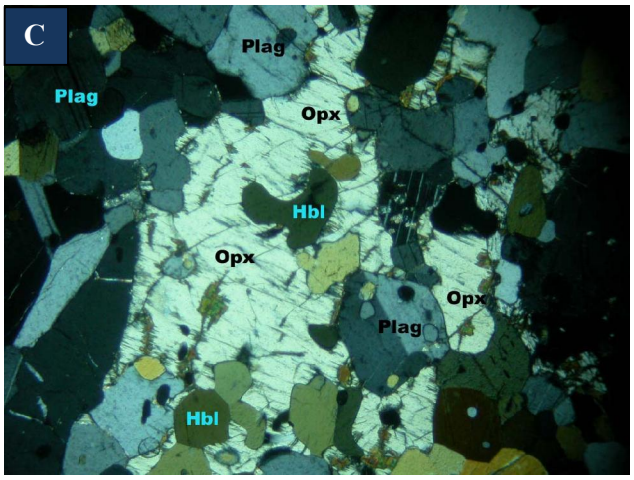

9-C: Porphyroblasts orthopyroxene (Opx) with inclusions of hornblende (Hbl), plagioclase (Plag) and quartz (Qtz) (Under crossed nicols).

Plate - 10

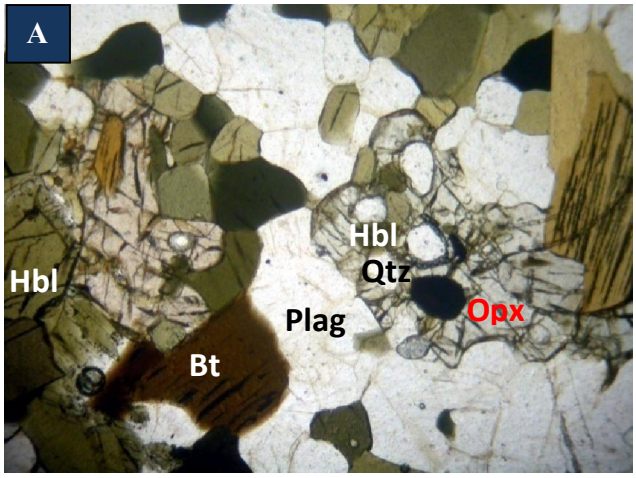

10-A: Inclusion of hornblende (Hbl) and quartz within orthopyroxene (Opx) (Under plane polarized light) suggesting prograde reaction:

Hornblende + Quartz ↔ Ortho-pyrxene + Clino-pyroxene + Plagioclase + H_2O.

.

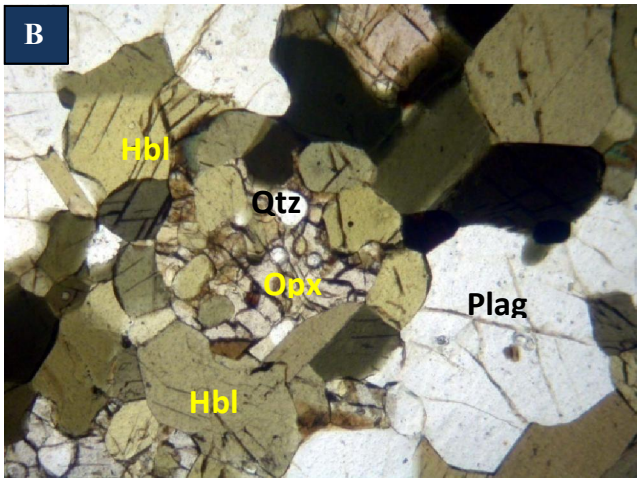

10-B: Orthopyroxene (Opx) grain completely rimmed by hornblende (Hbl) suggesting the reversal of the reaction. (Under plane polarized light)

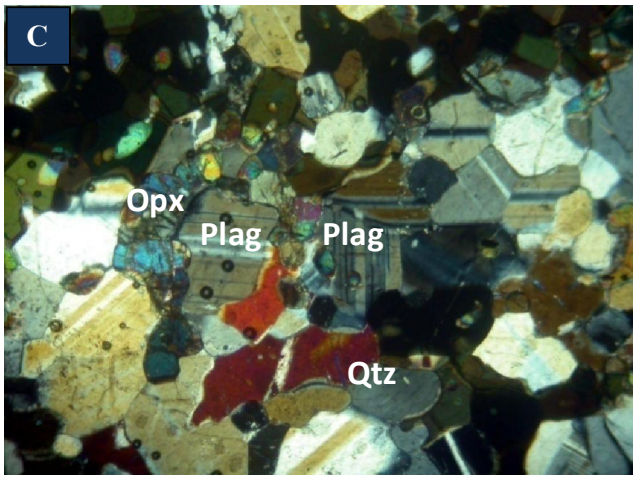

10-C: Deformed polysynthetic twinning of plagioclase (Plag) crystals suggesting post crystal-line deformation (Under crossed nicols).

3.4 QUARTZ – SILLIMANITE SCHISTS

3.4.1 MEGASCOPIC CHARACTERS

These are fine to medium grained, leucoratic rocks (Plate 4). It exhibits a well developed foliation defined by alternate laminae/bands rich in quartz and Sillimanite. Biotites are also commonly observed in these rocks. The schistosity is defined by the preferred orientation of biotite flakes and sillimanite needles. Quartz sillimanite schists are generally composed of quartz, sillimanite with minor amounts of biotite.

3.4.2 **Microscopic characters**

The Quartz Sillimanite Schists are fine to medium–grained, display well defined schistosity and contain quartz, sillimanite, biotite with accessory rutile and zircon. The mineral associations identified are: a) Quartz – Sillimanite – Biotite ± Ru tile ± Zircon and b) Quartz - Sillimanite – Biotite ± K- feldspar.

3.4.2.1 Quartz

Quartz occured as polycrystalline aggregates defining foliation, but some are randomly oriented crystals (Plates 11A, B). In general, quartz grains shows uniform twinning, but some grains exhibit wavy extinction. Two generations of quartz are evident. The first one is coarser grained, usually anhedral and elongated parallel to the fabric. The finer grained variety occurs as localized granoblastic aggregates and show uniform extinction. This variety may likely be of secondary origin.

3.4.2.2 Sillimanite

Sillimanite commonly occurs as radiating needles, acicular and sometimes prismatic crystals (Plate 11A). It is the major constituents of the assemblages. Sillimanites are oriented sub parallel to the principal foliation. In some cases, sillimanites are intergrowth with biotite.

3.4.2.3 Biotite

Biotites are less dominant mineral in quartz sillimanite schists. It occurs as flakes, which are sometimes feebly deformed. It shows high order interference colour (Plate 11B). It is pleochroic from pale yellowish to brownish yellow**.** Flakes of biotite along with sillimanite are oriented parallel to schistosity. Biotites are most commonly associated with flattened grains of quartz.

Plate - 11

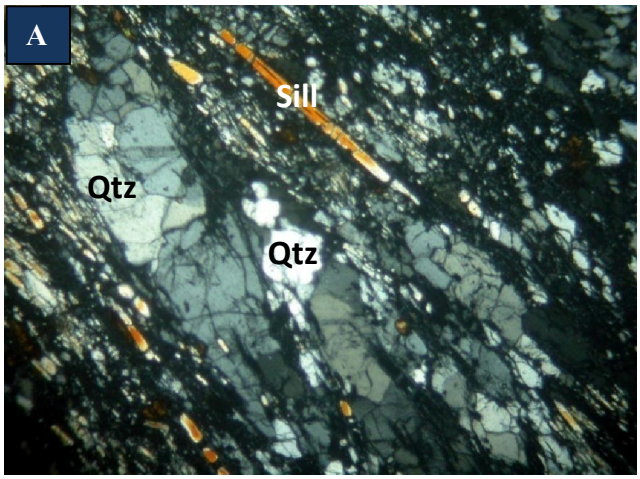

11-A: Polycrystalline quartz (Qtz) and needle sillimanite (Sill) defining foliation in quartz sillimanite schists. (Under crossed nicols)

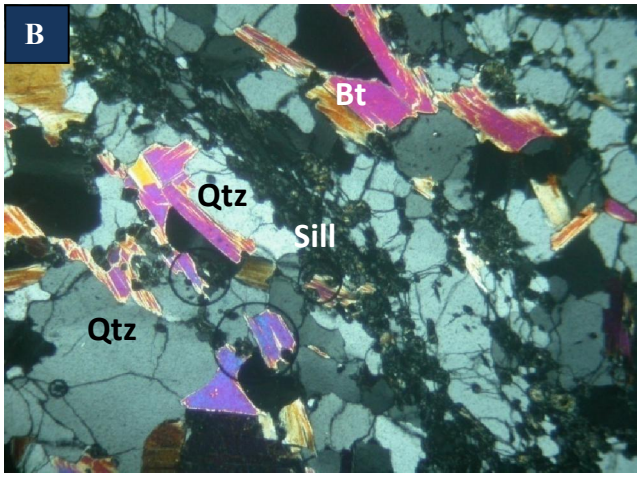

11-B: Mineral association of sillimanite (Sill), quartz (Qtz) and biotite (Bt) in quartz sillimanite schists. (Under crossed nicols).

Chapter- 4

WHOLE ROCK GEOCHEMISTRY

WHOLE ROCK GEOCHEMISTRY

4.1 SAMPLING AND ANALYTICAL TECHNIQUES

Fresh samples of the granite gneisses, metapelites, quartz-sillimanite schists and basic granulites were collected from the outcrops. Utmost care has been taken to collect the samples from the outcrops. Prior to geochemical analysis, the rocks were studied under microscope and the effects of weathering and alterations were observed in thin sections. Samples showing least alteration effects were selected for geochemical analysis.

Altogether, 30 (thirty) representative samples (Ten granite gneisses; Ten metapelites; Six basic granulites and Four quartz-sillimanite schists) were selected for geochemical analysis after careful petrographic studies from the point of view of alterations and weathering and also to represent maximum possible geographic locations within the study area.

The rock samples were reduced to smaller size (~3cm) to observe any traces of mineral veins. The chips were further crushed to yet smaller sizes (~2mm), then washed with distilled water and sundried. These samples were then pulverized using an agate mortar at National Geophysical Research Institute (NGRI), Hyderabad, India. Major elements were analysed by XRF and trace elements including REE were analysed by ICP-MS at National Geophysical Research Institute (NGRI), Hyderabad. The details of the instruments and the procedures followed for both the instruments are presented below.

4.1.1 **X-ray fluorescence (XRF)**

It is a Philips MagiX PRO model PW 2440 wavelength dispersive X-ray fluorescence spectrometer coupled with automatic sample changer PW 2540. The magiX PRO is a sequential instrument with a single goniometer based measuring channel covering the complete elemental measurement range from F to U in the concentration range from few parts per million (ppm) to percentage (%) level. The instrument is microprocessor controlled for a maximum flexibility and consists of end – window X-ray tube with Rh anode and maximum voltage /current of 60kV/125mA at a maximum power level of 4KW.

Software used in computer is able to take care of dead time correction, background and line overlap corrections and matrix effects giving the output directly as the concentration in weight percentage or in ppm after converting the counts into concentration with the help of calibration curves. Concentration based corrections using the model proposed by De Jongh (1973) which allows the use of fundamental influence coefficients (ALPHAS) were applied to convert the count into elemental concentrations.

A Spinner was used to spin the sample inside the spectrometer while measuring the counts to have uniform counts and to remove in homogeneity effect from the pressed sample. A 32mm primary beam aperture mask was used to restrict the x-ray beam to the sample surface only. Flow and scintillation detectors were used to count the x-ray photons. Pulse height discriminator and fine collimator were used for greater sensitivity for most of the trace and minor elements.

Whole rock major element data of the granite gneisses, metapelites, quartz-sillimanite schists and basic granulites area presented in appendix- I, II, III and IV.

4.1.2 Inductively Couple Plasma Mass Spectrometer (ICP-MS)

It is a Perkin Elmer SCIEX, Model ELAN DRC II ICP-Mass Spectrometer (Toronto, Canada). The instrumentation procedures are described at length by Balaram *et al*., (1996). The precision of the data are <5 % RSD. The sample introduction system consisted of a standard Meinhard nebuliser with a cyclonic spray chamber. Instrumental and data acquisition parameters, including the oxide and hydroxide formation levels are presented below.

Instrumental Parameters:	
RF Power	1100 W
Argon gas-flow:	
Nebuliser	0.86 l min^{-1}
Auxiliary	1.20 l min^{-1}
Plasma	15 l min^{-1}
Lens voltage	5 V

Data acquisition parameters	Quantitative mode
Measuring mode	Peak hopping Point
per peak	1
Number of sweeps	50
Dwell time	50 μs
Integration time	2500 ms
Replicates	3
Internal standard	103Rh a
Sample uptake rate	0.80 ml min^{-1}

Oxide and hydroxide formations levels (%)	
CeO^+	2.046
$CeOH^+$	0.065
a At an overall concentration of 20 ng ml^{-1}	

All quantitative measurements were performed using instrument software, which used knowledge- driven routines in combination with numerical calculations to perform an automated interpretation of the whole spectrum. Several well-known isobaric interferences were programmed and corrections applied automatically. An external calibration procedure was adopted for the analysis.

For the dissolution of the samples, an open digestion method has been adopted.

Open acid digestion method: A test portion (0.05 g) of the sample was added to PTFE Teflon beakers. Each sample was moistened with a few drops of ultra- pure water. Then, 10 ml of an acid mixture (containing 7:3:1 HF-HNO_3-$HClO_4$) was added to each sample. Samples were swirled until completely moist. The beakers were then covered with lids and kept overnight for digestion after adding 1 ml of 5 μg ml^{-1} Rh solution (to act as an internal standard). The following day, the beakers were heated on a hot plate at ~ 200^0C for about 1 hour, the lids were removed and the contents were evaporated to incipient dryness until a crystalline paste was obtained. The remaining residues were then dissolved using 10 ml of 1:1 HNO_3 and kept on a hot plate for 10 minutes with gentle heat (70^0C) to dissolve all suspended particles.

Finally, the volume was made up to 250 ml with purified water (18 MΩ) and stored in polyethene bottles.

During analysis, natural standards viz. JG-2, AG-2 and SDC-1 were also analyzed simultaneously to check the precision and accuracy of analytical data. The procedures followed in the preparation of the rock samples for analyses on XRF and ICP-MS are of national and international standards (Chao and Sanzolone, 1992; Roy, *et al*., 2007).

4.2 GEOCHEMICAL CHARACTERISTICS

4.2.1 **Granite gneiss**

4.2.1.1 *Major elements*

Appendix- I represents the major element abundances of the gneisses of the Shillong Plateau. The granite gneisses of the Shillong Plateau are highly siliceous ($64.63 \leq SiO_2 \leq 77.76$ wt %) with SiO_2 content averages 71.41 wt %. The granite gneisses are chemically characterized with Al_2O_3 (11.85 – 16.70 wt %), Fe_2O_3 (0.79 – 6.84 wt %), Na_2O (1.59 – 3.83 wt %) and K_2O (1.16 – 5.37 wt %), MnO (0.01 – 0.08 wt %), MgO (0.08 - 3.31 wt %), TiO_2 (0.19 – 0.81 wt %) and CaO (0.36 – 2.89 wt %). In Harker`s variation diagram, SiO_2 values show a pronounced inverse correlation with Al_2O_3, Fe_2O_3, MgO, MnO, P_2O_5 and TiO_2 (Fig. 4.1.1). No discernible trends were observed with K_2O and CaO. While Na_2O show a positive correlation (Fig. 4.1.1).

The molar saturation index $Al_2O_3/CaO + Na_2O + K_2O$ (A/CNK: Shand, Shand, 1927; Clark, 1981) values for the granite gneisses ranges from 1.03 – 2.10 and thus the gneisses can be group as peraluminous. The alkali content of the gneisses is moderately low ($4.89 \leq Na_2O+K_2O \leq 8.26$ wt %) with an average of 6.45 wt %.

Negative linear trends of Al, Fe, Mn, Mg and Ti oxides versus SiO_2 on the Harker`s variation diagrams indicate fractionation of early formed aluminous and ferromagnesian phases from the precursor magma for the gneisses. Total alkali concentrations are generally variable and range from 4.89 to 8.26 wt %, which are mainly controlled by K_2O abundance.

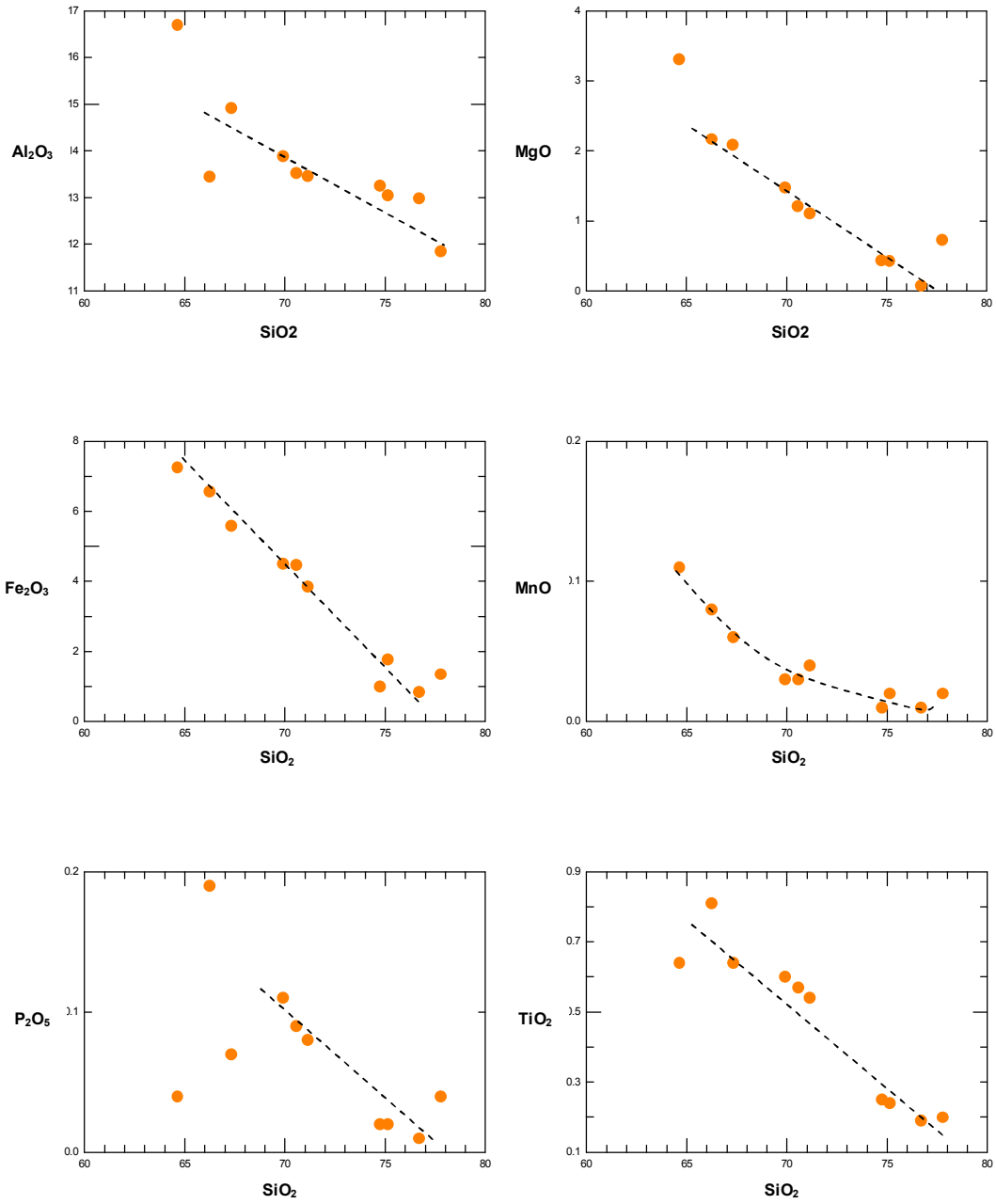

Figure 4.1.1: Harker`s variation diagram for major oxides of granite gneisses of the Sonapahar area, Shillong Plateau

.

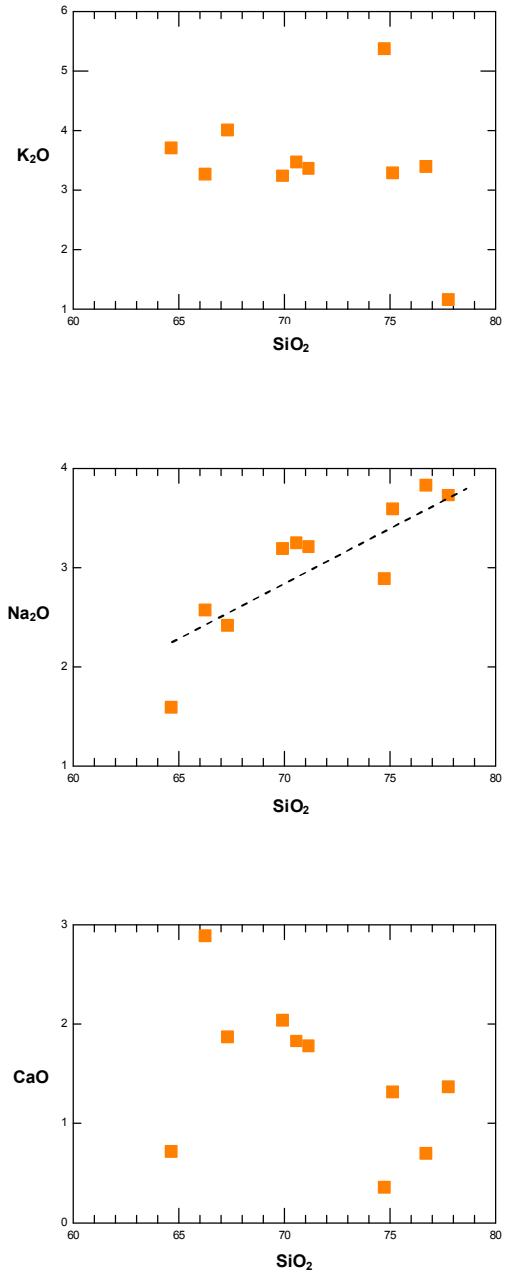

Figure 4.1.1: Harker`s variation diagram for major oxides of granite gneisses of the Sonapahar area, Shillong Plateau.

On the Na_2O/Al_2O_3 versus K_2O/Al_2O_3 diagram of Garrels and McKenzie (1971) discriminating the fields of Igneous and sedimentary/metasedimentary fields for the protoliths, the granite gneiss samples plot dominantly within the igneous field with only two sample granites plotting close to the boundary (Fig. 4.1.2a). On Al_2O_3 versus MgO diagram of Marc (1992) discriminating fields of ortho- and para-gneisses, the granite gneisses of Shillong Plateau plot within the orthogneiss field samples except two samples which fall within the paragneiss field (Fig. 4.1.2b). These two samples are characterized with high MgO concentrations.

The $Al_2O_3/(Na_2O + K_2O)$ versus $Al_2O_3/(CaO + Na_2O + K_2O)$ binary diagram of Shand (1943) deals with discriminating peraluminous, metaluminous and peralkaline magma series. This diagram also reveals that the samples are peraluminous (Fig 4.1.3). However, the samples straddle the field boundary defining I-type and S-type granite.

In the normative Ab-Or-An diagram of Barker (1979), the granite gneisses plot within the fields of granite with only one sample plot within the field of trondjhemite (Fig. 4.1.4). Variation diagram for SiO_2 vs. K_2O (after Peccerillo and Taylor, 1976) indicates that granite gneisses are high-K Calc-alkaline having continental margin affinity (Fig. 4.1.5).

When granite gneisses were plotted on the phase diagram of Von Platen, (1965), most of the samples lie in the field of eutectic melt, except one sample which is away from the granite field (Fig. 4.1.6). This suggests that granite gneisses of the Sonapahar area were the product of melting which is consistent with the field and petrographic observations. On the AFM ($Na_2O + K_2O$ - $Fe_2O_3^t$ - MgO) ternary diagram with the dividing lines of Irvine and Baragar (1971) to discriminate between tholeiitic and calc-alkaline suites, granite gneisses follow a calc-alkaline trend (Fig. 4.1.7).

4.2.2 *Trace elements*

Appendix- I represent the trace element abundance of the granite gneisses of Shillong Plateau.

The Rb and Sr content of the granite gneisses ranges from 53.48 ppm to 230.94 ppm averaging 140.30 ppm and 54.76 ppm to 106.55 ppm averaging 78.67 ppm repectively. The Zr, Nb, Y content of the granite gneisses ranges from 35.44

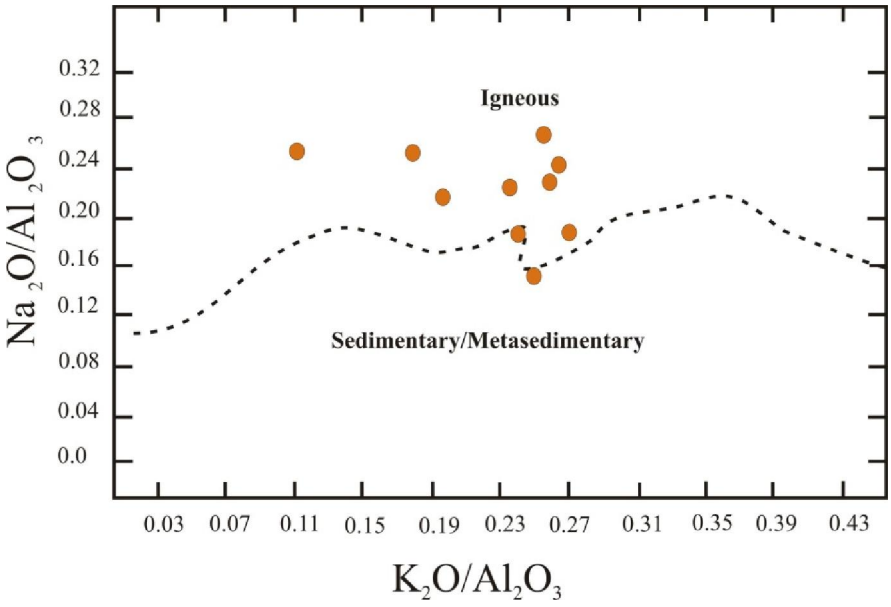

Figure 4.1.2a: Na_2O/Al_2O_3 vs K_2O/Al_2O_3 diagram for granite gneisses of the Sonapahar area, Shillong Plateau (after Garrels and Mc Kenzie, 1971).

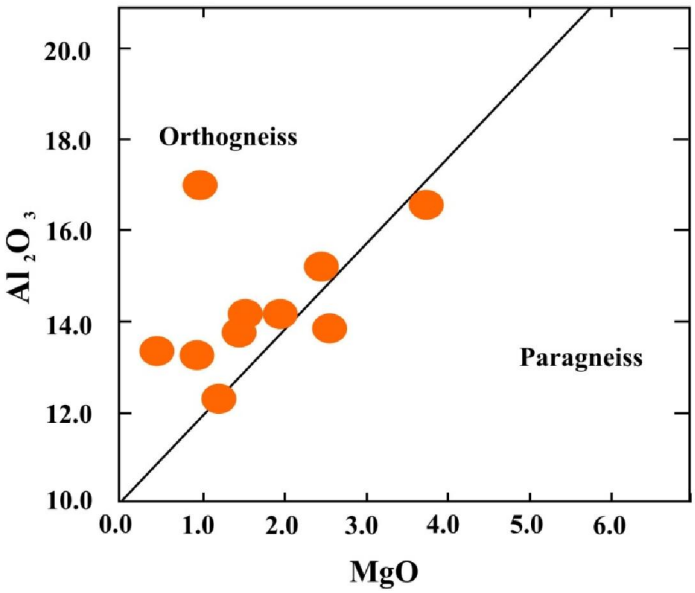

Figure 4.1.2b: Al_2O_3 vs MgO discrimination diagram for granite gneisses of the Sonapahar area, Shillong Plateau (after Marc, 1992).

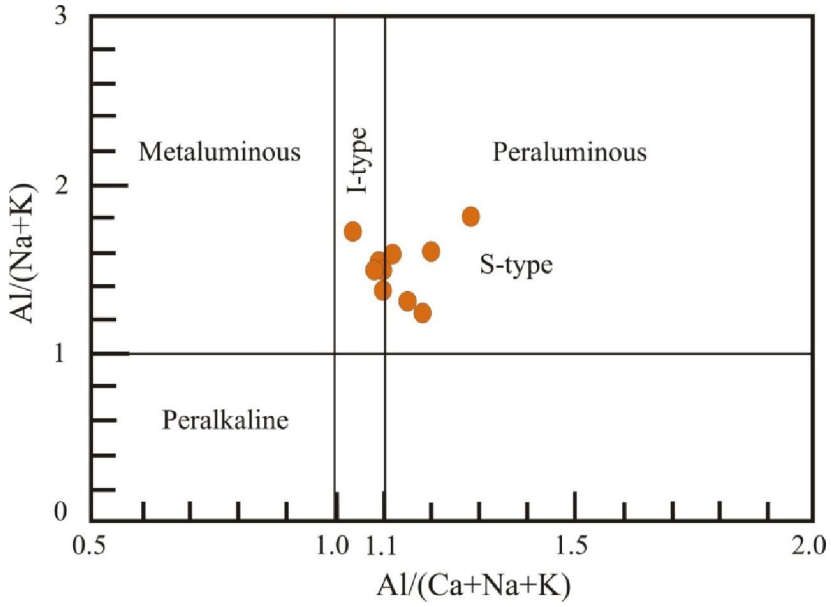

Figure 4.1.3: The A/CNK vs. A/NK diagram for granite gneiss of the Sonapahar area (after Shand, 1943). Boundary line for I-type and S-type granite field taken from Maniar and Piccoli (1989).

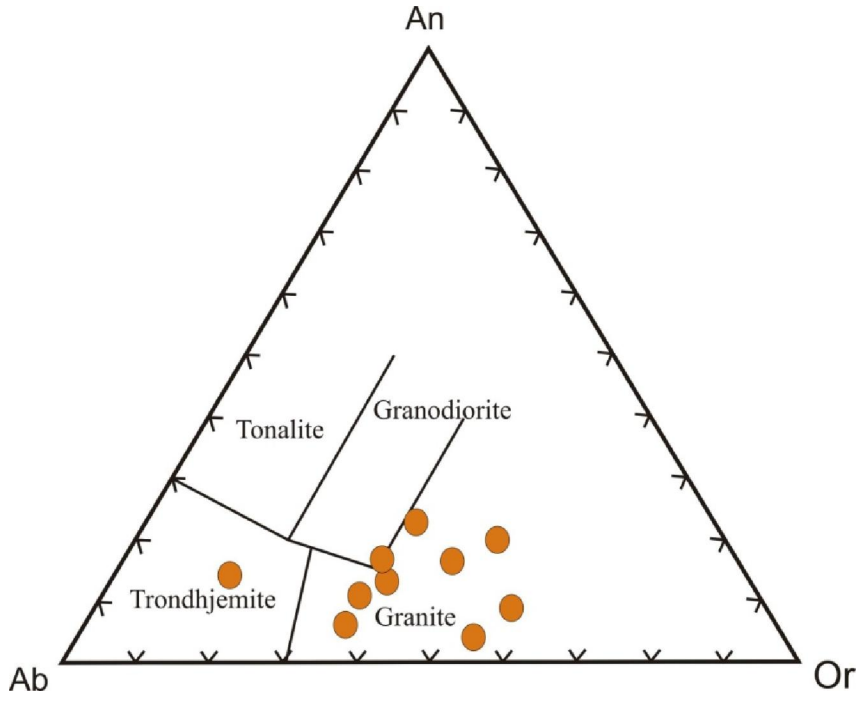

Figure 4.1.4: Rock classification of Sonapahar granite gneiss based on normative feldspar variation (after Barker, 1979).

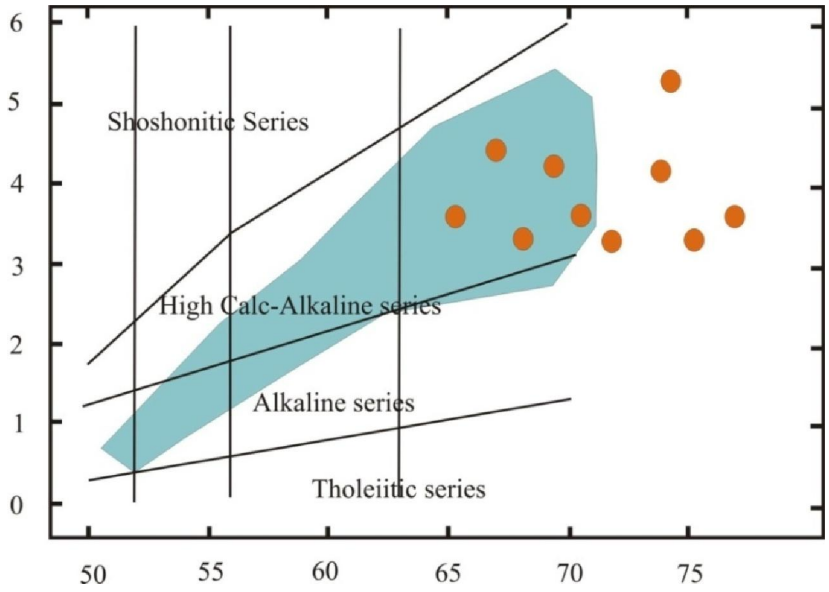

Figure 4.1.5: SiO_2 vs. K_2O variation diagram for Sonapahar granite gneisses (after Peccerillo and Taylor, 1976). The shade field represents continental margin affinity.

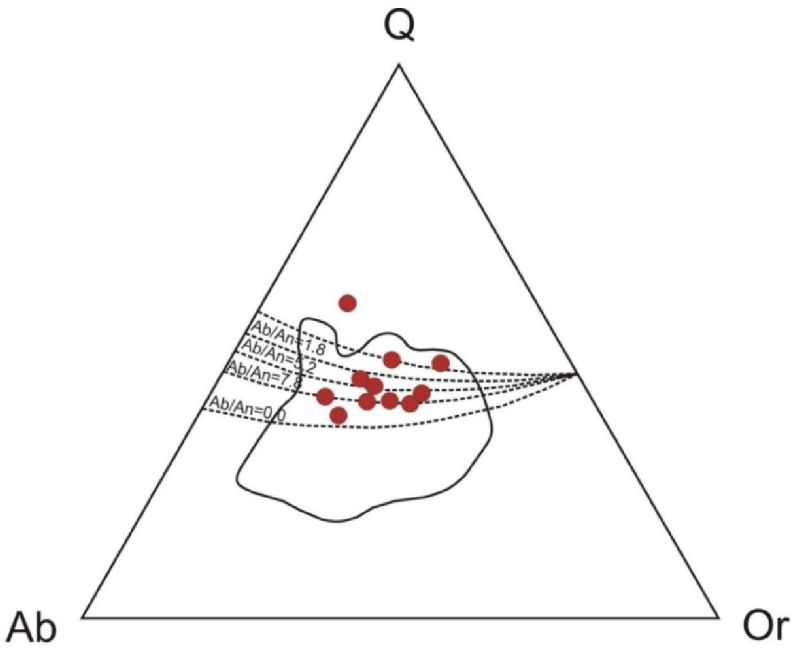

Figure 4.1.6: The plot of cotectic lines with compositions of minimum points, when anorthite (An) is added to albite (Ab)-K-feldspar (Or)- Quartz (Qz) system with addition of variable amount of anorthite, all the gneissic samples plot within the field of granitic composition (after Von Platen, 1965).

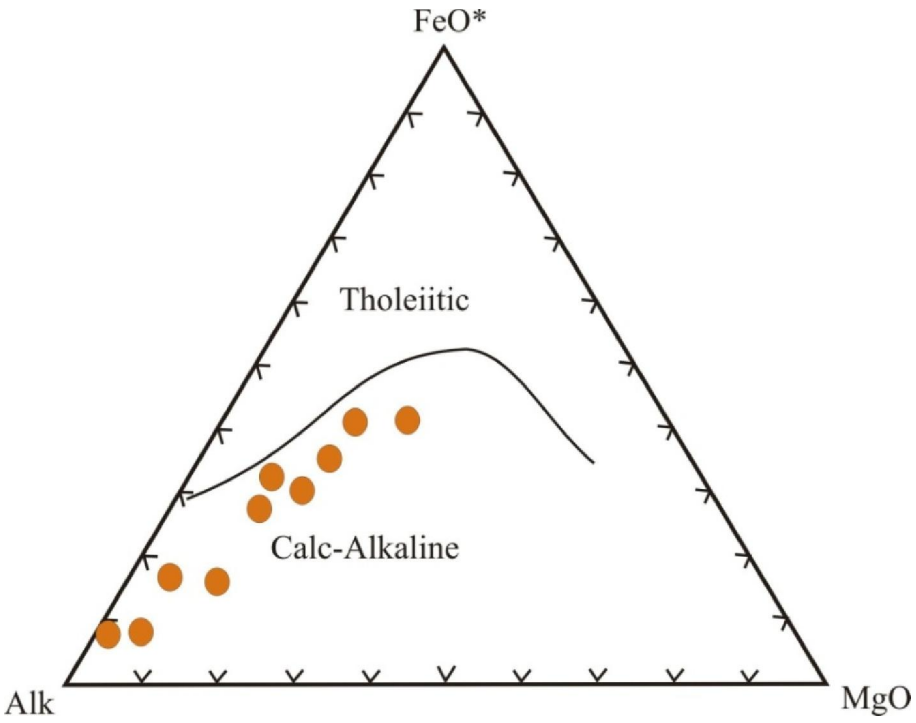

Figure 4.1.7: AFM ($Na_2O+K_2O-Fe_2O_3^t$ -MgO) ternary diagram for Sonapahar granite gneisses with the dividing lines of Irvine and Baragar (1971) to discriminate between tholeiitic and calc-alkaline suites.

ppm to 155.02 ppm averaging 94.63 ppm, 2.58 ppm to 16.85 ppm, averaging 10.82 ppm, 4.88 ppm to 77.11 ppm averaging 29.11 ppm respectively. Th content ranges 12.41 to 60.89 ppm, (averaging 25.67 ppm) and U ranges from 1.09 ppm to 7.31 ppm (averaging 2.94 ppm). The Ba content of gneisses ranges from 182.63 ppm to 989.98 ppm and average 737.75 ppm. The concentrations of Cr (3.29 -7.51 ppm), Co (0.95 – 23.62 ppm) and Ni (0.64 – 3.79 ppm), Sc (1.84 – 9 ppm) in granite gneiss are all of low values.

Among the trace elements, Sc, V show clear negative correlation with SiO_2 and Cr, Co, Ni, Cu, Rb, Nb, Cs, Ba, Ta, Ga shows limited data spread (Fig. 4.1.8). This indicates that all these trace elements probably behaved in a less mobile way during metamorphism. Whereas Zn, Th, U, Y, exhibits broad data scatter indicative of substantial mobility.

The trace elements are plotted in the mantle normalized multielemental spider diagram (Fig. 4.1.9). The elements are arrange in the order of increasing incompatibility from right to left for a normal upper mantle spinel-peridotite mineral assemblage (Sun and Mc.Donough, 1989) with high field strength element (HFSE) on the right and Large Ion Lithofile (LILE) on the left of the diagram (Fig. 4.1.9). The elemental concentration for the gneisses shows overall enrichment with respect to the primitive mantle alongwith the inter-elemental variation (Primitive mantle values are from from Sun and Mc Donough, 1989). The LILEs such as Rb, Ba, Th, U and K of the gneisses exhibit enrichment while HFSEs display strong depletion at Ti, P, Sr, Zr and Nb. The depletion of these elements of the gneisses can account for fractional crystallization of phases like rutile, ilmenite, apatite and plagioclase of its precursor melt or retention of these phases at the site of partial melting during the generation of the precursor melt of these gneisses.The Harkar`s variation diagram for the trace element of the gneisses vs. SiO_2 (Fig. 4.1.8) also corroborates the phenemenon of fractional crystallization of the trace elements for the precursor melts of the gneisses of the Shillong Plateau.

4.3.4 **Rare Earth Elements (REE).**

The total Rare Earth Elements (ΣREE) of the gneisses ranges from 107.23 ppm to 518.34 ppm. Chondrite normalize REE concentrations (normalizing values are from Sun and Mc Donough, 1989) shows variable LREE/HREE ratios

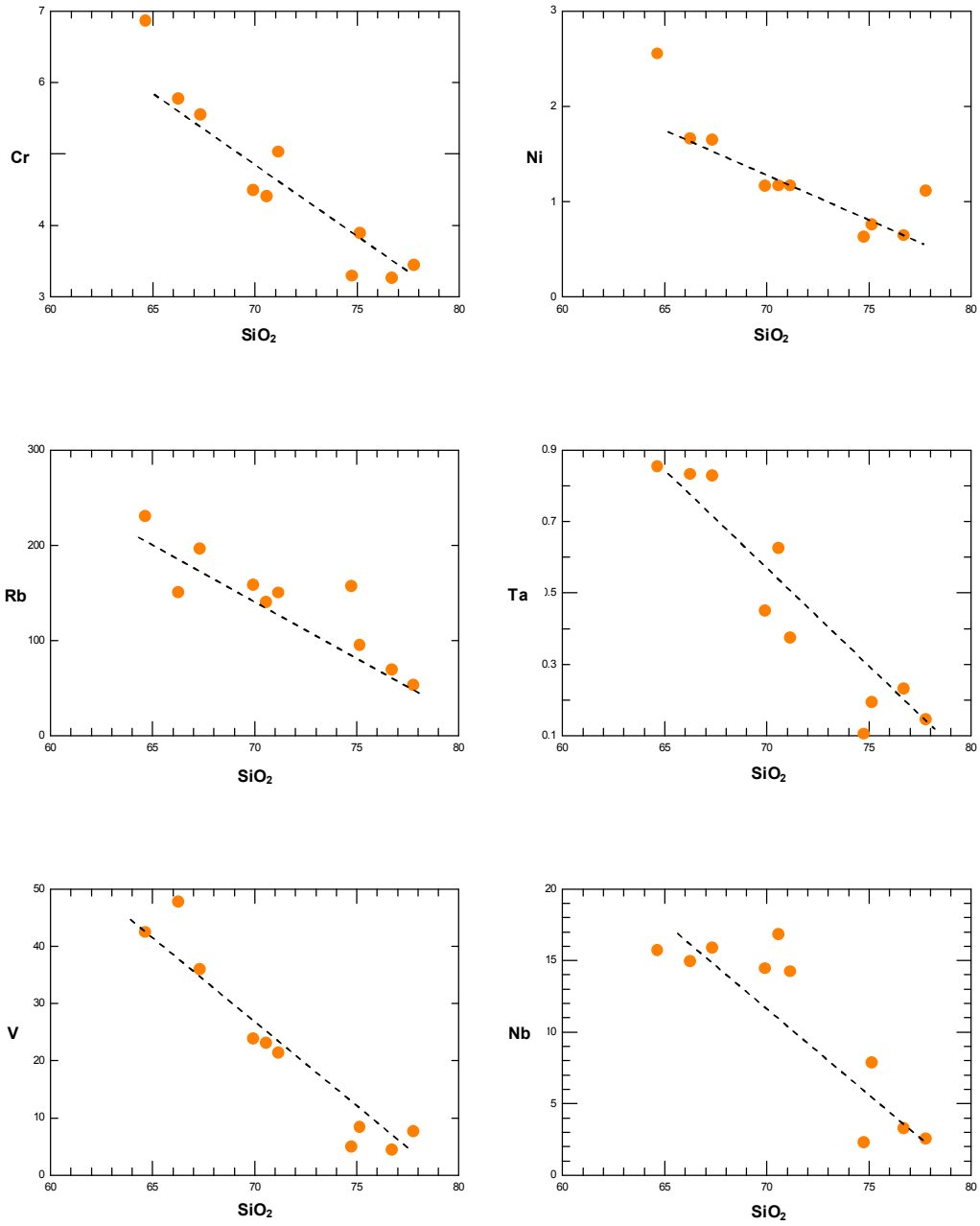

Figure 4.1.8: Harker`s variation diagram for selected trace element vs. SiO_2 of granite gneisses of the Sonapahar area, Shillong Plateau.

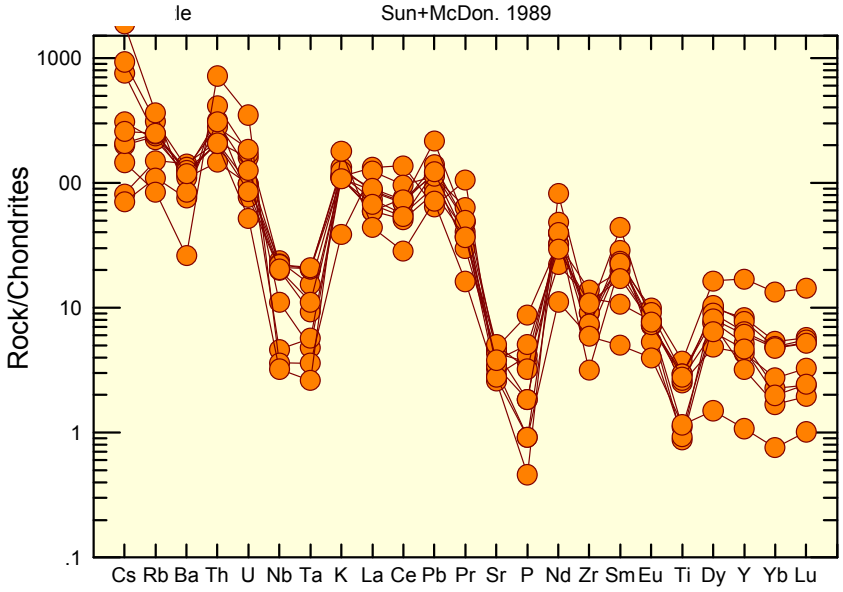

Figure 4.1.9: Multi- element spider diagram for granite gneisses of the Sonapahar area. Normalizing values are from Sun and McDonough (1989).

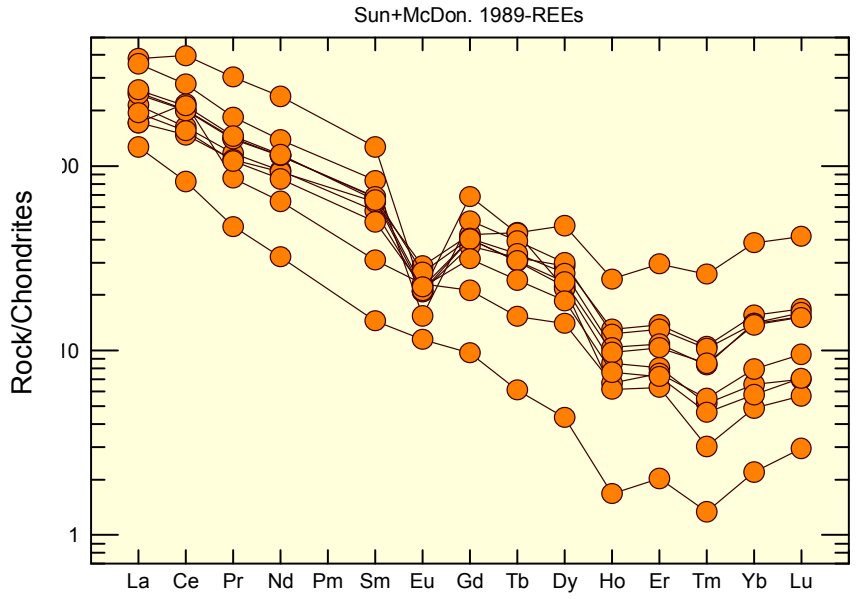

Figure 4.1.10: Chondrite normalised REE patterns for the granite gneisses of Shillong Plateau. Normalizing values are from Sun and McDonough, (1989).

[$(La/Yb)_N$ = 4.47–78.6]. The normalized patterns shows moderate to steeply inclined with highly enriched LREEs and flatter and less fractionated HREEs and with prominent Eu anomaly (Eu/Eu* = 0.21- 0.94) (Fig. 4.1.10).

4.2.2 **Cordierite bearing granulitic gneisses (Metapelites)**

4.2.2.1 *Major elements*

Appendix- II represents the major element abundances of the cordierite bearing granulitic gneisses (Metapelites) of the Shillong Plateau. The metapelites are moderately siliceous with SiO_2 ranging from 57.42 – 68.61 wt %. They are characterized by high Al_2O_3 (11.35 – 19.91 wt %), MgO (2.23- 4.80 wt %) and Fe_2O_3 (4.09 – 10.9 wt %) and low CaO (0.23 -1.12 wt %).

In general, the metapelites are more potassic than sodic. The K_2O content ranges from 1.14 - 4.19 wt % and averages 2.77 wt % and Na_2O content ranges from 0.40 - 2.30 wt % and averages 1.48 wt % except only one sample having Na_2O content 4.47 wt %. In Harker`s variation diagram, SiO_2 shows a pronounced inverse correlation with Al_2O_3, MgO and TiO_2 (Fig. 4.2.1). A strong positive correlation between SiO_2 and Fe_2O_3, a weak positive correlation between SiO_2 and Na_2O are observed. CaO, K_2O and MgO show no discernible trend against SiO_2 in the variation diagram (Fig. 4.2.1).

On the Na_2O/Al_2O_3 versus K_2O/Al_2O_3 diagram of Garrels and McKenzie (1971) discriminating the fields of Igneous and sedimentary/metasedimentary fields for the protoliths, the metapelitic samples plot dominantly within the sedimentary/ metasedimentary field with only two samples plotting in the Igneous field (Fig. 4.2.2a). On Al_2O_3 versus MgO diagram of Marc (1992) discriminating fields of ortho- and para-gneisses, the metapelitic samples of Shillong Plateau plot within the paragneiss field except only one samples which fall within the orthogneiss field and two samples are straddling along the boundary (Fig. 4.2.2b). On the Niggli 100mg-c-(al-alk) triangular diagram of Leake (1964), all the samples lie within the boundary field of typical shales except one sample which is plotting away.

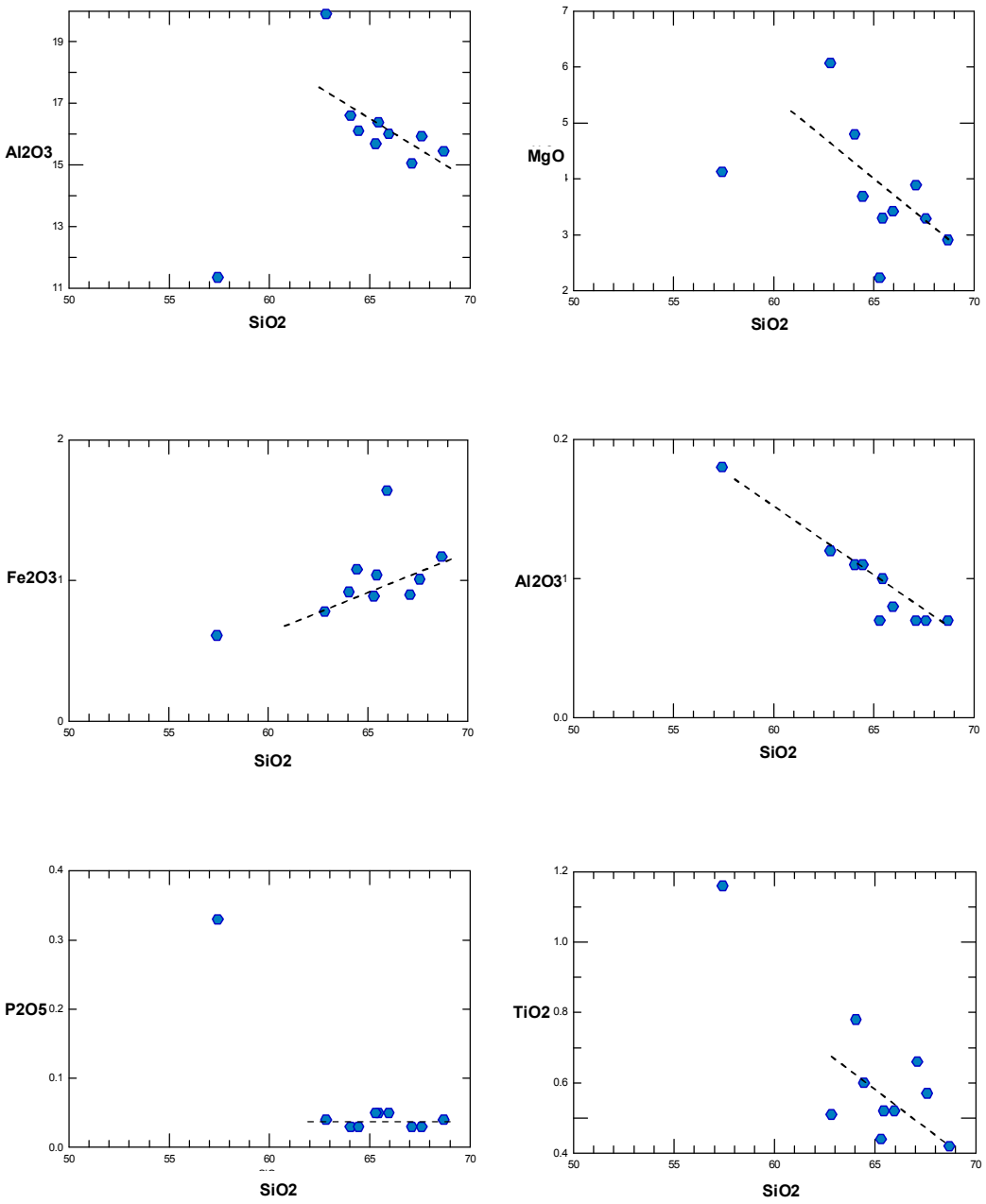

Figure 4.2.1: Harker`s variation diagram for major oxides of metapelites of the Sonapahar area, Shillong Plateau.

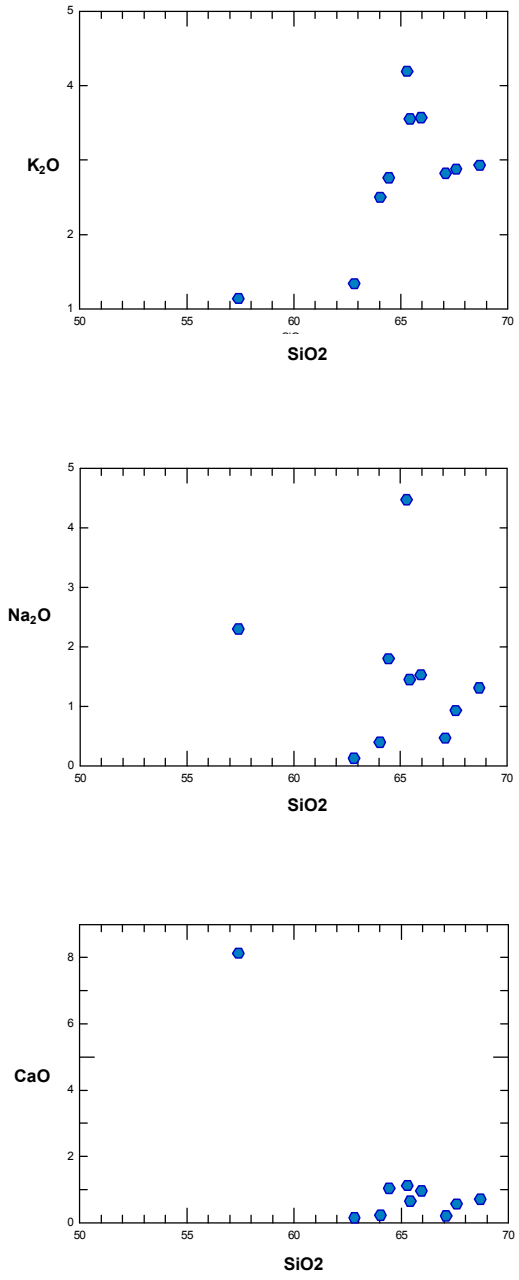

Figure 4.2.1: Harker`s variation diagram for major oxides of metapelites of the Sonapahar area, Shillong Plateau.

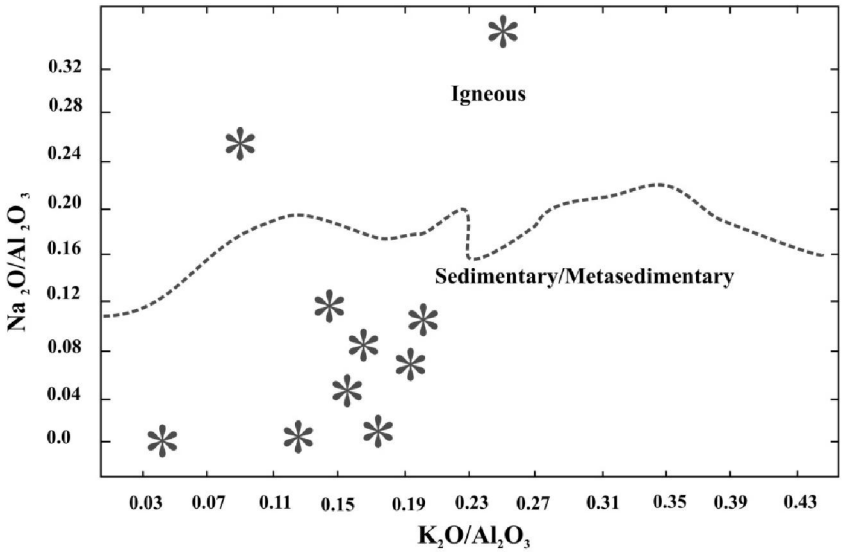

Figure 4.2.2a: Na_2O/Al_2O_3 vs K_2O/Al_2O_3 diagram for metapelites of the Sonapahar area, Shillong Plateau (after Garrels and Mc Kenzie 1971).

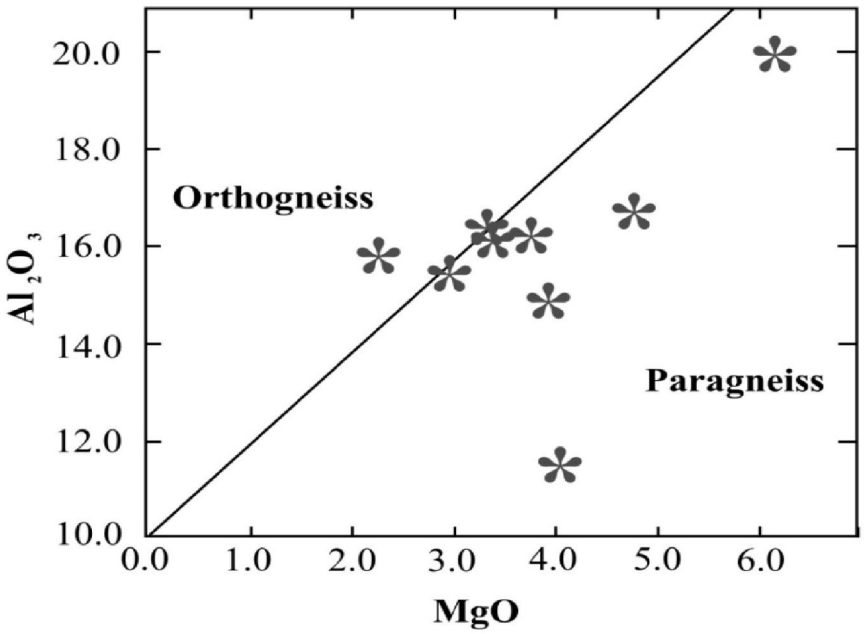

Figure 4.2.2b: Al_2O_3 vs. MgO discrimination diagram for metapelites of the Sonapahar area, Shillong Plateau (after Marc, 1992).

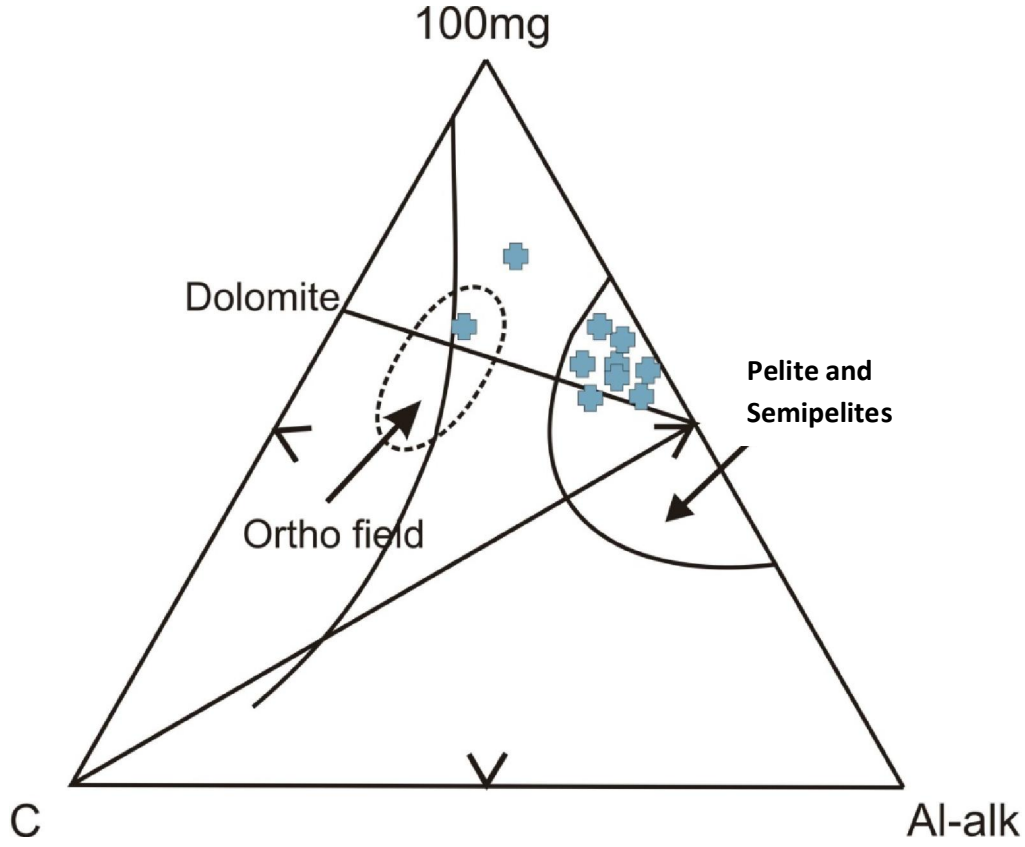

Figure 4.2.3: The Niggli 100mg-c-(al-alk) triangular diagram of metapelites of the Sonapahar area, Shillong Plateau (after Leake, 1964).

4.2.2.2 *Trace elements*

Appendix- II represents the trace element abundance of the metapelites of the Shillong Plateau. The Rb and Sr content of the metapelites ranges from 101.75 ppm to 211.95 ppm averaging 170.52 ppm and from 9.32 ppm to 94.64 ppm averaging 57.76 ppm repectively. The Zr, Nb, Y content of the metapelites ranges from 12.46 ppm to 96.66 ppm averaging 36.98 ppm; from 8.01 ppm to 17.15 ppm averaging 12.48 ppm; and from 16.46 ppm to 29.63 ppm, averaging 20.57 ppm respectively. Th content ranges 15.76 ppm to 36.22 ppm (averaging 25.02 ppm) and U ranges from 2.02 ppm to 4.35 ppm (averaging 2.92 ppm). The Ba content of metapelites ranges from 156.26 ppm to 586.19 ppm and averages 447.14 ppm. The concentrations of Cr (3.57 – 7.86 ppm), Co (9.59 – 18.06 ppm), and Ni (1.43 – 4.80 ppm), Sc (4.42 - 8.26 ppm) of the metapelites are all of low values.

In the Harker's variation diagram most of the trace elements e.g. Rb, Ni, Cr, Y, Nb, Pb show strong negative correlation against SiO_2 (Fig. 4.2.4). Sr, Ba, U, Th etc are all showing scattered plotting (Figures not shown).

4.2.2.3 *Rare Earth Elements (REE)*

The total Rare Earth Elements (ΣREE) of the metapelites ranges from 204.11 ppm to 375.58 ppm. Chondrite normalize REE concentrations (normalizing values are from Sun and Mc Donough, 1989) shows variable LREE/HREE ratios [$(La/Yb)_N$ = 16.67 – 68.98]. The normalized patterns are steeply inclined with highly enriched LREEs and fractionated HREEs along with prominent Eu anomaly (Eu/Eu* = 0.17 – 0.68) (Fig. 4.2.5).

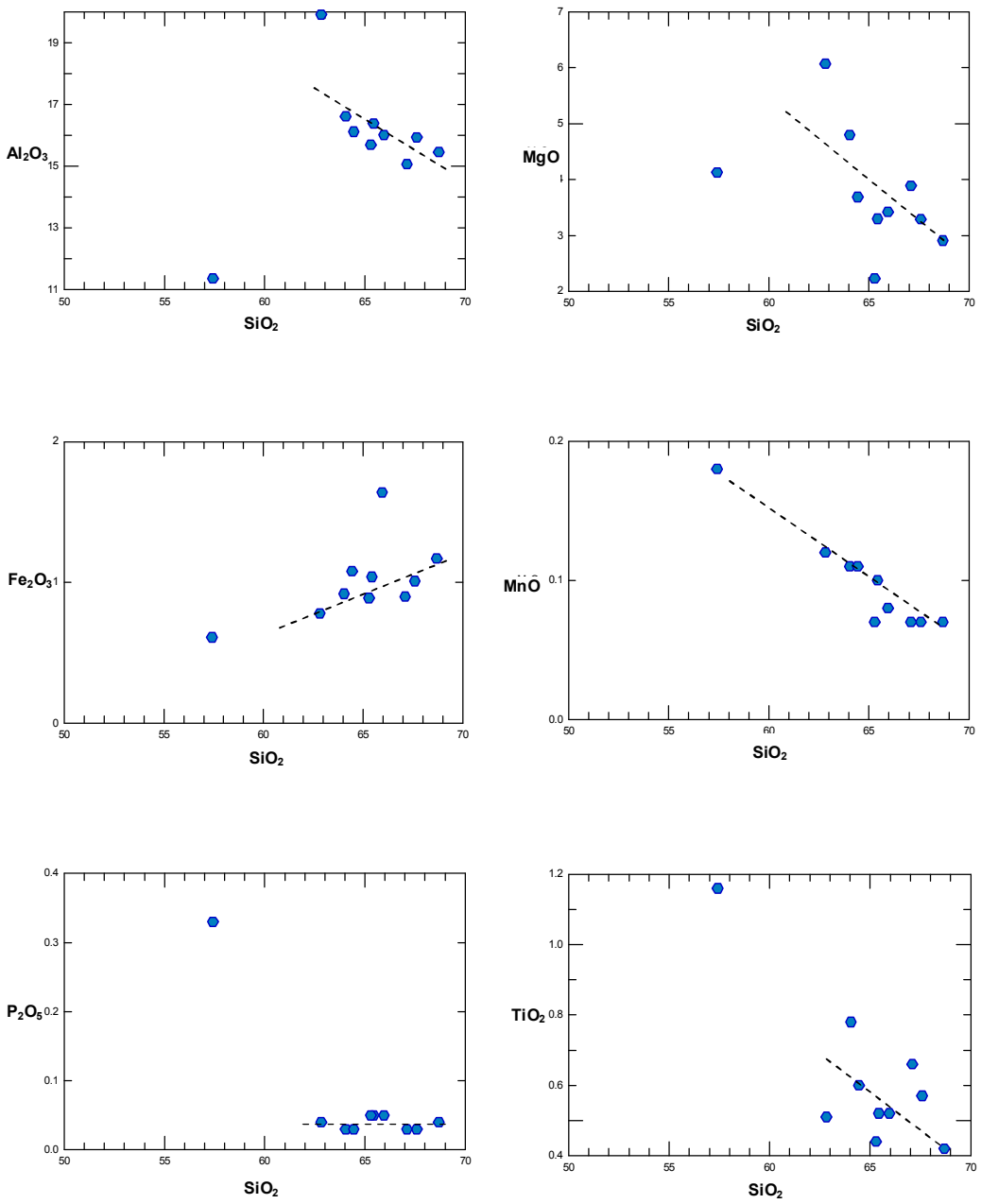

Figure 4.2.4: Harker`s variation diagram for selected trace element vs. SiO_2 of metapelites of the Sonapahar area, Shillong Plateau.

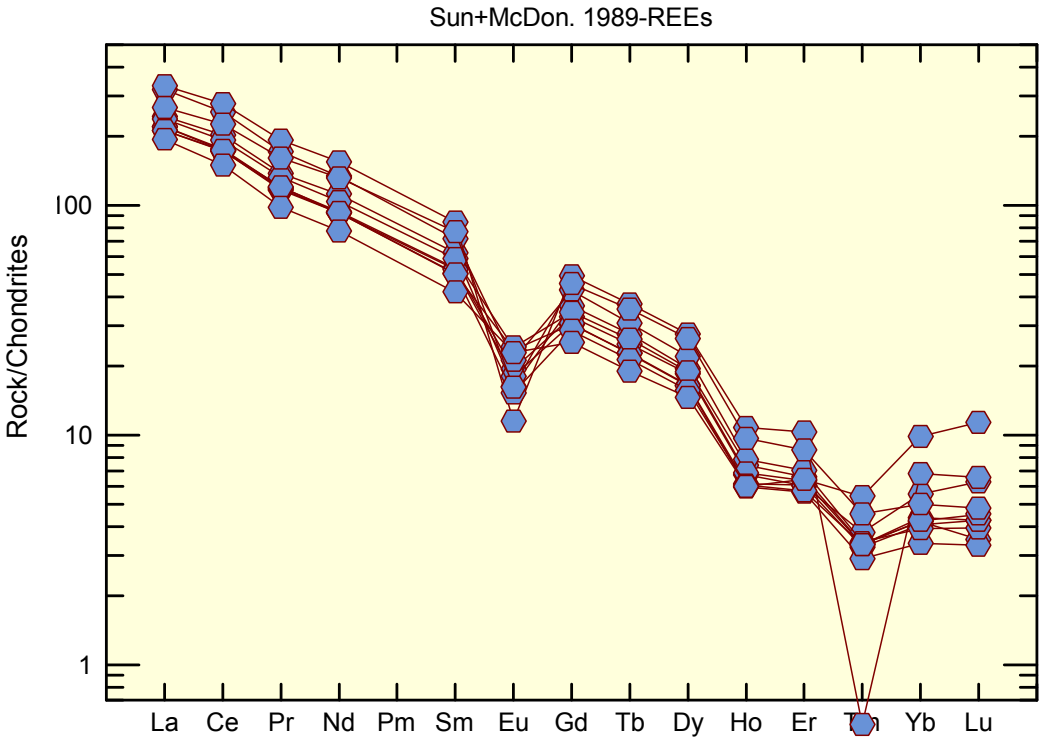

Figure 4.2.5: Concentration patterns of REE in metapelites, normalized with the values of CI chondrite (Sun and McDonough, 1989).

4.2.3 **Basic Granulites**

4.2.3.1 *Major Oxides*

Appendix- III represents the major element abundance of the basic granulites of the Shillong Plateau. The SiO_2 content of basic granulites are moderately high and ranges from 47.63 wt % to 64.62 wt % and averages 54.62 wt %. The basic granulites are characterized by medium to low MgO content ($4.53 \leq MgO \leq 7.9$ wt %). Mg numbers [Mg# = 100MgO/ (FeO^t+MgO)] of the basic granulites range between 46 – 58 and averages 51. It has moderate Fe_2O_3 content ranging between 4.3 and 8.7 wt %. TiO_2 shows low to moderate concentrations (0.71 to 1.32 wt %). Most of the samples were characterized by high Al_2O_3 (13.42-15.22 wt %) and CaO (5.6- 8.14 wt %) content except one sample with CaO equals 0.11 wt %.

The granulites are characterized by low alkali contents with Na_2O (1.62 – 2.7 wt %) and K_2O (0.84 – 1.65 wt % except one sample which show high K_2O values of 3.53 wt %). The total alkalis range from 3.31wt % to 5.11 wt % and have Na_2O/K_2O ratios ranging from 0.45 to 2.94 wt %. The molar A/CNK ratios for the basic granulites range between 0.68 to 0.85. As all the studies rocks have been affected by granulite facies metamorphism, it is necessary to assess effect of metamorphism on the major element composition of these rocks. To evaluate this feature, a variation diagram plotted between SiO_2 with other oxides is prepared (Fig. 4.3.1). Harker diagrams show negative correlation of SiO_2 with FeO^t, TiO_2, MgO, CaO, MnO and P_2O_5, while positive correlation is observed with Na_2O and Al_2O_3 (Fig. 4.3.1). From this diagram it is observed that, most of the samples show good crystallisation trends. No significant irregular pattern is observed. This probably suggests closed-system metamorphism of these samples. This observation rules out possibility of substantial mobilisation of elements during the metamorphism and suggests that these oxides reflect magmatic features. Any open-system metamorphism may lead mobility of elements and show erratic trend on the variation diagrams (Srivastava, 2006). Thus, it is believed that major oxides such as MgO, SiO_2, Al_2O_3, CaO and alkalis are not mobilized during the metamorphism and can be used for classification purpose.

The alkali vs. silica diagram of Irvine and Barager (1971) discriminating the fields of alkaline and subalkaline magmas, for the basic granulites of Shillong Plateau indicates that the precursor melts for the granulites are of subalkaline characteristics

(Fig. 4.3.2). The silica-alkali relationships also indicate that the basic granulites are mainly basalt with marginal overlap to basaltic andesite. In the TAS (total alkali-silica) diagram of Le Bas *et al*. (1986) the basic granulite falls in the field of basalt to basaltic andesite (Fig. 4.3.3). The FeO^t/MgO ratios of Sonapahar basic granulites range from 1.05 to 1.50 except one sample having a value less than one (0.94). Most of the arc basalts have FeO^t/MgO ratios higher than one (Tatsumi *et al*., 1983) suggesting that considerable amount of Mg rich mineral has been separated from the magmas.

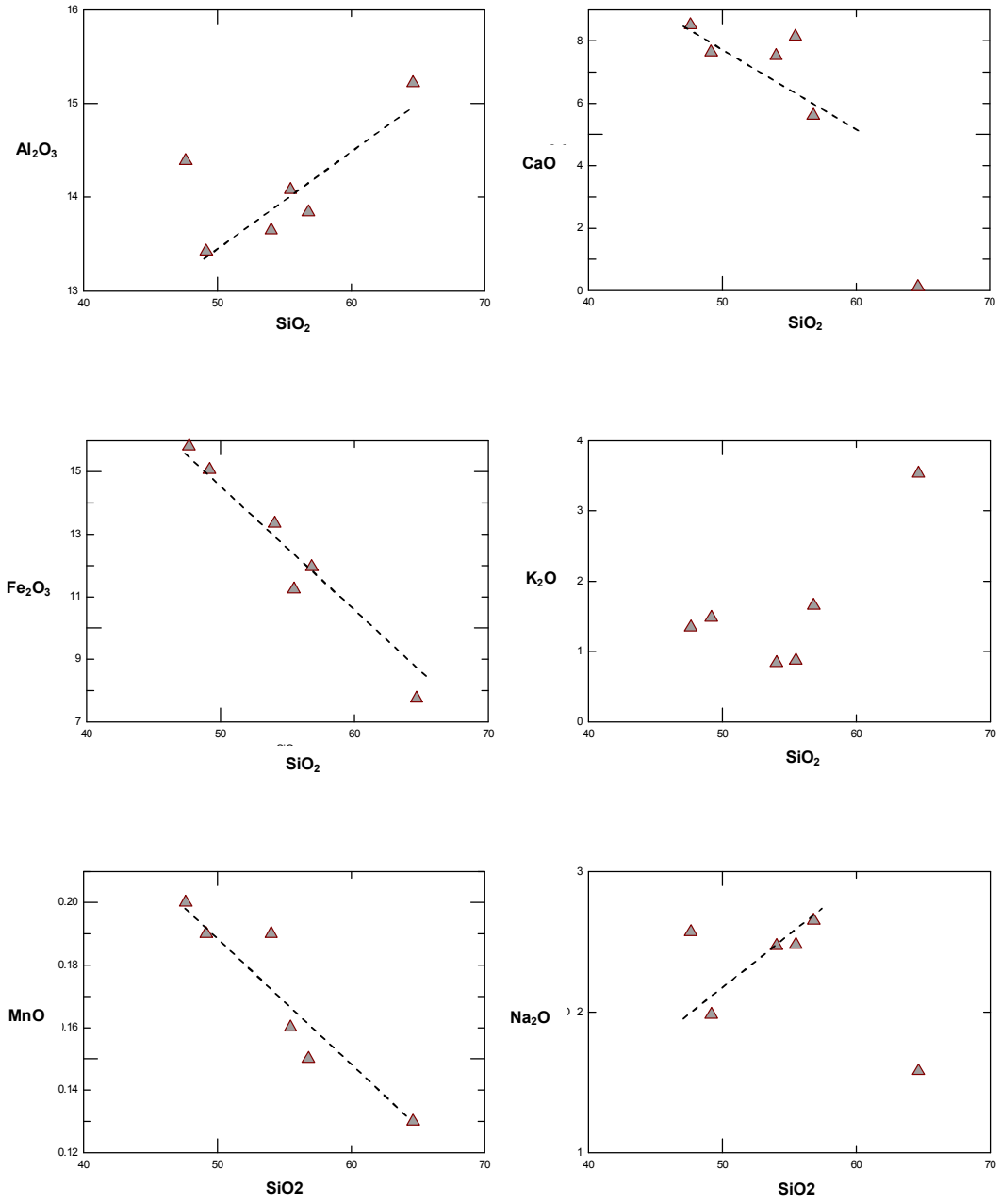

Figure4.3.1: Harker`s variation diagram for major oxides of basic granulites of the Sonapahar area, Shillong Plateau.

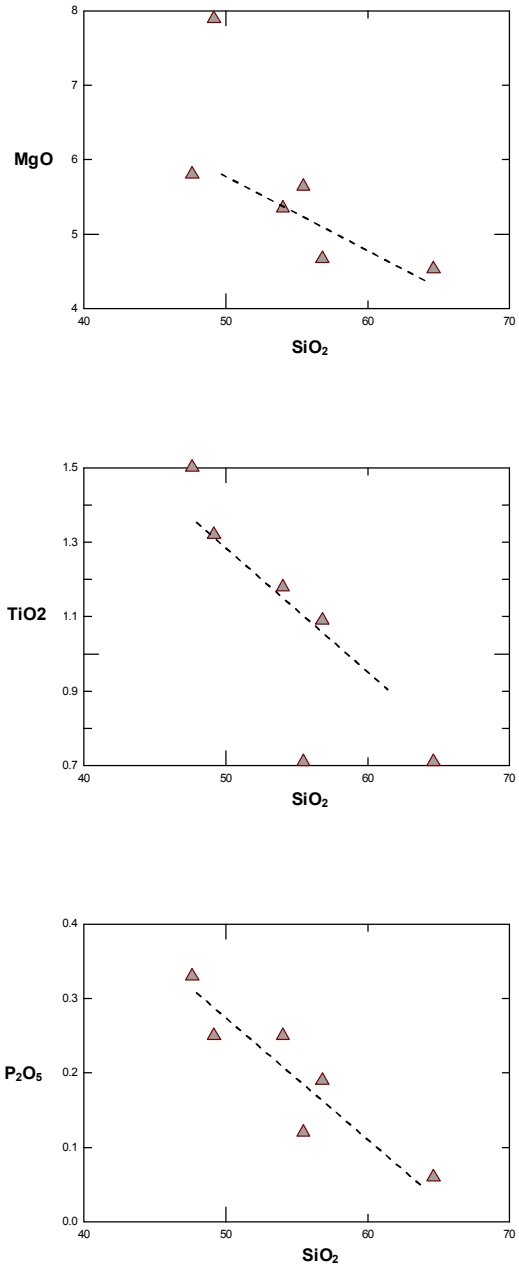

Figure 4.3.1: Harker`s variation diagram for major oxides of basic granulites of the Sonapahar area, Shillong Plateau.

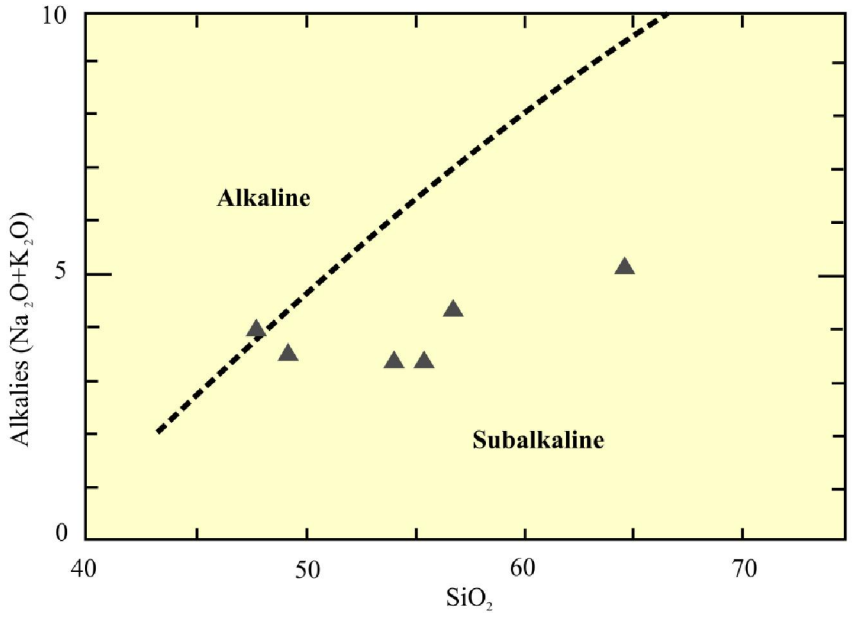

Figure 4.3.2: Alkalies-SiO_2 diagram for basic granulites from the Sonapahar area (after Irvine and Baragar, 1971).

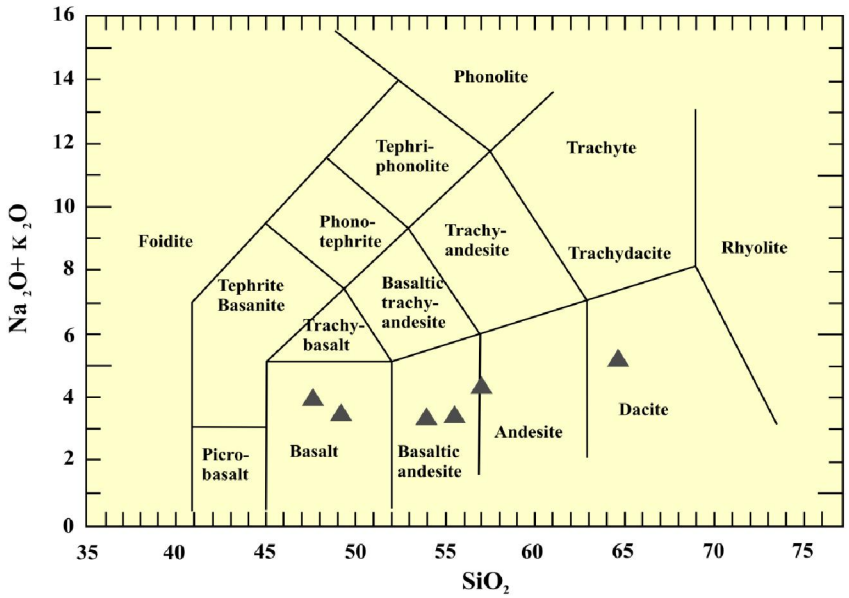

Figure 4.3.3: The TAS (total alkali-silica) diagram for basic granulites of the Sonapahar area, Shillong Plateau (after Le Bas *et al*. 1986).

4.2.3.2 **Trace elements**

Appendix- III represents the trace element abundance of the basic granulites of the Shillong Plateau.

Granulite facies metamorphism often causes depletion of Rb to K and Sr, resulting in increase of K/Rb ratios to over 1000 in certain case, and decrease of Rb/Sr ratios to less than 0.02 sometimes (Tarney *et al.,* 1977). But the present granulite samples have K/Rb ratio (318.65 – 608.46 except one sample which is 1822.47 that are very similar to typical upper continental crust. A decrease in Rb/Sr ratio is observed, all the data rangess between 0.08 to 0.29 and thus indicating the limited effect of metamorphism. The maximum U and Th concentrations for the upper crustal average values are 2.8 and 10.7ppm respectively (Taylor and McLennan, 1985). In contrast to the upper crustal averages, Sonapahar intrusive basic granulites have average of 0.62 and 2.89ppm of U and Th respectively. In the present studied samples, the Th/U ratios are 4.79 – 6.67 which indicates a slight effect by metamorphism.

Discrimination diagrams such as Zr-P_2O_5 diagram (after Floyd and Winchester 1976), Zr/P_2O_5 vs TiO_2 diagram (after Winchester and Floyd. 1976) has been applied to classify basic granulites of the Sonapahar area (Figs. 4.3.4, 5). Both the figures indicated that these rocks have relations to tholeiitic and alkali basalt. However, Al_2O_3- $Fe_2O_3^t$+TiO_2 – MgO diagram of Jensen (1976) shows that these rocks have calc alkali basalt characterictics (Fig. 4.3.6).

The mantle normalized multi-elemental patterns of the basic granulites exhibit a moderately fractionated trends with strong negative anomalies at Zr, Sr and Ti and small negative aonmalies at Rb, Nb and Sr (Fig. 4.3.7). Though the LILE and HFSE level of abundances are enriched than primordial mantle but have high LILE/HFSE ratios and define the degree of fractionation.

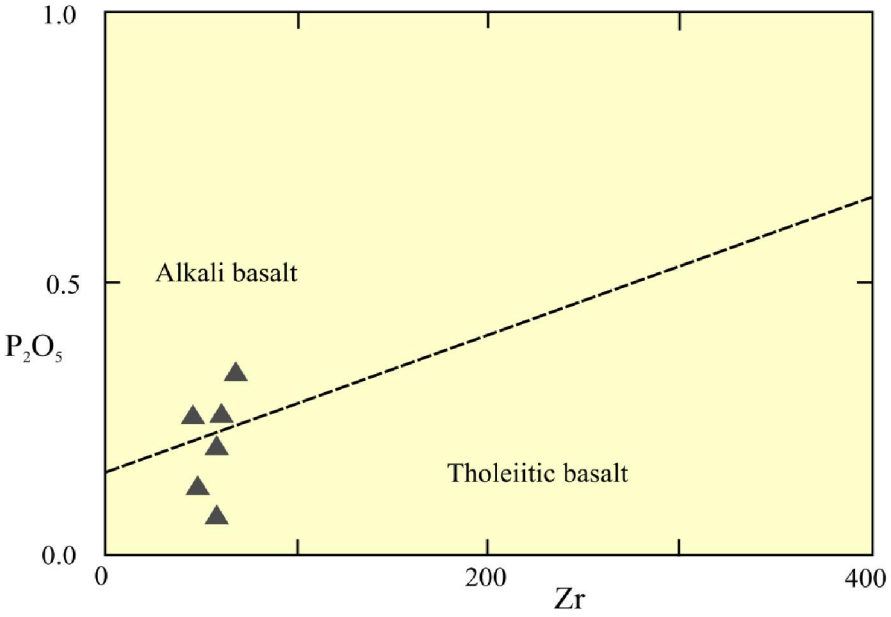

Figure 4.3.4: Zr-P_2O_5 diagram for basic granulites of the Sonapahar area (After Floyd and Winchester, 1976).

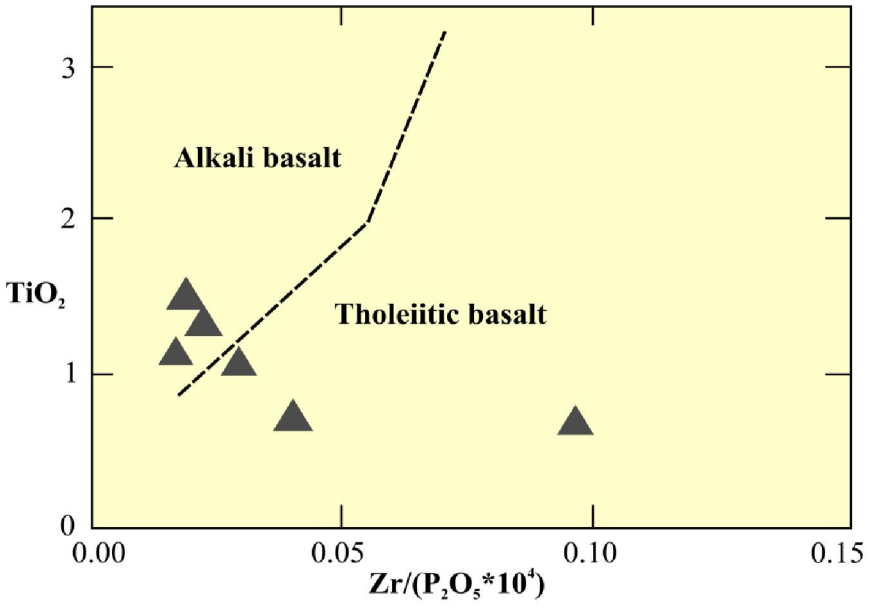

Figure 4.3.5: Zr/P_2O_5 vs TiO_2 diagram for basic granulites of the Sonapahar area (after Winchester and Floyd. 1976).

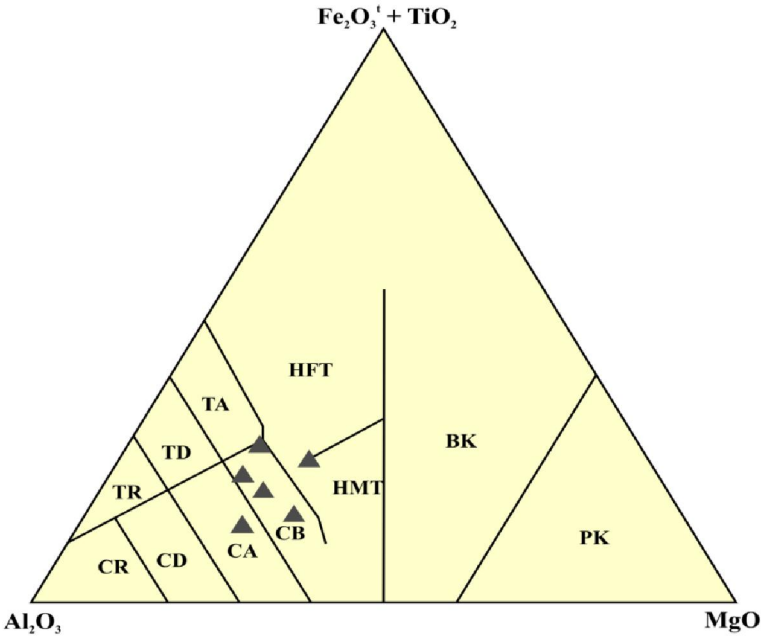

Figure 4.3.6: Al_2O_3- $Fe_2O_3^t$+TiO_2 – MgO diagram (Jensen, 1976) for the Sonapahar basic granulites. TA: tholeiitic andesite, TD: tholeiitic dacite, TR: tholeiitic rhyolite, CA: calc alkaline dacite, CD: calc alkaline dacite, CB: calc-alkaline basalt, CR: calc alkaline rhyolite, BK: basaltic komatite, PK: peridotitic komatite, HFT: high Fe- tholeiitic, HMT: high Mg- tholeiitic.

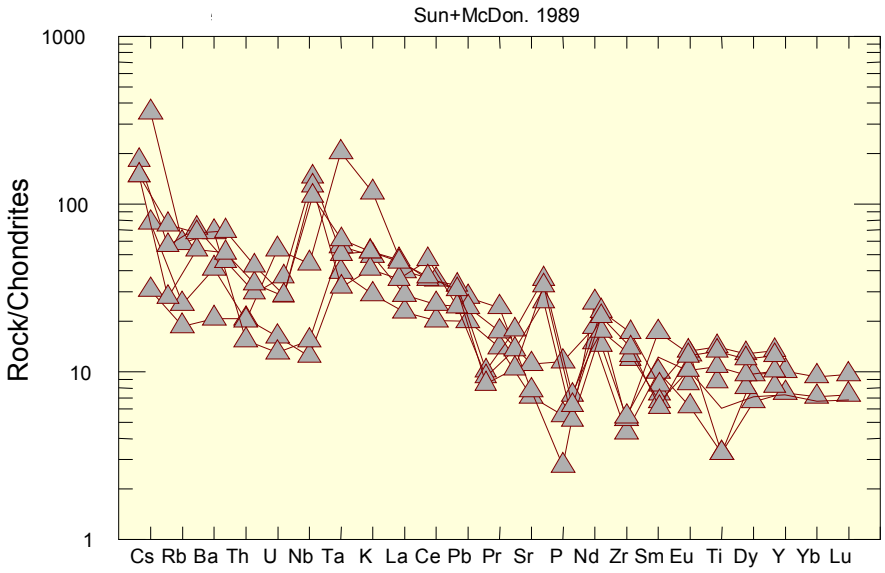

Figure 4.3.7: Multi- element spider diagrams of basic granulites from the Sonapahar area, Shillong Plateau (normalizing values are after Sun and McDonough, 1989).

4.2.3.3 Rare **Earth Elements (REE)**

Chondrites normalize REE patterns (Sun and McDonough, 1989) of the granulites reveal overall enrichments of light rare earth elements (LREE) (Fig. 4.3.8) and fractionated LREE/HREE patterns. Basic granulites have REE patterns with a moderate enrichment in LREE $(Ce/Yb)_N$ = 2.34 – 3.25). The REE pattern is characterized by prominent negative Eu-anomaly, in which Eu/Eu* = 0.17- 0.63. A significant negative slopes as follows from the values of $(La/Yb)_N$ = 3.21 – 4.58. Despite the limited number of analysed samples, different levels of the ΣREE have been observed. The ΣREE content in basic granulites ranges from 101.89 to 201.57 ppm. Such low values are typical rather of post Archean granulites (Rudnick and Presper 1990). The total REE increase with increase in acidity of the rocks. LREE patterns are inclined, whereas HREE patterns are flat. The flat HREE patterns suggest that the rock suites may be derived from depleted mantle source with no residual garnet (Pearce, 1983). The negative Eu anomaly could indicate that plagioclase was an important fractionating phase in the andesitic-basaltic rocks (Wheller, *et al.,* 1987). Negative Eu anomalies can also derive from the breakdown of plagioclase during hydrothermal alteration, which Eu is more mobile than the other REEs.

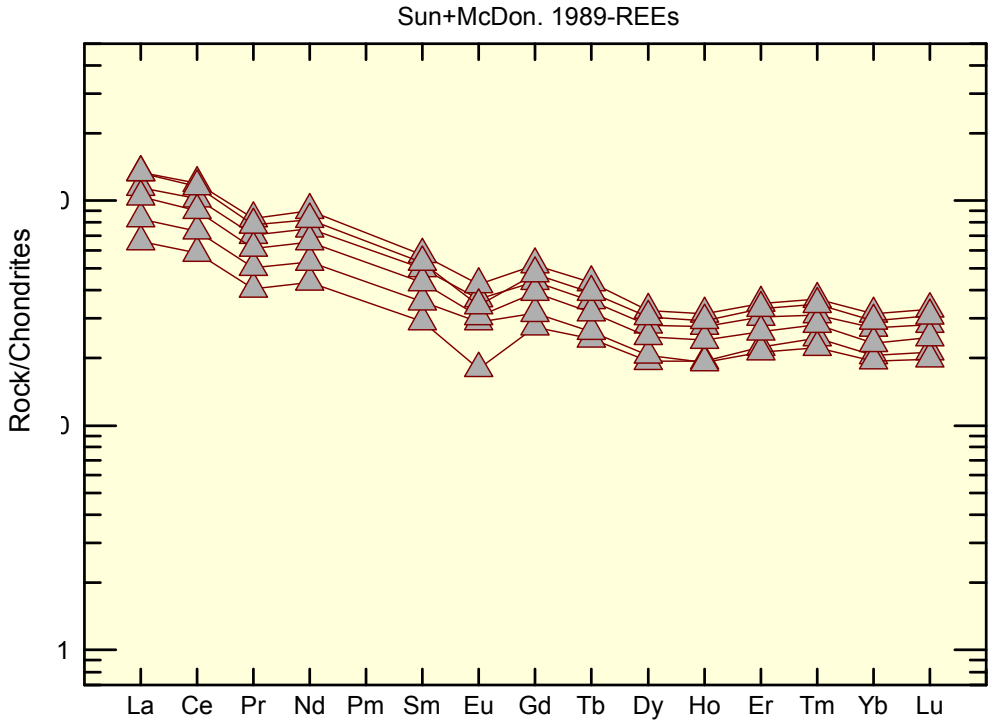

Figure 4.3.8: REE patterns of basic granulites from the Sonapahar area, Shillong Plateau (normalizing values are after Sun and McDonough, 1989).

4.2.4.0 **QUARTZ SILLIMANITE SCHISTS**

4.2.4.1 MAJOR OXIDES

Appendix- IV represents the trace element abundance of the quartz sillimanite schists of the Shillong Plateau. The quartz sillimanite schists are generally siliceous, SiO_2 (60.59 – 76.82 wt %) and are characterized by high Al_2O_3 content with average value (27.22 wt %), low P_2O_5, Fe_2O_3 and MgO, MnO Na_2O, K_2O and TiO_2. The values are however within the range for metasediments (Weaver, 1989). Average MgO, CaO, K_2O and Na_2O values are generally less than 0.15 wt %. TiO_2 values range from 0.13-0.35 wt %.

Compared with the post Archean metasediments, the Sonapahar schists are richer in SiO_2 and Al_2O_3 while depleted in other oxides. In general, Al_2O_3 and SiO_2 constitute more than 97 wt % in most of the samples. In Harkers variation diagram, SiO_2 shows a linear inverse correlation with Al_2O_3 and TiO_2, but there are no significant correlations observed with other oxides (Fig. 4.4.1). This may be due to limited number of samples. However, a strong positive correlation is also observed between Al_2O_3 and TiO_2 (Fig. 4.4.2).

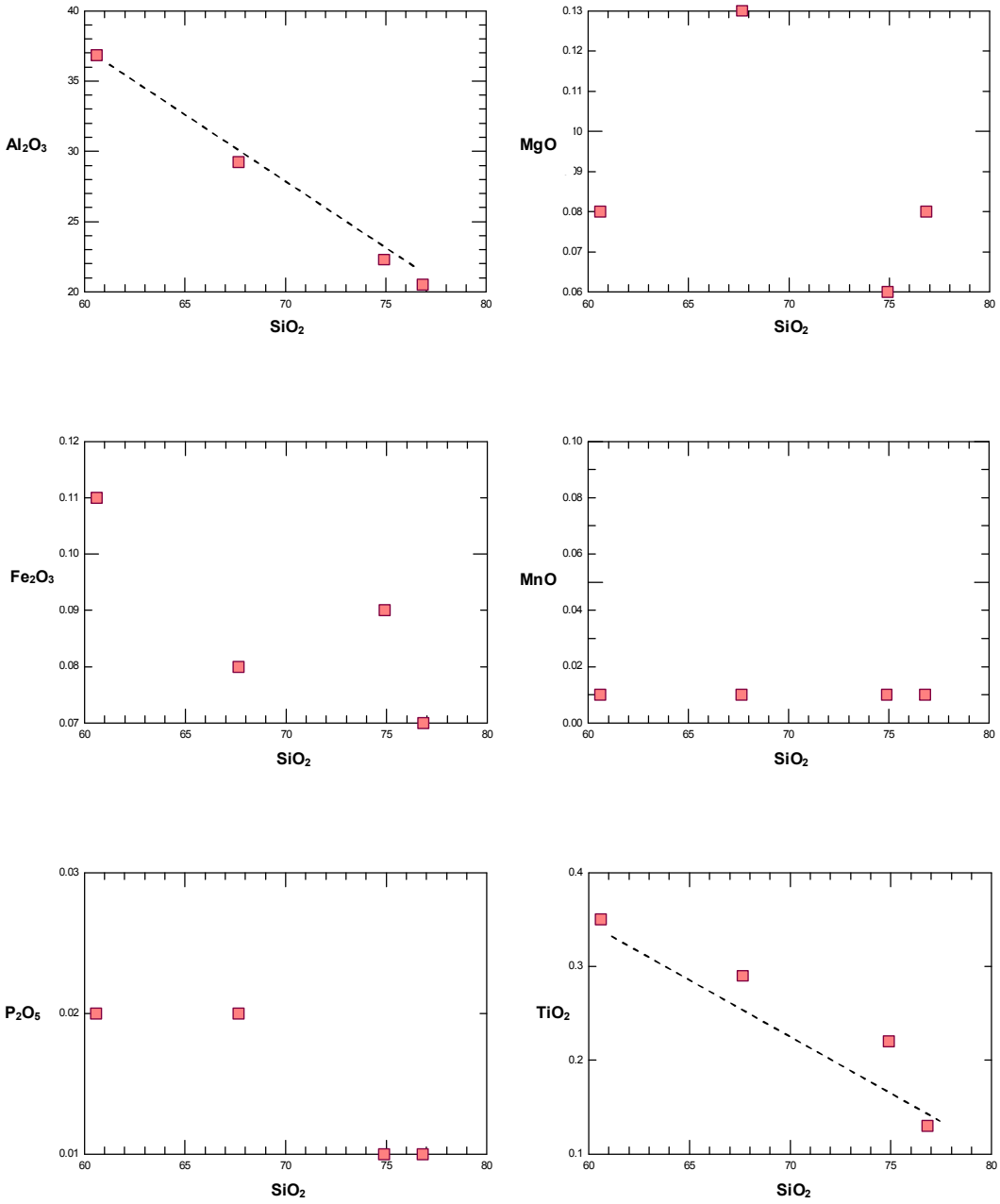

Figure 4.4.1: Harker`s variation diagram for major oxides of quartz sillimanite schists of the Sonapahar area, Shilong Plateau.

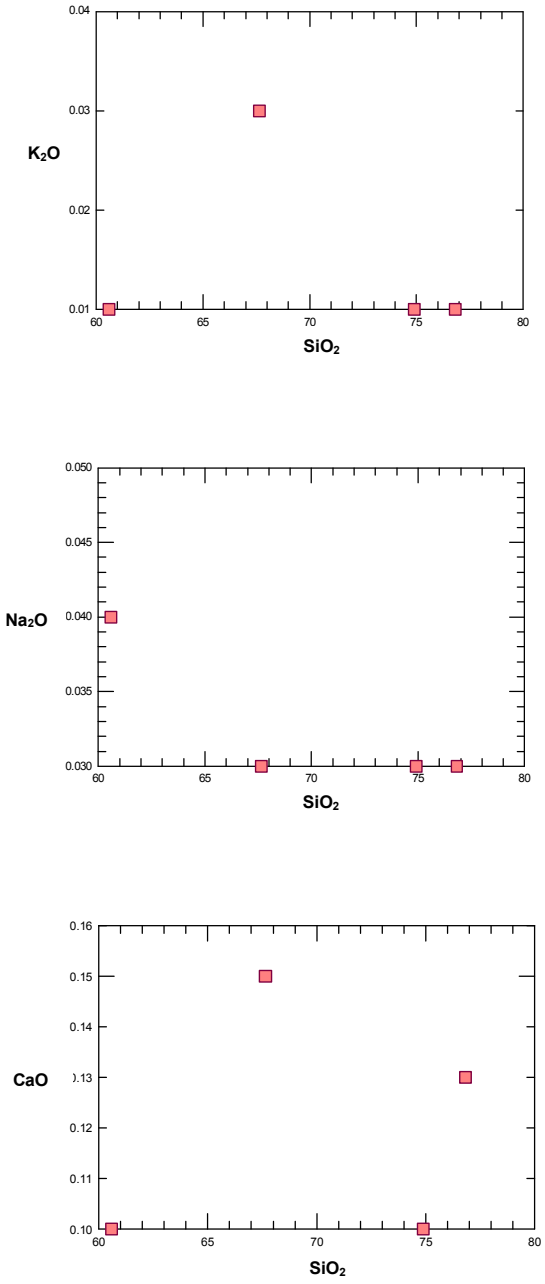

Figure 4.4.1: Harker`s variation diagram for major oxides of quartz sillimanite schists of the Sonapahar area, Shilong Plateau.

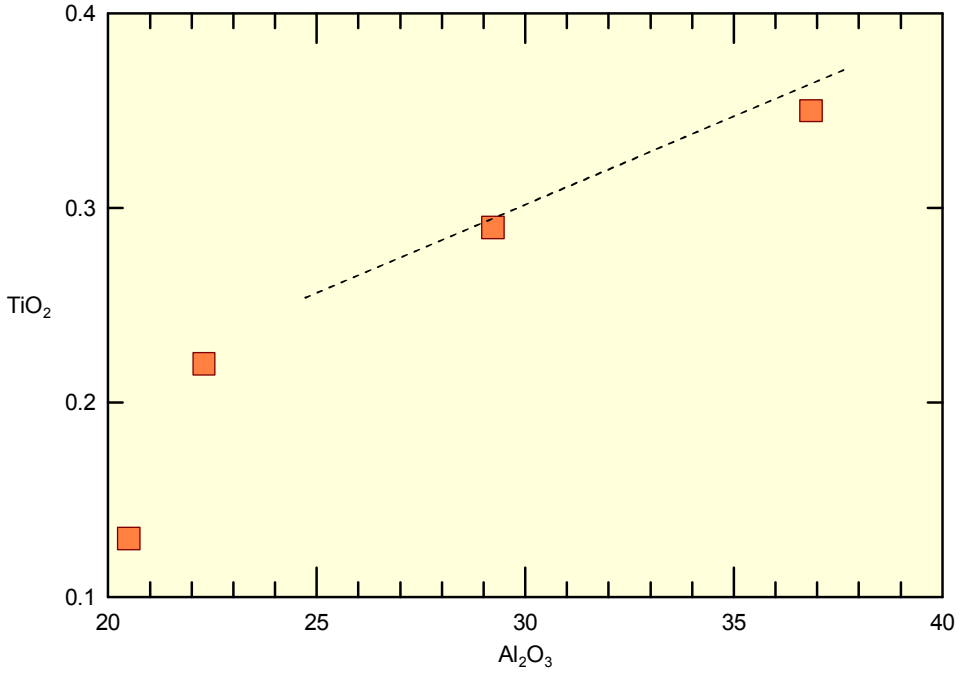

Figure 4.4.2: Al_2O_3 vs TiO_2 variation diagram for quartz sillimanite schists from the Sonapahar area, Shillong Plateau.

4.2.4.2 **Trace Elements**

Among trace elements, Zr, Hf and Pb are characterized by high concentration relative to other. In particular, the high Zr content may reflect the presence of detrital zircon in the rocks (Elueze, 1981). Zn, Cu and Co content is generally low. The schistose rocks are generally low in Sr/Ba ratios (< 0.88 %). The relatively high content of Rb in contrast to Ba indicates the contribution of felsic components can be rule out since Ba indicates K-feldspar-rich source rocks (Okonkwo, 1992; Okonkwo and Winchester, 1998). All the LILEs e.g.Rb, K, Ba are characterized by low concentration.

Most of the samples analysed have low La/Th and Th/U. This feature is normally associated with post Archean recycled upper crust sources (Leyleroupet. al., 1977; Taylor et. al., 1986). V is known to be mobile under oxidising weathering conditions (Rye and Holland, 2000a). The concentration of V (10.28 – 51.49) suggests the apparent mobility in these quartz sillimanite schists and may indicate that oxidizing conditions prevailed during weathering.

4.6.4 **Rare Earth Elements**

Chondrite normalize REE patterns of the schists reveals a strongly fractionated patterns with enriched LREE and low HREE values [$(La/Yb)_N$ = 27.38 – 43.98]. (Fig.4.4.3). The REE patterns was characterized by prominent negative Eu-anomaly, Eu/Eu* = 0.14- 0.29. Despite the limited data set, different levels of the ΣREE have been observed. The ΣREE content in metapelites ranges from 142.32 ppm to 355.72 ppm.

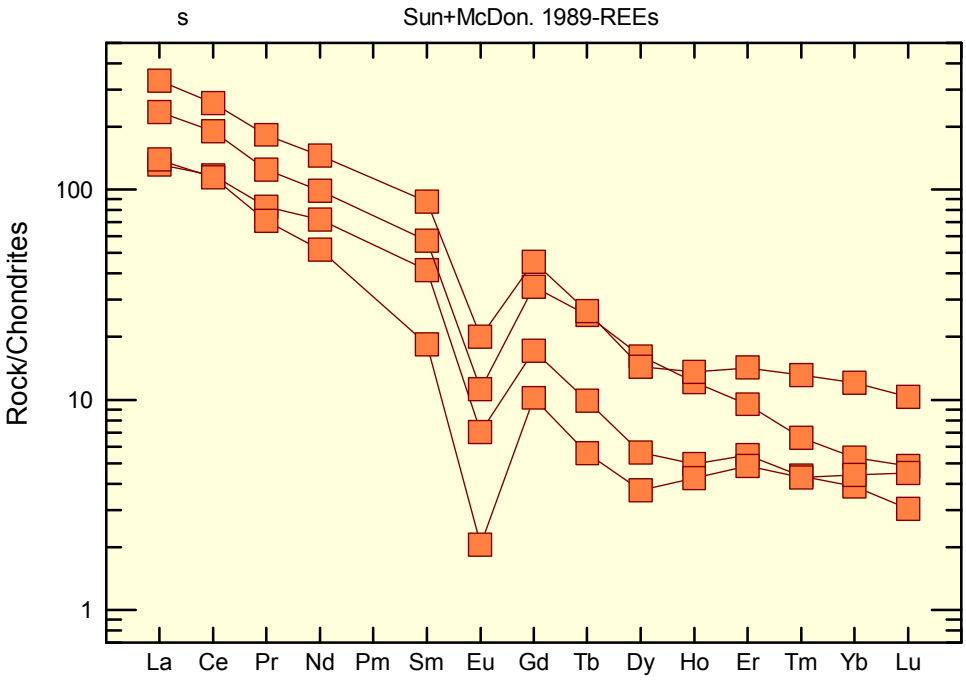

Figure 4.4.3: REE patterns of quartz sillimanite schists from the Sonapahar area, Meghalaya (normalizing values are after Sun and McDonough, 1989).

Chapter- 5

PETROGENESIS

PETROGENESIS

5.1 PETROGENESIS

5.1.1 **Granite Gneisses**

To understand the petrogenesis of the granite gneisses per say the precursor melts for the granite gneisses of Shillong Plateau, it becomes imperative to analyse the role of fractional crystallization, assimilation fractional crystallization (AFC), crustal contamination and partial melting processes, as these are the potential processes for magmatic differentiation of acidic rocks. Almost all the elements of granite gneisses of Shillong Plateau show negative correlation with SiO_2 except for K_2O, CaO, Rb, Th and U which show no discernible trends (Figs.4.1.1, 4.1.8) in the Harker's variation diagram. The trace elements of the granite gneisses of Shillong Plateau show slight scattering compared to the major elements on the Harker's variation diagram (Fig. 4.1.8). The observed trends for the rock suites indicate fractional crystallization of K-feldspars, plagioclase, biotite, ilmanite, apatite, rutile and other Fe-Ti oxides from the precursor melts of granite gneisses. The depletionary trends at Ba, Sr, P, Ti and Nb in the multielemental spider diagram (Fig. 4.1.9) also bear the evidence. The role of fractional crystallization of a mafic magma during Archaean, in producing trondhjemitic, calcalkaline and granodioritic magmas is considered to be minor due to paucity of intermediate crystallization products such as diorites and andesites (Glikson, 1968; Arth et al., 1978; Arth, 1979). Spulber and Rutherford (1983) further observed that a 90% fractional crystallization of tholeiitic magma is required to produce silica enriched residual melts. In Shillong plateau, no such large bodies of cumulate phases are observed by us nor reported by any other workers. Thus fractional crystallization of a basaltic source in alone seems to be a quite inefficient mechanism to characterize the petrogenesis of the Archaean volumetric calc-alkaline felsic rocks (Green and Ringwood, 1978) including the basement granite gneisses of Shillong plateau. However a combination of fractional crystallization and crustal contamination processes may explain generation of the precursor magmas for the granite gneisses of Shillong plateau. The relative enrichment trends of the most of incompatible elements e.g. Rb, Ba, Th and U in the multielement spider diagram points to some influence of assimilation fractional crystallization mechanism. Moreover such enrichments can also be ascribed due to

addition from subduction zone components (Saunders et al., 1980) and possible sediment incorporation into the mantle (see e.g. Tatsumi et al.,1986)

The primordial mantle normalized multi-elemental patterns for the gneisses show marked enrichment in the LILE with enriched abundance in Rb, Ba, K, Th and U (Fig. 4.1.9). The patterns simultaneously display lesser abundance of HFSE with strong negative anomalies at Ba, Nb, P and Ti, Zr. Such elemental pattern may be explained by magmatism in a subduction zone environment (Tatsumi *et al*., 1986; Peacock, 1990; Saunders *et al*., 1991; Hawkesworth, 1994). Fractionation of LILE from HFSE in the melts generated in a subduction environment can be due to dehydration of the subducting slab (Tatsumi *et al*., 1986; Saunders *et al*., 1991), whereas the melting of the subducting slab will not fractionate the LILE from the HFSE unless minor phases like rutile, titanite, alanite, phlogopite, hornblende etc. are present in the residual phases (Tatsumi *et al*., 1986; Saunders *et al*., 1991). The selective depletion of P and Ti in the granite gneisses of shillong plateu indicates that one or more mineral phases removed Ti and P selectively without causing larger depletion in other HFSE. Although Ti and P are the principal constituents of rutile and apatite, but at high pressures both Ti and P may have enhanced solubility in garnet (Saunders *et al*., 1991). The garnet retained at the site of partial melting can also act as a repository for Ti and P and can explain the depleted nature of the elements.

The REE patterns of the gneisses are characterized by moderately fractionated (La_N/Yb_N = 4.47–78.6) trends, HREE depletion and concave upward shape with curvature of the HREE ends along with prominent negative Eu anomalies (Fig. 4.1.10). Such REE patterns are similar to those of various Archaean silicic gneisses from around the world, which were explained by various workers (e.g. Martin, 1986, 1993, 1994) in terms of subduction zone magmatism. Partial melting of an Archaean mafic source (amphibolite and/or eclogite) with hornblende and/or garnet in the residuum can result in depletion of the heavy rare earth elements. Fractional crystallization of hornblende and plagioclase can account for the negative Eu anomaly.

5.1.2 **Cordierite bearing Granulitic Gneisses (Metapelites) and Quartz Sillimanite Schists**

The petrological and geochemical signatures indicate that the Cordierite bearing granulitic gneisses (metapelites) and the quartz sillimanite schists are

metasedimentary rocks. On the Na_2O/Al_2O_3 versus K_2O/Al_2O_3 diagram of Garrels and McKenzie (1971), most of metapelitic samples plot within the sedimentary/ metasedimentary field (Fig. 4.2.2a). On Al_2O_3 versus MgO diagram of Marc (1992) the metapelites also plot within the paragneiss field (Fig. 4.2.2b). On the Niggli 100mg-c-(al-alk) triangular diagram of Leake (1964), all the samples lie within the boundary field of typical shales.

Al_2O_3, MgO and TiO_2 show negative correlation against SiO_2 in the Harker`s variation diagram (Fig. 4.2.1). A strong positive correlation between SiO_2 and Fe_2O_3, a weak positive correlation between SiO_2 and Na_2O are observed while CaO, K_2O and MgO display no discernible trend against SiO_2 (Fig. 4.2.1**)**. Most of the trace elements e.g. Rb, Ni, Cr, Y, Nb and Pb show strong negative correlation against SiO_2 (Fig. 4.2.4) except Sr, Ba, U, Th which show scattered plotting. The major and trace element in particular the LILEs composition of metapelites and their behavior in the Harker's variation diagram thus indicate probable weathering of the protoliths of the metapelites.

As Aluminum increases, calcium and the alkalis decrease with progressive weathering, a good measure of the degree of weathering may be obtained from the major element chemistry by their so-called chemical index of alteration (CIA) (Nesbitt and Young 1982). The CIA is obtained from the following formula using molecular proportions:

$$CIA = [Al_2O_3/(Al_2O_3 + CaO + Na_2O + K_2O)] \times 100$$

The CaO is the amount of this oxide in the silicate fraction and should be corrected for any carbonate or apatite content. As carbonates are absent and the amount of apatite is negligible in our samples, such a correction was inappropriate in this particular case. As pointed out by Nesbitt and Young (1982), CIA values for average shales range from about 70 to 75 due to a large proportion of hydrous aluminum silicates and related minerals. CIA values of the metapelite samples range between 62 and 84 (average 81). Omitting S08-22 (CIA= 50) and S08-33 (CIA = 93), the eight remaining samples vary between 81 and 86 (average 75), indicating a highly weathered precursor that formed in a warm, humid climate. The quartz-sillimanite schists have an average CIA index of 99 and thus, the schists probably had a highly weathered precursor (see e.g. Nesbitt and Young, 1982).

Thorium correlate strongly with the LREE in many sedimentary rocks (McLennan *et al.,* 1980). In the metapelites of Shillong plateau, Th correlate well with La (LREE) (Fig. 5.1) and the La/Th ratio range from 2.06 – 2.91. In La vs. Th (McLennan, 1989) diagram, all the metapelite samples plot within the field of post-Archean cratonic deposits (Fig. 5.1). In addition, REE fractionated pattern and a pronounced negative Eu anomaly (Eu/Eu*: 0.17- 0.68), are well within the compositional range of various post-Archaean shale estimates (Taylor and McLennan, 1985). It follows therefore that the Sonapahar metapelites are metamorphosed post-Archean sediments. The erosion of acidic rocks is evident from the elevated values of Th/Sc = 2.6 – 3.4 and Th/U = 6.06 – 15.37 relative to those PAAS which strongly supports the presumed parent rocks for metapelites.

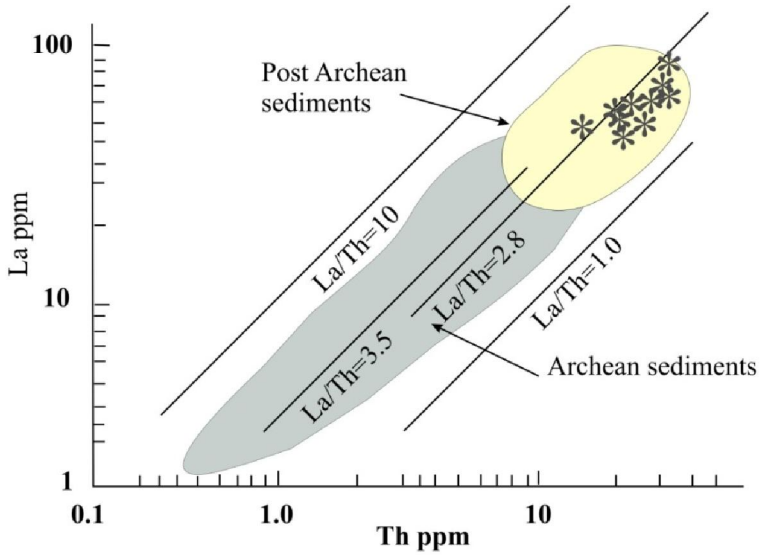

Figure 5.1: La vs. Th diagrams for the metapelites from the Sonapahar area (after McLennan, 1989).

5.1.2.1 *Sedimentary processes*

The previous discussions and plots support the cordierite bearing granulitic gneisses (metapelites) and the Quartz-sillimanite schists as metasedimentary rocks which were formed of weathered precursor sediments derived in a warm, humid climate. But it is important to emphasize the compositional complexity of sedimentary rocks as there are at least four main factors which have to be considered. Chemical weathering in situ or during transport may cause profound alteration of the

provenance rock(s) and judging from the previous plots this has obviously been an important factor. The source rock in the provenance area is also important; if there are several source rocks, a mixing of the debris or weathered material may cause different chemical trends. Other processes during sediment transport and deposition, such as grain-size sorting, adsorption and other syn- or post-depositional alterations may change the geochemical signature of the provenance rocks profoundly. Moreover, diagenesis and metamorphism may also cause element mobility. Unfortunately, the nature of the source rock is unknown. Since granite gneiss is the only basement rock older to the metapelites the sediments are most likely to be derived from the granite gneisses. Rare earth elements are not much affected during sedimentation (very short residence period in water), diagenesis and metamorphism, the REE plot of the metapelites shows a very conformable trend (Fig. 4.2.5) indicating a singular source for the precursor sediments and REE patterns of the metapelites conforms to the trend defined by the granite gneisses of Shillong plateau (Fig. 4.1.10). For the quartz sillimanite schists, both the granite gneisses and metapelites are the older rocks and were possible sources for precursor sediments of the Schists. The high CIA and CIW values indicate that the sillimanite schists might have been derived from both metapelites with larger proportions and granite gneisses in smaller proportions. The quartz fractions might have been derived from more granite gneisses and clay fraction most likely derived from the metapelites.

5.1.2.2 *Trace element distribution*

In a relatively wet climate, hydrous solutions are expected to play an important role in dissolving minerals and controlling the behaviour of elements during transportation and precipitation. Important in this connection is the Ionic Potential (IP) or Field Strength (FS) which is defined as Z/r, where 'Z' is the ionic charge and 'r' is the ionic radius. This factor will, to some extent, control the solution/precipitation behavior of the different elements. Elements with an ionic potential or field strength less than 2 (denoted LFSE or Low Field Strength Elements) will be easily dissolved. Thus, Sr, Ba, K and Rb will be removed in hydrous fluids as soluble cations during weathering and remain in solution during transportation. Elements with higher Field Strength (or HFSE with FS between 2.5 and 9.5) (Krauskopf and Bird 1995) become fixed to hydroxyl groups and are precipitated by hydrolysis. Elements with FS higher than approximately 10 or 11 will normally form

soluble anionic complexes. In the present investigation this includes phosphorus (P) and the spider diagrams in the present study are constructed with P (highest FS) on the left followed by elements with gradually decreasing FS values (Figs. 5.2, 3). The pH and redox potential also influence the element distribution during sedimentary processes. Colloidal processes, where sols and gels influence precipitation, may be an important factor, such as the adsorption of K, Rb and Ba to montmorillonite-rich clay. Some heavy metals, such as V, may also be adsorbed under certain conditions and thus be removed from solution by natural colloids. Despite these complications, which may influence the element distribution, an attempt to identify the nature of the protolith has been made by normalising all the analysed trace elements to Post Archaean Australian Shale (PAAS) (McLennan, 1989).

In the PAAS normalized spider diagrams, all the metapelite samples, with just one exception (S08-14), have pronounced negative P anomalies in the spider diagrams (Fig. 5.2). The metapelites have large negative anomalies for Zr, and Sr and small negative anomalies for Y, and K. The metapelite possess positive anomalies for Nb, Ti, Th, Ce, La, Ba and Rb. Th, Ce and La are enriched relative to PAAS. The quartz sillimanite schists exhibits a very fractionated trend with P, Nb, Ti, Y, Sr, Ba, K and Rb are highly depleted and Zr, Th, Ce and La are enriched relative to PAAS. The spider diagram exhibits pronounced negative anomalies for Y and K and positive anomalies for Zr (Fig. 5.3). The strong negative anomalies at P for almost all the metapelites and quartz-sillimanite schists may indicate that it stayed in solution in the form of soluble anion complexes during formation of the precursors to the sillimanite rocks. Alternatively, phosphorus may have been dissolved and removed during diagenesis or, less likely, during metamorphism. Niobium in the metapelite is in the range of 8 -17 (average 12.5); which is slightly lower than the PAAS (19 ppm). The Nb content of the schists is extremely low compared to PAAS in the range of 1.3 ppm to 6 ppm (average 2,5 ppm). Since Nb substitutes for Zr in zircon, the elevated concentration of Zr in the schists can therefore account for the substitution of Nb for Zr. Both the rock suites have higher Thorium (Th) Cerium and (Ce) values than the PAAS. Ce is the main element in monazite, a highly resistant mineral that is chiefly derived from the weathering of granites and granite pegmatites and there suggests the precursor sediments are possibly derived from felsic rocks and probably not mafic rocks.

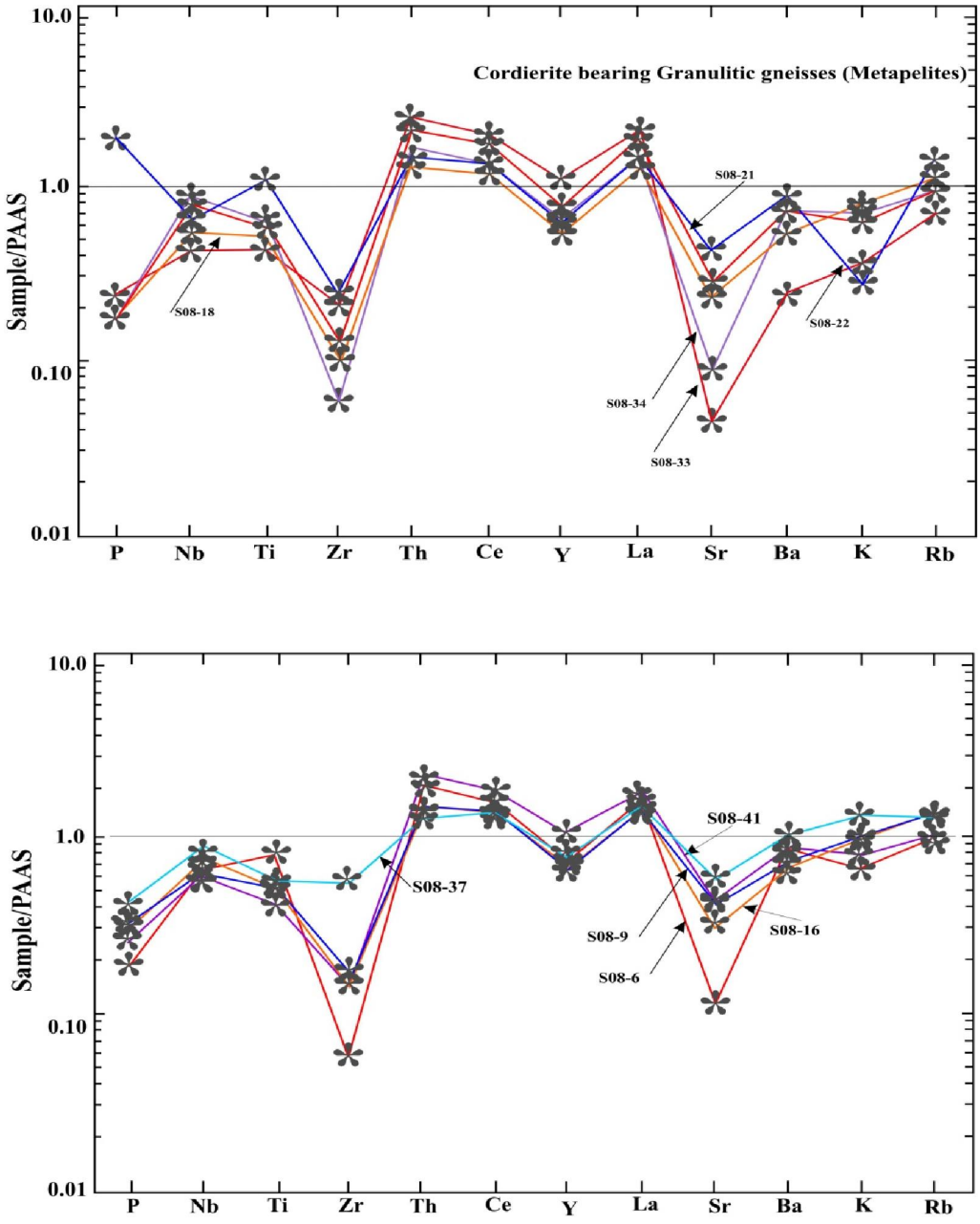

Figure 5.2: Spider diagram for the elements of the cordierite bearing granulitic gneisses (metapelites) normalised to PAAS (Post-Archaean Australian Shale; McLennan 1989). The elements are in succession with decreasing ionic potential towards the right.

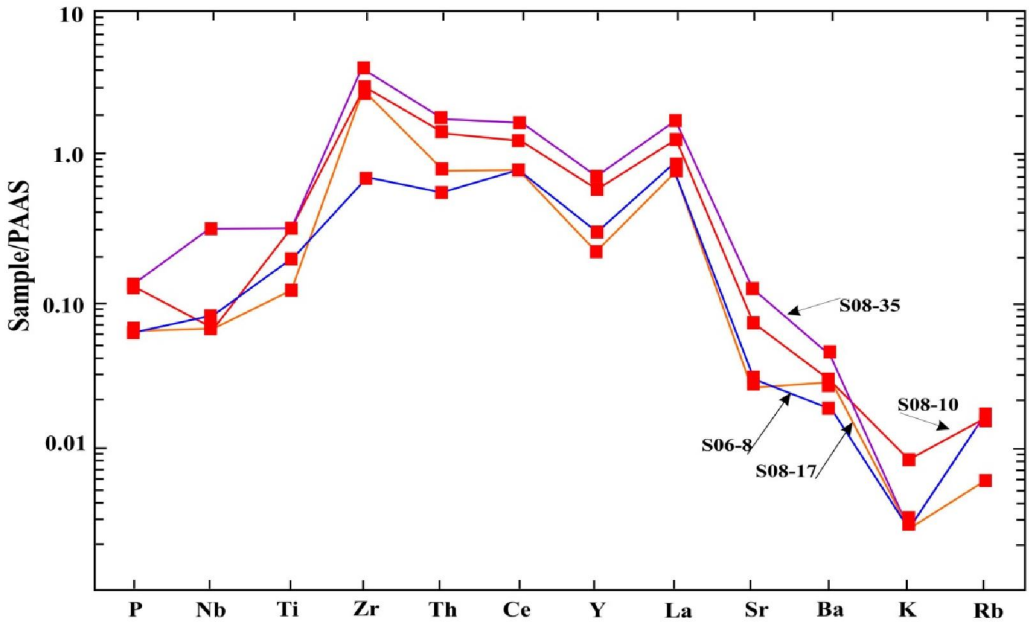

Figure 5.3: Spider diagram for the elements of the quartz-sillimanite schists normalised to PAAS (Post-Archaean Australian Shale; McLennan 1989). The elements are in succession with decreasing ionic potential towards the right.

The large-ion lithophile elements Sr, Ba, K and Rb should ideally form dissolvable ions in aqueous solutions owing to their low ionic potential or field strength, unless other processes, such as adsorption, have led to their precipitation in the clay fraction. In a sedimentary context, Sr is known from deposits formed in a dry climate. The negative Sr anomalies for both the rocks types may be taken as an indication that Sr was brought into solution during weathering in a humid climate and stayed in solution during formation of the precursor sediments. Barium is recovered from residual clay deposits where Ba is trapped because of its higher tendency for adsorption to clay minerals than Sr. The metapelites and quartz sillimanite schists have positive Ba anomalies. Relatively high Ba in the metapelites may be ascribed to the adsorption model. Potassium is commonly adsorbed to clay minerals under suitable conditions. Pettijohn (1975) estimated that Precambrian and Palaeozoic shales contained on average 3.2% K_2O and 1.1% Na_2O, close to Condie´s (1993) calculated averages for Proterozoic shales of 3.62% K_2O and 1.06% Na_2O compared to 3.7% K_2O and 1.2% Na_2O in PAAS. In primitive Precambrian paleosoil, K was mainly derived from the weathering of K-feldspar and/or muscovite and fixed in illite, whereas Ca and Mg were dissolved and removed from the sediments. The relatively

high K_2O values in the metapelitic samples may be explained by either diagenetic processes may give rise to some K-metasomatism (Nesbitt and Young 1989) or adsorption of K to clay minerals leads to higher K contents or K may also have been added at a later stage during metasomatism and/or magmatic injections. A variety of different processes may therefore have contributed to an increase in the K contents of the metapelites. Rubidium occurs in small concentrations in most K-bearing minerals. The metapelites have enriched Rb contents while the quartz sillimanite have depleted Rb content. During sedimentation dominated by clay precipitation, Rb will have a greater tendency to become adsorbed in clay minerals than K. The present distribution of Rb i.e. high Rb in the metapelites thus indicates that the precursor sediments to the metapelites were relatively clay rich than those for the schists.

The positive enrichment ratios for almost all trace elements, apart from P and Sr, Zr and Y in the metapelites suggest clay rich sediment from continental source rocks. However, high values for Zr, Th, Ce and La suggest that the precursors to the quartz-sillimanite Schists were probably sand-clay mixtures with zircon enrichment in the sand fraction. The major element geochemistry rules out some other possible models of origin for the sillimanite schists. Immature sediments, such as glacial clay or loess, can be excluded because the high CIA index suggests rather highly weathered sediments derived in a warm, humid climate. The quartz-sillimanite schists and cordierite bearing granulitic gneisses cannot be simple metamorphic derivatives of bauxite deposits, as bauxites normally contain more than 40% Al_2O_3, which is well above the level for the sillimanite schists. Pelagic red clays can also be excluded since they have different element distributions than the sillimanite rocks (McLennan *et al.,* 1990; Li 1991, 2000). Even if the protolith and paleoenvironmental condition for the precursor sediments of the cordierite bearing granulitic gneisses and sillimanite-bearing schists remains somewhat elusive, there seems to be ample support for the notion that clay-rich sedimentary precursors for the gneisses and sandy-clay mixture for the schists developed during weathering in a warm, humid environment.

Chondrite normalize REE concentrations for the metapelites show variable LREE/HREE ratios [$(La/Yb)_N$ = 16.67 – 68.98]. The normalized patterns are steeply inclined with highly enriched LREEs and fractionated HREEs along with prominent Eu anomaly (Eu/Eu* = 0.17 – 0.68) (Fig. 4.2.5). When compared with the patterns of the granite gneisses, the rare earth elemental patterns of the metapelites show a

remarkable similarity. From the field relationships with the granite gneisses hosting the metapelites and their ages [granite gneisses: ca. 1600 Ma (Yin *et al*., 2010); metapelites: ca. 520 Ma (Chatterjee *et al*., 2007)] it is reasonable to assume that the metapelites were derived from granite gneisses.

5.1.3 **Basic Granulites**

Both major and trace elements vary significantly in basic granulite samples. Some distinct trends have been noted in the variation diagrams, ratio-ratio plots, multi-elemental spider diagram and also in the REE patterns (Figs. 4.3.1- 4.3.8). These trends were either likely to be results of the individual processes like fractional crystallisation, crustal contamination, mantle metasomatism of the primary precursor basaltic magma for the granulites or a combined effect of these processes. In the primitive mantle-normalized multi-element plot (Fig. 4.3.7), the trace element data show typical island arc basalt trace element patterns, with enriched LILEs such as Rb, Ba, Pb and K relative to HFSEs such as Hf, Zr and Ti. Typical island arc lavas are enriched in LILE and LREE but depleted in HFSE, particularly in Nb, Ta, and Ti on normalized trace element diagrams (Saunders et al., 1991; Hawkesworth et al., 1993; Hawkins, 2003; Murphy, 2007). However, primitive mantle normalized multi-element plot displaying prominent positive Ta suggests OIB like trace element patterns and which might have originated in a subduction zone geodynamic setting.

5.1.3 a. *Crustal Contamination*

Negative Nb anomaly in the multi-element patterns (Fig. 4.3.7) along with enriched LREE patterns (Fig. 4.3.8) for the basic granulites indicate possibility of crustal contamination for its precursor magma. Further, high La/Nb ratios (0.86 – 1.78) with an average value of 1.5 for the basic granulites also indicate crustal involvement (see e.g. Hasse *et al*., 2000). But the high Ce/Pb values (18.94 – 31.63) and low Ba/Nb values (9.14 – 23.87) do not reflect any such contamination signature. Incompatible elements such as La or Ba should increase relative to Nb if basaltic magma is contaminated by crustal material, which usually has high La/Nb, Ba/Nb and low La/Ba (Weaver and Tarney, 1984; Wedepohl, 1995). The studied samples show increase in La with increase in Nb, but the correlation of Ba/Nb and La/Ba is not very clearly established which can also be due to limited number of samples. It follows therefore that contributions of crustal material is very limited. The observed LREE

enrichment may be either due to subduction of crustal material into the mantle or due to metasomatism of mantle.

The basement rocks of shillong plateau consist of granite gneisses, which are exposed quite ubiquitous throughout the plateau. For comparison and to check for the possibility of any contamination at crustal level, the mantle normalized data of the host granite gneisses are plotted in the multi-elemental spider diagram (Fig. 5.4). The host granite gneisses share similar patterns and similar level of enrichment for individual element in the spider diagram. These are enriched in both large ion lithophile elements (LILE) and high field strength elements (HFSE) compared to primordial mantle (PM) except for Ti, P Y, Yb and Lu of only one sample. The patterns have distinct Nb, Sr, P, Zr and Ti negative anomalies. Moreover, the level of enrichment of Nb, Sr, P, Zr and Ti contents of the basic granulites are higher than those in the host granite gneisses. Thus considering the whole set of data it becomes apparent that the geochemical signatures of the granulites are not much affected by crustal contamination. Their geochemical characteristics represent source characteristics or contamination of crustal material at mantle level.

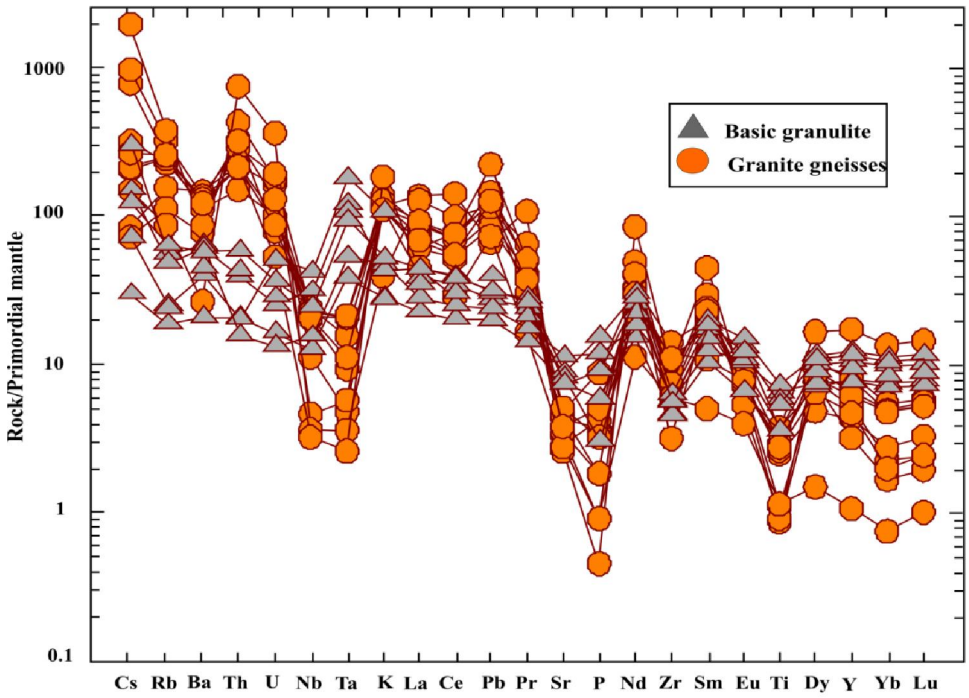

Figure 5.4: Primordial mantle normalized multi-element patterns for the Basic granulites and the basement granite gneisses of Shillong Plateau. Normalizing values are from Sun and McDonough, (1989).

5.1.3 b. *Fractional crystallization*

Both major and trace element data are sensitive to the effects of fractional crystallization (Cox et al., 1979). Basic granulites are characterized by high SiO_2, Al_2O_3 and CaO moderate high Fe_2O_3 medium to low MgO and low to moderate TiO_2 and low Na_2O and K_2O. These geochemical features point towards fractional crystallization of some of the mineral phases. Both CaO and Al_2O_3 for the basic granulites show a decreasing trend against Mg # plot (Figure not shown). CaO/Al_2O_3 of basic granulites is always lower than that of chondrite (0.9). These features account for clinopyroxene, olivine ± plagioclase fractionation for the basic granulites. Ni and Cr show positive relationship with Mg # **(**Figure not shown**)**. Negative anomalies of Sr in the multi elemental spider diagram for the dykes (Fig. 4.3.7) and negative anomalies at Eu in the REE plot (Fig. 4.3.8) of the granulites also indicate plagioclase fractionation.

Alle`gre *et al*., 1976 deduced that Ni concentrations between 130 and 200 ppm can be derived by 15% fractional crystallisation of olivine from a mantle derived primitive magma with 300–450 ppm Ni. The low Ni content of the basic granulites (13 – 67 ppm) thus indicates that the precursor basaltic magma was derived from a olivine-poor source material or this may be derived from a less primitive magma. Nb and Y show increases with decreasing MgO as predicted by the fractionation of plagioclase, olivine and pyroxene. The low Ni/V (0.04 – 0.34) and Zr (~56.49) contents also suggest olivine fractionation.

5.2 TECTONIC IMPLICATIONS

5.2.1 **Granite gneisses**

Several attempts have been made to discriminate granitoids of different tectonic settings based mainly on some critical trace element abundances; because the major element concentration of granitoids from different tectonic environments are observed to exhibit gross similarities. Besides, the major elements being mobile, any inferences on the mode of emplacement of magma based on their concentrations may not be reliable. However, anorogenic, orogenic, syn-collisional and post-collisional granitoids probably cannot be distinguished in any straight forward basis based on their trace element chemistry either, because they share a common range of trace element concentrations. Since trace element discrimination diagrams more accurately

reflect distinct chemical source reservoirs than tectonic setting characteristics (Pearce et al., 1984), therefore it is not surprising that the same source region might have been tapped during the evolving tectonic setting scenario. For instance, present arc or syn-collisional sources might have been tapped as "within plate" sources and may have become source for collision magmatism. However the compositional diversity of the magma of different tectonic settings is also not unexpected and as a result, a lot of empirical tectonic discrimination diagrams are drawn based on the study of the geochemical characteristics of rocks of known tectonic settings and later, these diagrams are extrapolated to understand the geodynamic environment for other suites (Pearce et al., 1984; Harris et al., 1986) and construct paleo-tectonic environment. Pearce et al. (1984) have empirically drawn tectonic discrimination diagrams using some trace elements into four main groups: (i) Ocean ridge granite (ORG) - associated with ophiolite or belongs to oceanic crust (ii) Volcanic arc granite (VAG) – formed due to subduction of oceanic crust (iii) Within plate granite (WPG) – anorogenic granite and (iv) Syn-collisional granite (syn-COLG) – evolved as a consequence of continent-continent, arc-continent or arc-arc collisions. The granite gneisses of Shillong plateau are plotted on a number of tectonic discrimination diagrams (Figs. 5.5) of Pearce et al. (1984) and Pearce (1996) based on Rb vs. Y+Nb; Nb vs. Y; Rb vs. Yb+Ta and Ta vs. Yb. In the Nb vs Y discrimination diagram the gneissic suites plot within the common field for VAG and syn-COLG. In the Rb vs. Yb +Ta diasgram the granite gneisses are plotting within the Volcanic Arc Granite (VAG) field. In the Ta vs. Yb granite gneisses are plotting confined within VAG. In the Rb vs. Y+Nb granite gneisses are mostly plotting within VAG filed except two samples plot within WPG and one within Syn-COLG. Thus with a view to reconstruct the paleo-tectonic settings of the emplacements of the protoliths for the Granite gneisses of Shillong plateau it appears that these rock suites were emplaced in an arc related magmatic setting.

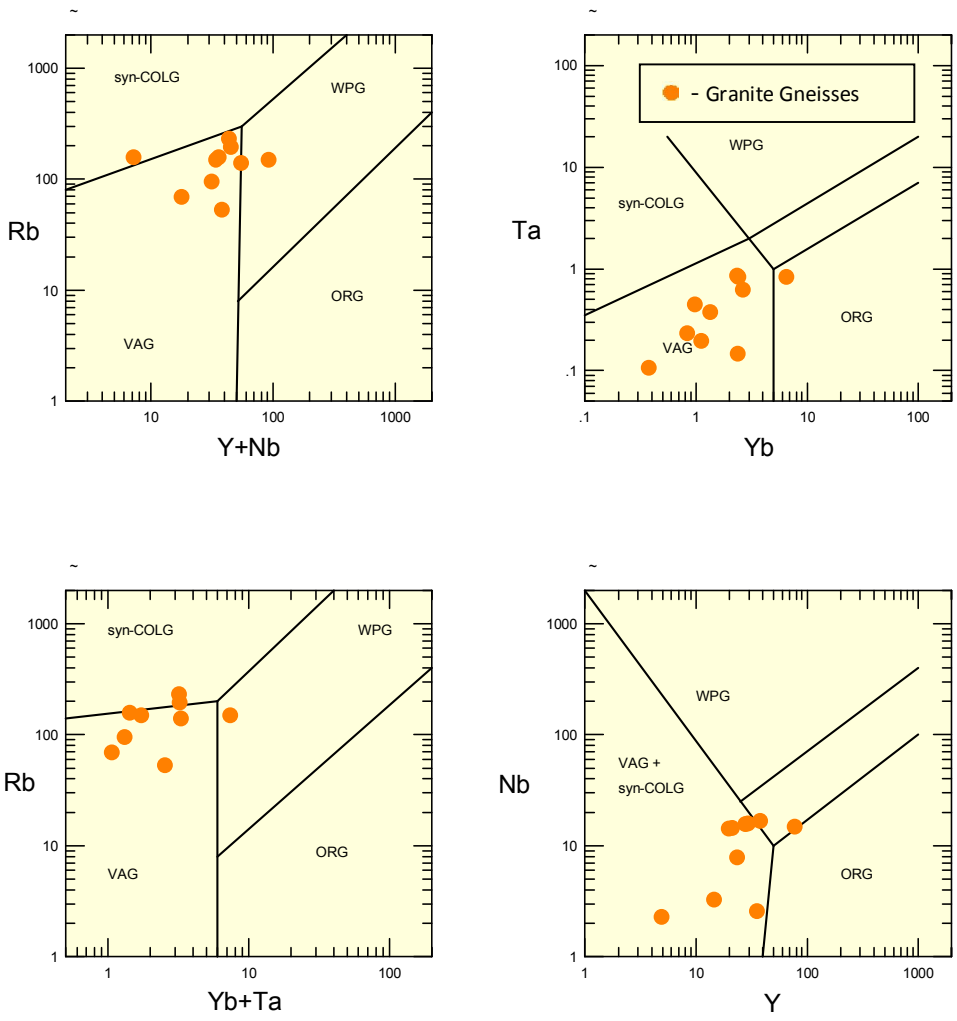

Figure 5.5: (a) Rb vs. Y + Nb (b) Rb vs. Yb + Ta, and (c) Nb vs. Y (d) Ta vs. Yb discriminant diagrams for the granite gneisses of the Sonapahar area allowing reproducing the tectonic environments in which the granitoids were produced. Compositional fields of the granitoids: post-COLG—postcollision, syn-COLG—collision, VAG—island-arc, WPG—within-plate, ORG—oceanic ridges. The dashed lines in the Nb vs. Y and Ta vs. Yb diagrams mark the ORG boundary for normal rifts.

5.2.2 **Basic granulites**

Based on major and trace element abundance and ratios of modern basaltic rocks many tectonomagmatic geochemical discriminant diagrams have been proposed (e.g. Pearce, 1982, 1983; Pearce and Norry, 1979; Pearce and Cann, 1973; Mullen 1983, Pearce et al., 1984). These discriminant diagrams are now being widely used in paleo-tectonic reconstruction. But it has been observed that many of these discrimination diagrams always overlap some portion of the fields of other tectonic setting and as a result, interpretation becomes more misleading and ambiguous. Most of the diagrams are not very useful to discriminate continental basalt, from oceanic basalt; the majority of the data on continental basalts plot in every fields except within plate basalt field. Because the data on continental basalt do plot in other fields such as MORB and arc basalts, the discriminating ability of these diagrams is impaired. Nevertheless these diagrams are widely used by geologists since these were propounded.

Four discrimination diagrams based on Ti, Mn, P, Sr, Zr and Y contents (Mullen, 1983; Pearce and Cann, 1973; Pearce and Gale, 1977 and Pearce and Norry, 1979) were chosen to constrain the tectonic setting of the protolith of basic granulites of Shillong plateau. On Zr – TiO_2 discrimination diagram (after Pearce and Cann, 1973), all the samples plot within the field of arc basalt overlapping MORB (Fig.5.6a). In the TiO_2 - MnO- P_2O_5 tectonomagmatic discrimination diagram (Mullen, 1983) (Fig. 5.6d), all the basic granulites fall in the field of island arc tholeiites (IAT). Other diagrams such as Zr - Ti/100 - Sr/2 and Ti/Y vs. Zr/Y are also applied to the discrimination of the tectonic environment. In all these diagrams, the basic granulite samples fall within the field of island arc tholeiite or Plate Margin basalts (Figs. 5.6b, c). These results indicate that the protolith of basic granulites of Shillong plateau probably formed in a volcanic island arc tectonic setting.

Condie (1989) proposed basalt classification schemes using the ratios of immobile elements (e.g, Ti/V, Ti/Y, Zr/Y and Ti/Zr) for Archean and Proterozoic basic rocks. According to Condie (1989), Ti/V =30 is the boundary between the arc basalt (ARCB) [or N-type mid oceanic ridge basalt (NMORB)] and the MORB [or within plate basalt (WPB)]. Ti/V values of the basic granulites of Shillong plateau ranges between 33.08 and 41.14 minus two samples with Ti/V values less than 30. The basaltic rocks of tholeiitic to calc- alkaline composition are found almost

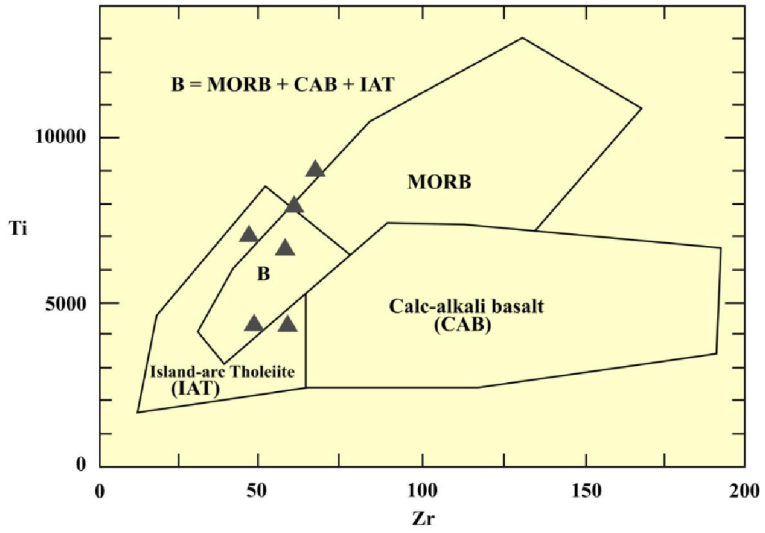

Figure 5.6a: Zr vs. Ti discrimination diagram for basic granulites of the Sonapahar area, Shillong Plateau (after Pearce and Cann 1973).

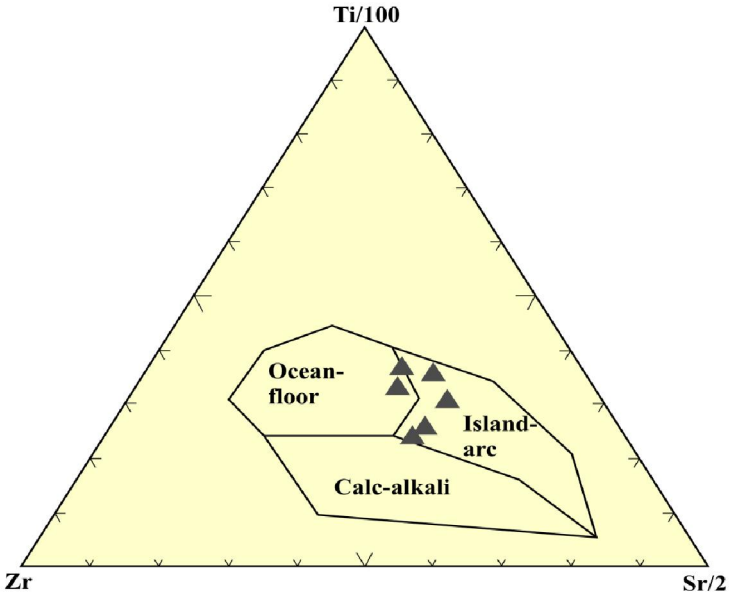

Figure 5.6b: Zr - Ti/100 -Sr/2 tectonic discrimination diagram for basic granulites of the Sonapahar area, Shillong Plateau (after Pearce and Cann, 1973).

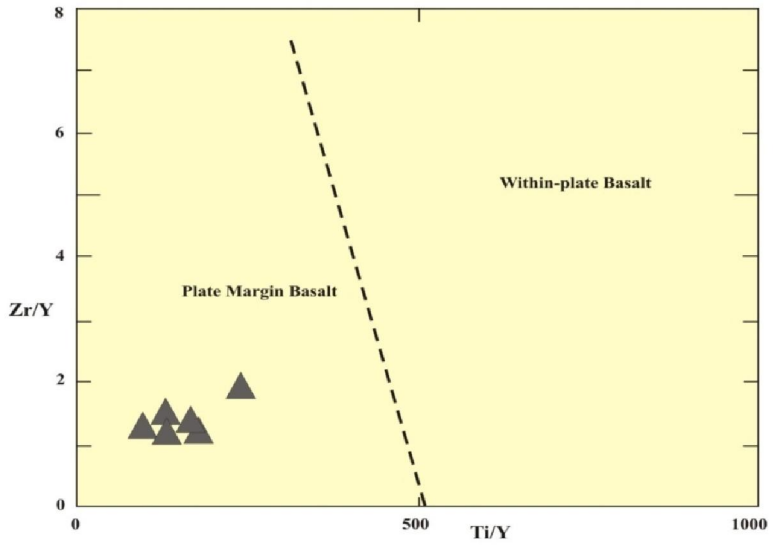

Figure 5.6c: Ti/Y vs. Zr/Y chemical discrimination diagram for tectonic environments of basic granulites from the Sonapahar area, Meghalaya (after Pearce and Galle, 1977)

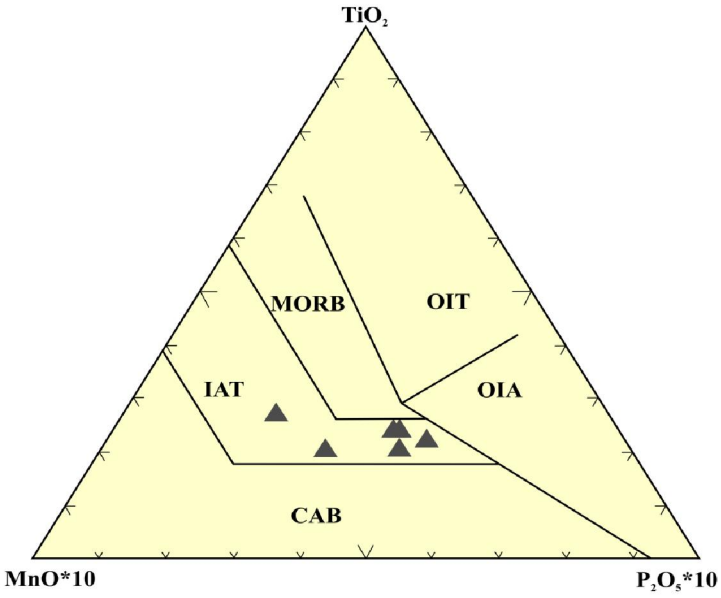

Figure 5.6d: TiO_2-MnO-P_2O_5 tectonomagmatic discrimination diagram (after Mullen, 1983) for basic granulites of the Sonapahar area. OIT: Oceanic island Tholeiite, OIA: Oceanic island alkali; MORB: Mid ocean ridge basalt, IAT: Island arc tholeiite, CAB: Island arc calc alkali basalt.

exclusively in subduction related tectonic environment (Pearce, 1983). The LILE enrichment and low HFSE abundances of the basic granulites of Shillong Plateau also attest to subduction related magmatism for their precursor magma.

5.3 PETROGENETIC EVOLUTION

Reliable geochemical as well as geochronological data on the basement rocks of Shillong Plateau consisting of granite gneisses, metapelites, sillimanite schists and basic granulites are very scarce. Thus in absence of quality geochronological data and geochemical data on the basement rocks, it seems difficult to constraints the evolution of Shillong Plateau. An approach is made to constraint the evolution of the Shillong Plateau using the few available geochronological data on the basement rocks and geochemical data synthesized for this present work.

As observed in the field, granite gneisses constitute the host rock for other rock units in the basement rocks of the Sonapahar area. Metapelites are intimately associated with the host rocks. Basic granulites occur as concordant and discordant intrusive within metapelites.

Ghosh *et al*., (2005) assigned ages for the basement gneisses to vary between 1714 and 1150 Ma. Mitra (1988) obtained Pb–Pb detrital zircon ages of 1530–1550 Ma for the Shillong Group of supracrustals. The detrital zircons are probably derived from the basement gneisses. There is periodic granite plutonism within the basement gneisses. Different works (e.g Ghosh *et al*., 1991; 1994; Chimote *et al*., 1988; Selvan *et al*., 1995) are assigning ages of emplacement for the emplacement for the undeformed granite pluton ranging between ca. 890 – 480 Ma.

Maibam and Deomurari (2007) carried out ^{207}Pb–^{206}Pb zircon age data of basement gneisses in different parts of the Shillong Plateau and obtained an Archaean age of about 2600 Ma. However they have yielded ages of about 1500 Ma for the gneisses from Riangdo which is very close to the present study area. A very recent geochronological work done by Yin *et al*., (2010), suggests an age of about ca. 1600 Ma for the basement gneisses.

The timing of metamorphism in the basement rocks has been determined by chemical ages of metamorphic monazites from the metapelites of Shillong Plateau by Chatterjee et al., (2007) with ages clustering at 1600 – 1400 Ma, 1000 – 1300 Ma, and

ca. 500 Ma respectively. Similarly, the timing of tectonothermal activity within the basement rocks has been determined by Yin *et al.,* (2010) conducting U-Pb datings on zircons from undeformed granitoids and basement gneisses and on detrital zircons from Shillong Group of Sedimentary rocks. Their works reveals three distinct episodes of tectonothermal events at ca. 1600 Ma, ca. 1100 Ma and ca. 500 Ma and three ductile deformation events at ca. 1100 Ma, ca. 520 – 500 Ma and during the Cretaceous. Thus looking from the geochronological data, it appears that the Shillong Plateau experienced episodic rather than semi-continous tectonothermal events.

Yin *et al*., (2010) described the first two tectonomagmatic events (i.e ca. 1600 Ma and ca. 1100 Ma) within Shillong Plateau as contractional and suggested these are possibly induced by assembly of Rodinia and Eastern Gondwana. The tectonomagmatic events have been related to magmatic arc developments and subsequent terminal continental collision that form the proto-continent (Shillong Plateau) (Yin *et al*., 2010) (Fig. 5.7). The geochemical signatures of the basement gneisses with multi-element spider diagrams, REE patterns and tectonic discrimination diagrams (Figs. 4.1.9, 10; 5.5) accord well with volcanic magmatism signatures.

The 1100 Ma event in Northeastern India correlates well with the development of the Eastern Ghats orogenic belt during collision between India and Antartica (Kelly *et al*., 2002). They further suggested that the first separation from Antartica did not occur until the late Proterozoic during the deposition of the Shillong Group. It was likely that the depositions of metapelites are coeval with deposition of Shillong Group of sediments. After deposition of these sediments, the westward oceanic subduction started below the eastern Indian margin and produced arc magmatism between 520 - 480 Ma and the closure of the ocean between India and Antartica led to the formation of Eastern Gondwana (Meert, 2003; Collins and Psarevsky, 2005; Collins *et al*., 2007). Intense regional contraction occurred between 520 Ma and 500 Ma, which was expressed by the development of the central Shillong thrust and isoclinals folding in the Shillong Group of metasediments and the post kinematic plutons with ages ranging from ca. 500 Ma – 480 Ma or even younger, might have generated after the collision between Antartica and India (Yin *et al*., 2010).

The tectonomagmatic events at ca. 1600 Ma of Yin *et al*., (2010) could therefore be correlated with the emplacement of the precursors for basement gneisses

of Shillong Plateau which subsequently might have suffered the ductile-deformation at ca.1100 Ma possibly due to collision of Eastern Gondwana and Rodinia.

Despite gap in ages, granite gneisses and metapelites of the Shillong plateau shows a remarkable similarity in their geochemical characteristics in various aspects. It is therefore reasonable to assume that metapelites were derived from granite gneisses. The exhumation of granite gneisses possibly started subsequent to assemblage of Rodinia and Eastern Gondwana. As soon as these rocks were exposed to the surface, the deposition of sedimentary materials, mainly derived from these granite gneisses took place. This assumption was strongly supported by the fact that all analysed samples of metapelites display Post Archean nature of sediments.

For the basic granulites, no geochronological data are available so far. Therefore it is difficult to make assumption regarding the time of emplacement of the precursor magma to the basic granulites. However, on the basis of field relationship it can be ascertained that basic granulites are younger than metapelites as it occurs as intrusive within metapelites.

Chatterjee *et al*., (2007) interpreted four metamorphic episodes based on the textural relations in metapelites in which the last episode represent post-tectonic. In the present study, a spectacular example of synkinematic prophyroblast growth is provided by the so-called snowball garnets, which have spiral trails of biotite inclusions (Plate 7A). Keeping this in mind, ca. 520-500 Ma deformation events of Yin *et al*., (2010) seems responsible for the prograde metamorphism in metapelites and basic granulites of Shillong plateau.

Lal *et al.* (1978) suggested that the metamorphic equilibrium pressure–temperature (*P–T*) conditions of the Sonapahar granulites including the corundum–spinel–sapphirine metapelites are 750^0C and 5 kbar. Keeping the average geothermal gradient (35^0/Km) in mind, such a high temperature could be expected only deep inside the crust, specifically middle to lower continental crust. However, it is not very likely for metapelites to be buried at such depth. Therefore, it is possible to assume that the last igneous activity proposed by Yin *et al*., 2010 could be also responsible for high temperature conditions of metamorphism within Shillong plateau.

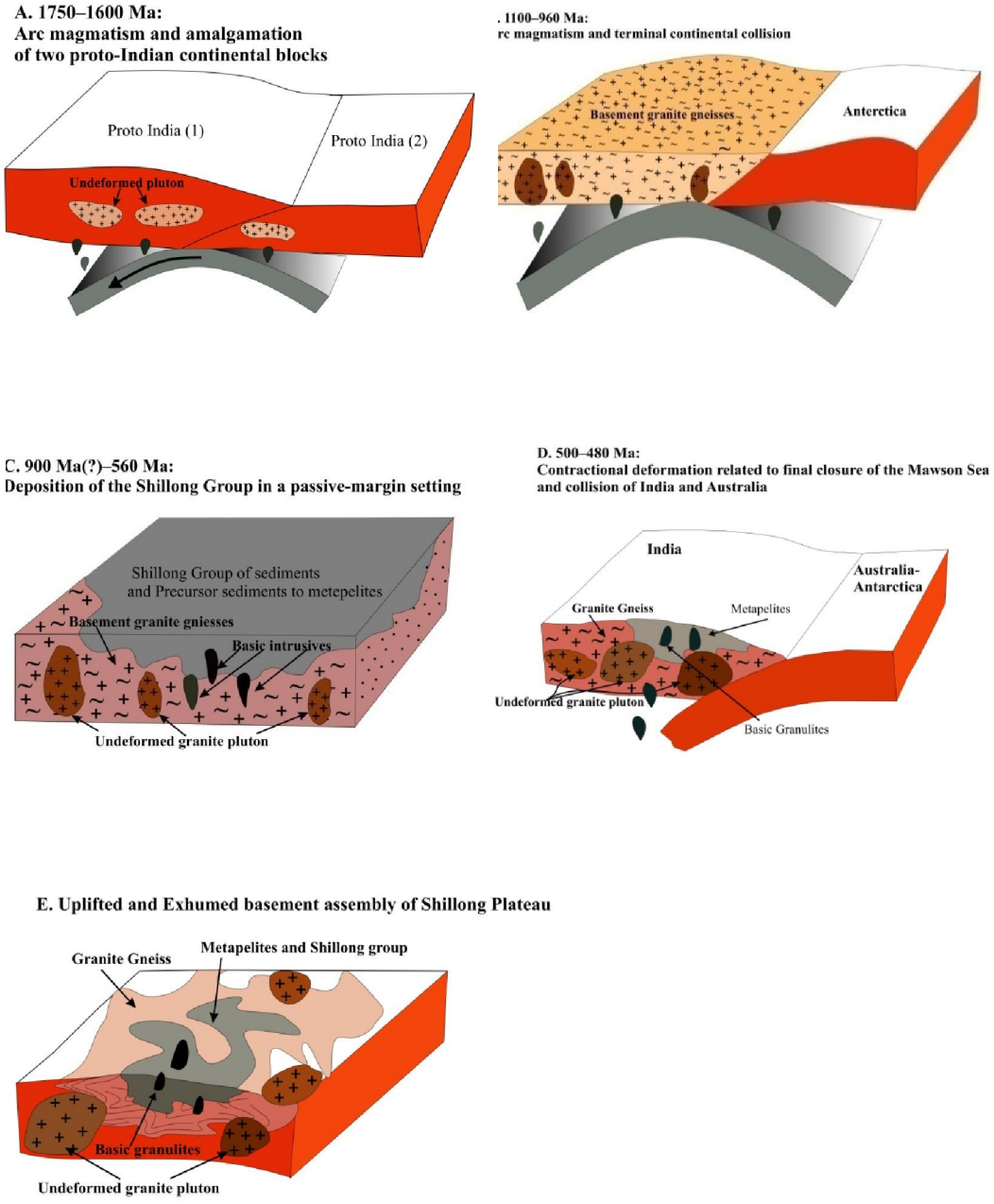

Figure 5.7: Schematic diagrams showing possible evolutionary history of basement rocks Shillong plateau. (A) 1750–1600 Ma: magmatism and amalgamation of two proto-Indian continental blocks. (B) 1150–950 Ma: arc magmatism and collision of India-Antarctica and Australia belt. (C) 900 Ma(?)–560 Ma: deposition of the Shillong Group in a passive-margin setting. (D) 500–480 Ma: Contractional deformation related to fi nal closure of the Mawson Sea and collision of India and Australia (E) Exhumed basement rocks of Shillong plateau

Chapter- 6

SUMMARY AND CONCLUSION

SUMMARY AND CONCLUSION

Shillong plateau is a prominent Precambrian Gneissic Complex, occurs in Northeast India. The basement of Shillong plateau consists of granite gneisses, metapelites, basic granulites and quartz bearing sillimanite schists. The Proterozoic Shillong Group of meta-sedimentary rocks overlies the basement and the granitic plutons (881 to 479 ma old) intrusive into both the basement and the Shillong group of rocks. Detailed geochemical and geochronological data are not available, where available; they are sketchy and not qualitative. As a result, petrogenetic history of these rocks and their geodynamic setting has remained elusive. Detailed work including good quality geochemical data are warranted to understand the evolution of Shillong plateau.

The quartzofeldspathic gneisses are the most voluminous and ubiquitous rock type of the plateau, and form the basement for the other rock suites of the plateau. In the field the gneisses show variation in terms of deformation, mafic contents, and texture making it difficult to map the individual gneissic units separately. Hence the entire have been taken as a single rock unit termed “granite gneisses”. In the present study we made an approach to understand the nature of the protolith of the gneisses and the petrogenesis and tectonometamorphic evolution of the granite gneisses.

Cordierite bearing granulitic gneisses (metapelites) and Quartz-Sillimanite schists are the meta-sedimentary rock suites of Shillong plateau. The metapelites overlies the granite gneisses and show gneissic foliation to massive, while quartz-sillimanite schists occur within the metapelites. We have undertaken the geochemical studies of the metapelites and the schists to understand the nature of precursor sediments and paleoenvironmental conditions of provenance area and the area of deposition of the precursor sediments to the metapelites and the schists.

Basic granulites are the intrusive rock bodies occurring within the granite gneisses and metapelites. We have undertaken the geochemical studies of the basic granulites to assess the source characteristics of the precursor mafic magmatism and to ascertain the tectonic settings for the basic granulites.

Granite-gneisses are characterized by medium to coarse grained mosaic of inequigranular, polyonal grains of mesoperthitic K-feldspar, biotite, plagioclase and quartz displaying interlocking boundaries. Various reaction, exsolution and symplectitic textures e.g. Perthite, antipertite, myrmekite and graphic intergrowth textures are well developed in the granite-gneisses. The various mineral associations of granite gneisses are*:* a) Quartz – K-feldspar – Plagioclase – Biotite, b) Quartz – Plagioclase – Biotite – K-feldspar – Garnet and c) Quartz – K- feldspar – Plagioclase – Biotite – Hornblende.

The cordierite bearing granulitic gneisses (Metapelites) are medium to fine grained melanocratic rocks with gneissose structure with exception of a few samples which are massive and showing no trace of foliation. The metapelites are mainly characterized a medium to fine grained mosaic of equant, polyonal, strain free grains of mesoperthitic K-felspar, quartz, biotite, cordierite, sillimanite, plagioclase and garnet. Four mineral associations of metapelites that are identified include: a) Garnet – Cordierite – Biotite – Sillimanite – Quartz – K-feldspar ± Plagioclase, b) Cordierite – Biotite - Sillimanite – K-feldspar – Quartz ± Plagioclase (± spinel), c) Cordierite – Biotite – Sillimanite – Quartz and d) Garnet – Cordierite – Biotite – Sillimanite - Quartz (± spinel).

Basic granulites are medium to coarse grained rocks with granulitic textures. They are mainly massive but a few samples exhibit foliation due to orientation of hornblende and biotite. The basic granulites are characterized by granulose texture of medium to coarse subidioblastic to xenoblastic crystals of orthopyroxene, clinopyroxene, hornblende, biotite and plagioclase. Two prominent mineral associations are identified which include: a) Hornblende – Clinopyroxene – Orthopyroxene – Plagioclase – Biotite – Quartz and b) Hornblende – Orthopyroxene – Plagioclase – Biotite – Quartz.

The Quartz Sillimanite Schists are characterized by well defined schistosity and contain medium–grained quartz, sillimanite, biotite with accessory rutile and zircon. Two mineral associations are identified which includes: a) Quartz – Sillimanite – Biotite ± Rutile ± Zircon and b) Quartz- Sillimanite – Biotite ± K-feldspar.

The granite gneisses of the Shillong Plateau are highly siliceous with SiO_2 content averages 71.41 wt %. The molar saturation index (A/CNK) values for the granite gneisses suggest the gneisses as being peraluminous. The granite gneisses show negative linear trends of Al, Fe, Mn, Mg and Ti, P oxides against SiO_2 on the Harker`s variation diagrams. Negative anomalies at Sr, Zr P, Ti and Nb in the spider diagram and negative anomalies at Eu in the REE patterns indicate fractional crystallization of the precursor melt to the granite-gneisses of Shillong plateau. It has been estimated that about 90% fractional crystallization of a mafic magma can yield silica-enriched rock. Felsic rocks of huge dimensions like those of the gneisses of Shillong plateau should have to be associated with even larger volumes of ultramafic and/or intermediate rocks, had these rocks been products of fractional crystallization. The absence of such large bodies of ultramafic and/intermediate rock suites within the plateau thus hints that fractional crystallization of a mafic parental melt alone was not the dominant petrogenetic mechanism associated to the precursor melts to the granite gneisses. However fractional crystallization and crustal contamination together can produce a greater volume of calcalkaline and granodioritic magmas. Enriched patterns of the incompatible elements like Rb, Th and U in the spider diagram for the granite gneisses indicate some influence of assimilation fractional crystallization mechanism. Moreover, such incompatible enrichments can also be produced due to addition from subduction zone components (Saunders et al., 1980) and possible sediment incorporation into the mantle. Major oxide data and various plots indicate the granite gneisses are of peraluminous characteristics. This indicates the possibility of contamination of a greater degree of crustal material. However, an early crystallization of hornblende can also account for the increase in alumina content of the melt and thereby can make the rocks peraluminous (McCarthy and Grooves, 1979).

The multi-elemental patterns for the granite-gneisses of Shillong plateau show moderately fractionated trends with highly enriched LILE and low abundances of HFSE along with negative anomalies of Sr, Zr P, Nb and Ti. Such elemental patterns point towards subduction zone magmatism for the precursor melts of the gneisses. The REE patterns of the granite-gneisses of Shillong plateau are strongly fractionated with enriched LREE and slightly depleted HREE along with concave upward curvature of HREE ends and negative anomalies at Eu. Such REE patterns represent

volcanic arc magmatic characteristics and invoke subduction mechanism(s) for the petrogenesis of the granite-gneisses of Shillong plateau. These petrogenetic interpretations on the granite-gneisses of Shillong plateau are also well in accordance with the tectonic discrimination plots of the rock suite. The granite-gneisses of Shillong plateau plot within the volcanic arc granite (VAG) field in the Rb vs. (Y+Nb); Rb vs. Yb+Ta; Nb vs. Y and Ta vs. Yb tectonic discrimination diagrams and thereby suggests the precursor melts to the granite-gneisses were emplaced in a subduction tectonic setting.

The metapelites are moderately siliceous with SiO_2 ranging from 57.42 – 68.61 wt % and are characterized by high Al_2O_3, MgO and Fe_2O_3 and low CaO. In general, the metapelites are more potassic than sodic.

The quartz sillimanite schists are generally siliceous and aluminous and are remarkably depleted in all other oxides. Al_2O_3 and SiO_2 together constitute more than 97 wt % in most of the samples. Among trace elements, Zr, Hf and Pb are characterized by high concentration relative to other; while all the LILEs e.g. Rb, K, Ba are characterized by low concentration. Most of the samples analysed have low La/Th and Th/U. Geochemical data and various discrimination plots suggest the protoliths of the metapelites and the quartz sillimanite schists are of sedimentary origin.

Chemical Index of Alteration (CIA) values of the metapelite samples range between 62 and 84 (average 81). Omitting S08-22 (CIA= 50) and S08-33 (CIA = 93), the eight remaining samples vary between 81 and 86 (average 75), indicating a highly weathered precursor that formed in a warm, humid climate. The quartz-sillimanite schists have an average CIA index of 99 and thus, the schists probably had a highly weathered precursor. Since granite gneiss is the only basement rock older to the metapelites, thus it appears that the precursor sediments were most possibly derived from the granite gneisses. As rare earth elements are not much affected during sedimentation, diagenesis and metamorphism, the REE plot of the metapelites shows a very conformable trend indicating a singular source for its precursor sediments and REE patterns of the metapelites conforms well to the trend defined by the granite gneisses of Shillong plateau. For the quartz sillimanite schists, both the granite gneisses and metapelites are the older rocks and were thus could have been possible sources for precursor sediments of the Schists. The high CIA and CIW values indicate

that the larger proportions of precursor sediments to quartz-sillimanite schists might have been derived from metapelites with smaller proportions from granite gneisses. More particularly, the quartz fractions might have been derived from more granite gneisses and clay fraction were most likely derived from the metapelites.

PASS normalized spider diagram exhibits that the metapelite samples, have pronounced negative P anomalies in the spider diagrams. The metapelites have large negative anomalies for Zr, and Sr and small negative anomalies for Y, and K. The metapelites possess positive anomalies for Nb, Ti, Th, Ce, La, Ba and Rb. Th, Ce and La are enriched relative to PAAS. The quartz sillimanite schists exhibits a very fractionated trend with P, Nb, Ti, Y, Sr, Ba, K and Rb are highly depleted and Zr, Th, Ce and La are enriched relative to PAAS. The spider diagram exhibits pronounced negative anomalies for Y and K and positive anomalies for Zr. The strong negative anomalies at P for almost all the metapelites and Sillimanite Schists may indicate that it stayed in solution in the form of soluble anion complexes during formation of the precursors to the sillimanite rocks. The elemental patterns for metapelites in the spider diagram with positive enrichment ratios for almost all trace elements, apart from P and Sr, Zr and Y suggest clay rich precursor sediment from continental source areas. However, the patterns for the quartz-sillimanite schists with high values for Zr, Th, Ce and La suggest that the precursors to the quartz-sillimanite schists were probably sand-clay mixtures with zircon enrichment in the sand fraction.

When compared with the REE patterns of the granite gneisses, the REE patterns of the metapelites show a remarkable similarity. From the field relationships with the granite gneisses hosting the metapelites and their ages [granite gneisses: ca. 1600 Ma (Yin *et al*., 2010); metapelites: ca. 520 Ma (Chatterjee *et al*., 2007)] it is reasonable to assume that the metapelites were derived from granite gneisses.

The basic granulites are characterized by moderately high silica, high Al_2O_3 and CaO, medium to low MgO, moderately high Fe_2O_3 and low TiO2. Mg numbers [Mg# = 100MgO/ (FeO^t+MgO)] of the basic granulites range between 46 – 58 and averages 51. The precursor melts of the basic are of subalkaline tholeiitic nature. In the primitive mantle-normalized multi-element plot for the basic granulites, the trace element data show typical island arc basalt trace element patterns, with enriched LILEs such as Rb, Ba, Pb and K relative to HFSEs such as Hf, Zr and Ti. Geochemical data and various plots including the primitive mantle normalized

comparative spider diagram of host rocks (granite gneisses) with the granulites indicate that the precursor magma bears source characteristics and was not much modified by contamination with crustal material.

While plotted on various tectonic discrimination diagrams, the basic granulite samples fall within the field of island arc tholeiite or Plate Margin basalts. These results indicate that the protolith of basic granulites of Shillong plateau probably formed in a volcanic island arc tectonic setting. The basaltic rocks of tholeiitic to calc-alkaline composition are found almost exclusively in subduction related tectonic environment (Pearce, 1983). The LILE enrichment and low HFSE abundances of the basic granulites of Shillong Plateau also attest to subduction related magmatism for their precursor magma.

The timing of metamorphism in the basement rocks has been determined by Yin *et al.,* (2010) conducting U-Pb datings on zircons from undeformed granitoids and basement gneisses and on detrital zircons from Shillong Group of Sedimentary rocks. Their works reveals three distinct episodes of tectonothermal events at ca. 1600 Ma, ca. 1100 Ma and ca. 500 Ma and three ductile deformation events at ca. 1100 Ma, ca. 520 – 500 Ma and during the Cretaceous. Thus, looking from the geochronological data, it appears that the Shillong Plateau experienced episodic rather than semi-continous tectonothermal events. The first two tectonomagmatic events (i.e ca. 1600 Ma and ca. 1100 Ma) within Shillong Plateau as contractional and these are possibly induced by assembly of Rodinia and Eastern Gondwana as suggested by Yin *et al*., (2010). The tectonomagmatic events have been related to magmatic arc developments and subsequent terminal continental collision that form the proto-continent (Shillong Plateau) (Yin *et al*., 2010). The geochemical signatures of the basement gneisses with multi-element spider diagrams, REE patterns and tectonic discrimination diagrams accord well with volcanic magmatism signatures.

The tectonomagmatic event at ca. 1600 Ma of Yin *et al*., (2010) could therefore be correlated with the emplacement of the precursors for basement gneisses of Shillong Plateau which subsequently might have suffered the ductile-deformation at ca.1100 Ma possibly due to collision of Eastern Gondwana and Rodinia.

Despite gap in ages, granite gneisses and metapelites of the Shillong plateau shows a remarkable similarity in their geochemical characteristics in various aspects.

It is therefore reasonable to assume that metapelites were derived from granite gneisses. The exhumation of granite gneisses possibly started subsequent to assemblage of Rodinia and Eastern Gondwana. As soon as these rocks were exposed to the surface, the deposition of sedimentary materials, mainly derived from these granite gneisses took place. This assumption was strongly supported by the fact that all analysed samples of metapelites display Post Archean nature of sediments. After deposition of these sediments, the westward oceanic subduction started below the eastern Indian margin and produced arc magmatism between 520 - 480 Ma and the closure of the ocean between India and Antartica led to the formation of Eastern Gondwana (Meert, 2003; Collins and Psarevsky, 2005; Collins *et al*., 2007).

For the basic granulites, no geochronological data are available so far. Therefore it is difficult to make assumption regarding the time of emplacement of the precursor magma to the basic granulites. However, on the basis of field relationship it can be ascertained that basic granulites are younger than metapelites as it occurs as intrusive within metapelites. Therefore, it is possible to assume that the last igneous activity proposed by Yin *et al*., 2010 could be responsible for high temperature conditions of metamorphism within Shillong plateau.

REFERENCES

REFERENCES

Acharya, S.K., and Ghosh, S.K., 1986b. Geology and coal resources of Siju Coalfield (eastern part) Garo Hills District, Assam. *Unpub*. *Rep of Geol. Surv. Ind. F.S,* 1967 – 68.

Alle`gre, J.C., Treuil, M., Minster, B., and Albarede, F., 1976. Systematic use of trace elements in igneous processes in volcanic suites. *Contrib. Min. Petrol,* **12**: 56 – 75.

Angelier, J., and Baruah S., 2009. Seismotectonics in Northeast India: a stress analysis of focal mechanism solutions of earthquakes and its kinematic implications. *Geophys. J. Int*, **178**: 303–326.

Arth, J. G., 1979. Some trace elements in trondhjemites – their implication to magma genesis and paleotectonic setting. In: Barker, F. (Ed.) Trondhjemites, Dacites and Related Rocks. Amsterdam: Elsevier, 123 - 132.

Arth, J. G., Barker, F., Peterman, Z. E., Friedman, I., 1978. Geochemistry of the Gabbro-diorite-tonalite-trondhjemite suites of southwest Finland and its implications for the origin of tonalitic and trondhjemitic magmas. *Jour. Petrol.*, **19**: 289 - 316.

Baksi, S.K., 1966. Stratigraphy of Barail series in south-eastern part of Shillong Plateau, Assam. *Geol. Surv. of India report.*

Baksi, A.K., 1995. Petrogenesis and timing of volcanism in the Rajmahal flood basalt province, Northeastern India. *Chem. Geo,* **121**: 73–90.

Balaram, V., Ramesh, S.L., and Anjaiah, K.V., 1996. New trace and REE data in thirteen GSF reference samples by ICP-MS. *Geostandards Newsletter*, **20**: 71-81.

Banerjee, M., Mitra, P., and Chakraborty, D.K. 1977. Ocurences of Lower Gondwana rocks in western Garo Hills, India IV. *Ind. Gond Symp India*, **1**: 71-75.

Barker, F., 1979. "Trondhjemites: Definitions, Environment and Hypothesis of Origin," in *Trondhjemites, Dacites and Related Rocks*, Ed. by F. Barker., Amsterdam: Elsevier, 1–12.

Bhattacharya, B.P., and Ray Barman., 2000. Precambrians of Meghalaya: a concept. *Geol. Surv. India. Spl. Pub,* **55**: 95-100.

Bhattacharya, P.M., Kayal, J.R., 2003. Mapping the b-values and its correlation with the fractal dimension in the northeast region of India. *J. Geol. Soc. India*, **62**: 680–695.

Bhattacharya, P.M., Majumder, R.K., and Kayal, J.R., 2002. Fractal dimension and b-value mapping in northeast India. *Current Science*, **82**:1486–1491.

Bhowmik, S.K., Basu Sarbadhikari, A., Spiering, B., and Raith, M., 2005. Mesoproterozoic reworking of Palaeoproterozoic ultrahightemperature granulites in the Central Indian Tectonic Zone and its implications. *J. Petrol*, **46**:1085–1119.

Bilham, R., and England, P., 2001. Plateau `pop-up` in the great Assam Earthquake. *Nature*, **410**: 806 - 809.

Bingen, B., and Stein, H., 2003. Molybdenite RE-Os dating of biotite dehydration melting in the high temperature granulites, S Norway. *Earth planet. Sci. Lett*, **208**:181-195.

Biswas, S., and Grasemann, B., 2005. Quantitative morphotectonics of the southern Shillong Plateau (Bangladesh/India). *Aust. J. Earth Sci*, **97**: 82 – 93.

Biswas, S., Coutand, I., Grujic, D., Hager, C., Sto¨ckli, D. and Grasemann, B., 2007. Exhumation and uplift of the Shillong plateau and its influence on the eastern Himalayas: New constraints from apatite and zircon (U-Th-[Sm])/He and apatite fission track analyses. *Tectonics*, **26**: TC6013, doi: 10.1029/2007TC00 2125.

Blein, O., Laflèche, M.R. and Corriveau, L., 2003. Geochemistry of the granulitic Bondy gneiss complex: A 1.4 Ga arc in the Central Metasedimentary Belt, Grenville Province, Canada. *Precamb. Res,* **120**:193–217.

Chao, T.T., and Sanzolone, R.F., 1992. Decomposition techniques. *Jour. Geochem. Explo,* **44**: 65-106.

Chatterjee, N., Mazumdar, A.C., Bhattacharya, A., and Saikia, R.R., 2007. Mesoproterozoic granulites of the Shillong–Meghalaya Plateau: Evidence of

westward continuation of the Prydz Bay Pan-African suture into Northeastern India. *Precamb. Res*, **152**: 1–26.

Chimote, J.S., Pandey, B.K., Bagchi, A.K., Basu, A.N., Gupta, J.N., and Saraswat, A.C., 1988. Rb–Sr whole rock isochron age from the Mylliem granite, Khasi Hills, Meghalaya. In: *Proceedings of the IVth National Smposium of Mass Spectrometry, Bangalore*, EPS 9/1-9/4.

Clark, G.S., and Subbarao, K.V., 1971. Rb–Sr isotopic age of the Kunavaram series, a group of alkaline rocks from India. *Can. J. Earth Sci*, **8**:1597–1602.

Clark, M.K., and Bilham, R., 2008. Miocene rise of the Shillong Plateau and the beginning of the end for the Eastern Himalaya. *Earth and Planetary Science Letters,* doi:10.1016/j.epsl.2008.01.045.

Coffin, M.F., Pringle, M.G., Duncan, R.A., Gladezenko, T.P., Storey, M., Millar, R.D., and Gahagan, L.A., 2002. Kerguelen hotspot magma output since 130 Ma. *J. Petrol,* **43**: 1121–1139.

Collins, A.S., and Pisarevsky, S.A., 2005. Amalgamating eastern Gondwana: the evolution of the circum-Indian orogens. *Earth- Science Reviews*, **71**: 229 – 270. Doi: 10.1016/j.earscirev.2005.02.004.

Collins, A.S., Santosh, M., Braun, I., and Clark, C., 2007. Age and sedimentary provenance of the southern granulites, South India: U-Th-Pb SHRIMP secondary ion mass spectrometry. *Precamb Res*, **155**: 125-138.

Condie, K. C., 1993. Chemical composition and evolution of the upper continental crust: Contrasting results from surface samples and shales. *Chem. Geol*, **104**: 1–37.

Condie, K.C., 1981. *Archean Greenstone Belts*. Amsterdam: Elsevier, 434.

Condie, K.C., 1989b. Geochemical changes in basalts and andesites across the Archean - Proterozoic boundary: Identification and significance. *Lithos*, **23**: 1- 18.

Cox, K.G., Bell, J.D., and Pankthrust, R.J., 1979. *The interpretation of Igneous Rocks*. London: George, Allen and Unwin.

Cox, R., Lowe, D.R., and Cullers, R.L., 1995. The influence of sediment recycling and basement composition on evolution of mudrock chemistry in the South Western United States. *Geochim. Cosmochim.Acta,* **59**: 2919 – 2940.

Crawford, A.R., 1974. Indo-Antarctica, Gondwana Land and pattern of the distortion of a granulite belt. *Tectonophysics*, **22**: 141–157.

Dasgupta, S. and Nandy, D.R., 1982. Seismicity and tectonics of Meghalaya Plateau, North-eastern India: *Proc.VII symp. On Earthquake engineering, Univ. of Roorkee,* **1**: 19-24.

Desikachar, S.V., 1974. A review of the tectonic and geological history of eastern India in terms of plate tectonics theory, *J. Geol. Soc. India*, **15**: 137 –149.

Dobmeier, C.J., and Raith, M.M., 2003. Crustal architecture and evolution of the Eastern Ghats Belt and adjacent regions of India. In: Yoshida, M., Windley, B.F., Dasgupta, S. (Eds.), Proterozoic East Gondwana: Supercontinent assembly and breakup, 206. *Geol. Soc., Special Publications, London*, 145–168.

Elueze, A. A., 1981. Dynamic metamorphism and oxidation of amphibolites, Tegina area, north western Nigeria. *Precamb. Res*, **14**: 368–379.

Evans, P., 1932. Tertiary succession in Assam. *Trans. Min. Geol. Met. Inst. Ind*. **27**: 3.

Evans, P., 1964. The tectonic framework of Assam. *J. Geol. Soc. India,* **5**: 80–96.

Fermor, L.L., 1935. General report, 1934. *Rec. Geol. Surv. Ind,* **69**: 82.

Fermor, L.L., 1936. An attempt at the correlation of the ancient schistose formations of Peninsular India. *Mem. Geol. Surv. India*, **70**: 217–324.

Fitzsimons, I.C.W., 2003. Proterozoic basement provinces of southern and southwestern Australia, and their correlation with Antarctica. In: Yoshida, M., Windley, B.F., Dasgupta, S. (Eds.), Proterozoic East Gondwana: supercontinent assembly and breakup, **206**. *Geol. Soc*., *Special Publications, London*, 93–130.

Floyd, P.A., and J.A. Winchester, 1978. Identification and discrimination of altered and metamorphosed volcanics using immobile elemnts. *Chem. Geol*, **21**: 291-306.

Fox, C.S., 1934 - 1935. Garo Hills Coal fields, Assam. Director`s General Report. *In Hero, A.M. Rec. Geol. Surv. Ind*, **71**: Pt. 1, 35.

Fox, C.S., 1934. The lower Gondwana Coal Fields of India. *Mem. Geol. Surv. Ind*, **59**: 1-386.

G.S.I., 1989. *Special Publication*, No. 23.

G.S.I., 2009. *Miscellaneous Publication*. No. 30 Part. IV. Vol. 2(ii) Meghalaya.

Garcia, M.G.M., Campos, N.M.C. and Fallick, A.E., 2003. Oxygen isotope composition and geothermometry of granulite to greenschist facies metamorphic rocks: A study from the Neoproterozoic collisionrelated nappe system, south of São Francisco Craton, SE Brazil. *Journal of South American Earth Sciences,* **15**: 871–83.

Garrels, R.M., and F.T. Mackenzie., 1971. *Evolution of sedimentary rocks*. New York: W. W. Norton & Co., 397.

Ghosh, S., Chakraborty, S., Bhalla, J.K., Paul, D.K., Sarkar, A., Bishui, P.K. and Gupta, S.N. 1991. Geochronology and geochemistry of granite plutons from East Khasi Hills, Meghalaya. *J. Geol. Soc. India*, **3**7: 331-342.

Ghosh, S., Chakraborty, S., Paul. D.K., Bhalla, J.K., Bishui, P.K. and Gupta, S.N., 1994. New Rb-Sr isotopic ages and geochemistry of granitiods from Meghalaya and their significance in middle to late Proterozoic crustal evolution. *Indian Minerals*, **48**: 33-44.

Ghosh, S., Fallick, A.E., Paul, D.K., and Potts, P.J., 2005. Geochemistry and origin of Neoproterozoic granitoids of Meghalaya, Northeast India: Implications for linkage with amalgamation of Gondwana Supercontinent. *Gond. Res,* **8**: 421–432.

Glikson, A. Y., 1978. Early Precambrian tonalite trondhjemite sialic nuclei. *Earth Sci. Res*., 151-173.

Godwin Austin, H.H., 1869. Notes to accompany geological map of the Khasi Hills. *Jour. Asiatic Soc. Bengal*, **38**: Pt. 2.

Gogoi, K., 1961-73. The Geology of the Precambrian rocks in the North- Western parts of the Khasi and the Jaintia Hills. Meghalaya. *Misc. Publ. Geol. Surv. Ind*, **23**: 37-48.

Green, T. H. and Ringwood, A. E., 1968. Genesis of the calc-alkaline igneous rocks of granitic composition. *Earth Planet. Sci. Lett*., **38**: 26-43.

Gupta, R.P., and Sen, A.K., 1988. Imprints of Ninety-East Ridge in the Shillong Plateau, Indian shield. *Tectonophysics*, **154**: 335–341.

Harley, S.L., 2003. Archean-Cambrian crustal development of East Antarctica: metamorphic characteristics and tectonic implications. In: Yoshida, M., Windley, B.F., Dasgupta, S. (Eds.), Proterozoic East Gondwana: Supercontinent Assembly and Breakup, 206. London: Geol. Soc., Special Publications, 203–230.

Harris, L.B., 1993. Correlations of tectonothermal events between the central Indian tectonic zone and the Albany Mobile Belt of Western Australia. In: Findlay, R.H., Unrug, R., Banks, M.R., Veevers, J.J. (Eds.), Gondwana Eight: Assembly, Evolution and Dispersal. Rotterdam: Balkema, 165–180.

Harris, N.B.W., Pearce, J.A., and Tindle, A.G., 1986. Geochemical characteristics of collision-zone magmatism. In: Coward, M.P., Ries, A.C. (Eds.), Collision Tectonics. London: Geological Society of London, Special Publication, 67–81.

Hasse, K.M., Műhe, R., and Stoffers, P., 2000. Magmatism during the extension of lithosphere: geochemical constraints from lavas of the Shaban Deep, Nothern Red Sea. *Chemical Geology*, **166**: 225 – 239.

Hawkesworth, C. J., Gallagher, K., Hergh, J. M., and McDermott, F., 1994. Mantle and slab contributions in arc magmas. *Annual Review of Earth and Planetary Sciences,* **21**: 175–204.

Hawkesworth, C.J., Gallanger, K., Hergt, J.M., and McDetmott, F., 1993. Mantle and slab contributions in arc magmas. Annu.Rev. *Earth Planet. Sci,* **21**: 175 – 204.

Hawkins, J.W., 2003. Geology of supra- subduction zones – implications for the origin of ophiolites. In: Dilek, Y., Newcomb, S, (Eds), Ophiolite concept and the Evolution of Geological Thought. *Geol. Soc. Am. Spec. Paper,* **373**: 227 – 268.

Irvine, T.N., and Baragar, W.R.A., 1971. A guide to the chemical classification of the common volcanic rocks. *Can. J. Earth Sci*, **8**: 523-54.

Jensen, L. S., 1976. A new cation plot for classifying sub-alkaline volcanic rocks; *Misc. Pub. Ontario, Div. Mines,* No. 66.

Johnson, S.J., and Alam, A.M.N., 1991. Sedimentation and tectonics of the Sylhet trough, Bangladesh. *Geol. Soc. Am. Bull*. **103**: 1513–1527.

Kayal, J.R. and Reena De., 1991. Microseismicitry and tectonics of northeast India, *BSSA*, **81(1)**: 131–138.

Kayal, J.R., 1987. Microseismicity and source mechanism study: Shillong Plateau, northeast India. *Seismological Society of America Bulletin*, **77**: 184–191.

Kayal, J.R., 2001. Microearthquake activity in some parts of the Himalaya and the tectonic model. *Tectonophysics*, **339**: 331–351.

Kayal, J.R., Arefiev, S.S., Barua, S., Hazarika, D., Gogoi, N., Kumar, A., Chowdhury, S.N. and Kalita, S., 2006. Shillong plateau earthquakes in northeast India region: Complex tectonic model. *Curr. Sci*, **91(1)**: 109 – 114.

Kayal, J.R., Zhao., and Dapeng., 1998. Three-Dimensional seismic structure beneath Shillong Plateau and Assam Valley, Northeast India. *Seismological Society of America Bulletin*, **88**: 667–676.

Kent, R.W., Pringle, M.S., Mu¨ller, R.D., Saunders, A.D., and Ghose, N.C., 2002. $^{40}Ar/^{39}Ar$ geochronology of the Rajmahal Basalts, India, and their relationship to the Kerguelen plateau. *J. Petrol*, **43**: 1141 – 1153.

Khan, P.K., 2005a. Mapping of b-value beneath the Shillong Plateau. *Gond. Research*, 8: 271–276.

La touch, T.H.D., 1887. Geology of Garo Hills Rec. *G.S.I*, **20**: 40-43.

Lal, R.K., Ackermand, D., Seifert, F., and Haldar, S.K., 1978. Chemographic relationships in sapphirine-bearing rocks from Sonapahar, Assam, India. *Contrib. Miner. Petrol*, **67**: 169–187.

Le Bas, M.J., Le Maitre, R.W., Streckeisen, A., and Zanettin, B., 1986. A chemical classification of volcanic rocks based on the total silica diagram. *J. Petrol,* **27**: 745 – 750.

Leake, B.E., 1964. Chemical distinction between ortho and para amphiboles, *J. Petrol*, **5**: 238 – 254.

Leyleroup, A., Dup y, C. and Andrian-mbolona, R., 1977. Chemical Compositionand consequence of Evolution of the French Massive Central Precambriancrust. *Mineral Petrol*, **62**: 283–300.

Li, Y.-H. 1991: Distribution patterns of the elements in the ocean: A Synthesis. *Geochimica et Cosmochimica Acta* 55: 3223-3240.

Li,Y.-H. 2000: *A compendium of Geochemistry*. New Jersey: Princeton University Press, 475.

Mahato, S., and Bhattacharya, A., 2006. Thermotectonic significance of the Eastern Ghats Belt Frontal Thrust, India. *Gond. Res.*, submitted for publication.

Mahoney, J. J., MacDougall, J. D., Lugmair, G. W., and Gopalan, K., 1983. Kerguelen hotspot source for the Rajmahal Traps and Ninetyeast Ridge?; *Nature,* **303**: 385–389.

Maibam, B., and Deomurari, M. P., 2007. Geochronological constraints onthe evolution of Meghalaya massif, northeastern India: An ion microprobe study. *Curr Sc*, **93**: No. 11, 1620-1623.

Mallet, F.R., 1876. On the coal field of Naga Hills, bordering the Sibsagar and Lakhimpur districts, *Mem. GSI*, **12**: 1-99.

Mamallan, R., Kumar, D and Bajpai, R. K., 1994. Jasra ultramafic–mafic–alkaline complex: A new find in the Shillong Plateau, northeastern India; *Curr. Sc,* **66**: 64–65.

Maniar, P.D., and Piccoli, P.M., 1989. Tectonic discrimination of granitoids. *Geol. Soc. America Bull*, **101**: 635-643

MARC, D. 1992. Granites and rhyolites from the northwestern USA: temporal variation in magmatic processes and relations to tectonic setting. Transactions of the Royal Society of Edinburgh, Earth Sciences **83**, 51-64.

Martin, H., 1993. The mechanisms of petrogenesis of the Archean continental crust. Comparison with modern processes. *Lithos*, **30**: 373-388.

Martin, H., 1994. The Archaean grey gneisses and the genesis of continental crust. *In*: K.C. Condie, Ed., The Archaean crustal evolution. *Developments in Precambrian geology*, Elsevier, **11**: 205-259.

Martin, H., 1986. Effect of steeper Archaean geothermal gradient on geochemistry of subduction-zone magmas. *Geology,* **14**: 753-6.

Mazumder, S.K., 1968. Geological mapping in parts of the Khasi Hills, Assam. *Geol. Surv. Ind. Prog. Rep. for field season 1967-1968* (unpublished).

Mazumder, S.K., 1976. A summary of the Precambrian geology of the Khasi Hills, Meghalaya. *Geol. Surv. India, Misc. Pubc*, **23**: 311 – 324.

Mazumder, S.K., 1965. A summary of the Precambrian geology of the Khasi Hills, Meghalaya. *Misc. Pub. Geol. Surv. India*, No. 23. (in press).

McCarthy, T. S. and Grooves, D. I., 1979. The Blue Tier Batholith, Northeastern Tasmania – a cumulate-like product of fractional crystallization. Contrib. *Miner. Petrol.,* **71**: 193-209.

McLennan, S.M., Lance, W.B., and Taylor, S.R., 1980. Rare Earth Element - Thorium correlation in sedimentary rocks, and the composition of continental crust. *Geochim. Cosmochim. Acta,* **44**: 1833-1839.

McLennan, S.M., 1989. Rare Earth Elements in Sedimentary Rocks: Influence of Provenance and Sedimentary Processes. *Geochemistry and Mineralogy of Rare Earth Elements*, **21**: 169–200.

McLennan, S.M., Taylor, S.R., McCulock, M.T., and Maynard, J.B., 1990. Geochemical and Nd-Sr isotopic composition of deep sea turbidites: Crustal evolution and plate tectonic associations: *Geochim. Cosmochim.Acta*, **54**: 2015-2050.

Medlicott, H.B., 1869. Geology sketch of the Shillong plateau, *Mem.G.S.I*, **7**: 151-207.

Meert, J.G., 2003. A synopsis of events related to the assembly of eastern Gondwana. *Tectonophysics*, **362**: 1-40, doi: 10. 1016/s0040-1951(02)00629-7.

Mezger, K., and Cosca, M.A., 1999. The thermal history of the Eastern Ghats belt (India) as revealed by U-Pb and 40Ar/39Ar dating of metamorphic and

magmatic minerals: implications for the SWEAT correlation. *Precamb. Res*, **94**: 251–271.

Mitra, S.K., 1988. Structure, sulphide mineralization and age of the Shillong Group of rocks, Meghalaya. *M.S. Krishnan Commemorative National Seminar, November 1–2, Calcutta*, 118–119.

Mukerjee, P.N., 1939. General report. *G.S.I. Rec*, **74**: 74.

Mukhopadhyay, M., 1984. Seismotectonics of transverse lineaments in the eastern Himalaya and its foredeep. *Tectonophysics*, **109**: 227–240.

Mullen, E.D., 1983. MnO/TiO2/P2O5: a minor element discriminant for basaltic rocks of oceanic environments and its implications for petrogenesis. *Earth Planet Science Letters,* **62**: 53–62.

Murphy, J.B., 2007. Arc magmatism II: geochemical and isotopic characteristics. *Geosci. Can,* **34**: 7- 35.

Murthy, M.V.N., Talukdar, S.C., Bhattacharya, A.C., and Chakraborty, C., 1967. Basement controlled volcanism, sedimentation and tectonics in the Assam Plateau, N.E India. *Paper presented at seminar on Geology of N.E India, Shillong*.

Nambiar, A.R., 1988. Petrology of the lamprophyres from East Garo Hills and West Khasi Hills District, Meghalaya; *J. Geol. Soc. India,* **32**: 125–132.

Nandy, D.R., and Das Gupta, S., 1986. Application of remote sensing in regional studies- A case study in Northeastern part of India. *Proc. Int. Sem. On Photogrametry and remote sensing for developing countries*, **1**: T.4-P/6.1-T.4-P/6.4.

Nandy, D.R., 2001. *Geodynamics of North Eastern India and the adjoining region*. Calcutta: ACB Publication, 120.

Nandy, D.R., 1980. Tectonic patterns in northeastern India. *Indian J. Earth Sci*, **7**: 103 – 107.

Nesbitt H.W. and Young G.M., 1982. "Early Proterozoic Climates and Plate Motions Inferred from Major Element Chemistry of Lulites," *Nature,* **299**: 715–717.

Okonkwo , C.T., 1992. Structural geology of basement rocks of Jebba area, Nigeria. *Journal of Mining and Geology*, **28(2)**: 203–209.

Okonkwo, C.T., and Winchester, J.A., 1998. Petrochemisry and Petrogenesis of Migmatitic Gneisses and Metagreywackes in Jebba area southwestern Nigeria. J*ournal of Mining and Geology*, **36 (1)**: 1–8.

Oldham., 1858. On the Geological Structure of the Khasi Hills, Bengal. *Mem. Geol.Surv. India*, 1, part 2.

Owen, J.V., Longstaffe, F.J., and Greenough, J.D., 2003. Petrology of sapphirine granulite and associated sodic gneisses from the Indian Head Range, Newfoundland. *Lithos*, **68**: 91–114.

Palmer, R.V., 1923. Geology of a part of the Khasi and Jaintia Hills. *Rec. G.S.I,* **55**: 143-187.

Pandey, B.K., Gupta, J.N., and Lall, Y., 1986. Whole rock and mineral Rb–Sr isochron ages for the granites from Bihar Mica Belt of Hazaribagh, Bihar, India. *Ind. J. Earth Sci,* **12**: 157–162.

Pascoe, E.H., 1973. *A manual of the Geology of India and Burma*, 3rd Ed. Calcutta: Geological Survey of India.

Peacock, S.M., 1990. Fluid processes in subduction zones. *Science*, **248**: 329-337.

Pearce J.A., Harris N.B.W., and Tindle A. G., 1984. "Trace Element Discrimination Diagrams for the Tectonic Interpretation of Granitic Rocks," *J. Petrol,* **25**: 956–983.

Pearce, J.A., and Gale, G.H., 1977. Identification of ore deposit environment from trace element geochemistry of associated host igneous rocks. In: Volcanic processes in ore genesis. *Geol. Soc. London. Pub*, **7**: 14 – 24.

Pearce, J.A., and Norry, M.J., 1979. Petrogenetic implications of Ti, Zr, Y and Nb variations in volcanic rocks. *Contrib. Mineral. Petrol*, **69**: 33-47.

Pearce, J.A., 1982. Trace element characteristics of lavas from destructive plate boundaries. In: Thorpe, R.S., Ed, 1982. *Andesites*, *Wiley, Chichester,* 525–548.

Pearce, J.A., 1983. Role of sub-continental lithosphere in magma genesis at active continental margins. In Hawkesworth C. J. & Norry M. J. (eds.) Continenta Basalts and Mantle Xenoliths, 230–49. *Shiva, Nantwich*.

Pearce, J.A., 1996. A user's guide to basalt discrimination diagrams. In Trace Element Geochemistry of Volcanic Rocks (D.A. Wyman, ed.). *Geol. Assoc. Can., Short Course Notes,* **12**: 79-114.

Pearce, J.A., and Cann, J.R., 1973. Tectonic setting of basic volcanic rocks determined using trace element analysis. *Earth Planet. Sci. Lett*, **19**: 290–300.

Peccerillo, A., and Taylor, S.R., 1976. Geochemistry of Eocene calcalkaline volcanic rocks from the Kastamonu area, northern Turkey. *Contrib. Miner. Petrol*, **58**: 63-81.

Pettijohn , T. J., 1975. *Sedimentary Rocks.* New York: Harper and brothers, 718.

Pharoah, T.C., and Pearce, J.A., 1984. Geochemical evidence for the geotectonic setting of early proterozoic metavolcanic sequences in Lapland *Precamb. Res*, **25**: 283-308.

Rahman, S., 1972. Petrology of Xenoliths in the Mylliem granite, Khasi and Jaintia Hills, Meghalaya. *Jour. Assam Sci. Soc*, **15(1)**: 76-81.

Rahman, S., 1981. Petrology and Petrochemistry of the greenstones occurring around Mylliem granite, Khasi Hills, Meghalaya. *Bull. Indian Geol. Assoc*, **14(2)**: 133-144.

Rahman, S., 1985. Petrochemistry of the Mylliem granite, Khasi Hills, Meghalaya. *Jour. Geol. Soc. India*, **22**: 356-359.

Rahman, S., 1987. Origin and emplacement of the Mylliem granite, Khasi Hills, Meghalaya. India. *Revista Brasileira de Geosciences*v. **17**: 660-662.

Rahman, S., 1991. Emplacement of some Precambrian granite plutons in the Shillong plateau, Meghalaya, N.E. India. *Internat. Symp. On "Granite and Geodynamics", Moscow; USSR*, 87-88 (extended abstract).

Rajendran, C.P., Rajendran, K., Duarah, B. P., Baruah S., and Earnest A., 2004. Interpreting the style of faulting and paleoseismicity associated with the 1897

Shillong, northeast India, earthquake: Implications for regional tectonism, *Tectonics,* 23, TC4009, doi:10.1029/2003TC001605.

Ramachandra, H.M., Roy, A., 2001. Evolution of the Bhandara- Balaghat granulite belt along the southern margin of the Sausar Mobile Belt of central India. *Proc. Indian Acad. Sci. (Earth Planet.Sci.),* 110/4, 351–368.

Ray Barman, T., Bishui, P.K., Mukhopadhyay, K., and Ray, J.N., 1994. Rb–Sr geochronology of the high grade rocks from Purulia, West Bengal, and Jamua-Dumka sector, Bihar. *Indian Min*, **48**: 45–60.

Rickers, K., Mezger, K., Raith, M.M., 2001. Evolution of the continental crust in the Proterozoic Eastern Ghats Belt, India and new constraints for Rodinia reconstruction: Implications from Sm–Nd, Rb–Sr and Pb–Pb isotopes. *Precamb. Res*, **112**: 183– 210.

Rollinson, H.R and Windley, B.F., 1980. Selective element depletion during metamorphism of Archean granulites, Scourie, NW Scotland. *Contrib. Min. Petrol,* **72**: 257-263.

Roy, P., Balaram, V and Kumar, A., 2007. New REE and trace element data on two kimberlitic reference materials by ICP-MS. *Geostandards and Geoanalytical Research,* **31**: 261-273.

Rudnick, R.L and Presper, T., 1990. Geochemistry of intermediate to high pressure granulites. *Granulites and Crustal Evolution, NATO ASI Series*, **311**: 523-550.

Rye, R., and Holland, H.D., 2000a. Geology and geochemistry of paleosols developed on the Hekpoort Basalt, Pretoria Group, South Africa. *Am. J. Sci*. **300**: 85–141.

Saha, A.K., 1987. Evolution of the continental crust of India: Growth of knowledge, 1900–1985. In: Saha, A.K. (Ed.), Geological Evolution of Peninsular India: Petrological and Structural Aspects, **13**. *Recent Researches in Geology*, 84–96.

Santosh, M., and Tsunogae, T., 2003. Extremely high density pure CO2 fluid inclusions in a garnet granulite from southern India. *J Geol*, **111**: 1–16.

Santosh, M., Tagawa, M., Taguchi, S., and Yoshikura, S., 2003a. The Nagercoil Granulite Block, southern India: Petrology, fluid inclusions and exhumation history. *Journal of Asian Earth Sciences,* **22**: 131–55.

Santosh, M., Yokoyama, K., Biju-Sekhar, S., and Rogers, J.J.W., 2003b. Multiple tectonothermal events in the granulite blocks of southern India revealed from EPMA dating: Implications on the history of supercontinents. *Gond Res,* **6**: 29–63.

Saunders, A.D., Norry, M.J., and Tarney, J., 1991. Fluid influence on the trace element compositions of subduction zone magmas. *Philos. Trans. R. Soc.Lond*, A 335, 377 – 392.

Saunders, A.D., Tarney, J., Marsh, N.G., and Wood, D.A., 1980. Ophiolites as ocean crust or marginal basin crust: A geochemical approach. In: Panayiotou, A., (ed). Ophiolite, *Geol. Surv. Dept. Cyprus*, 193-204.

Selvan, A.P., Prasad, R.N., Dhana Raju, R., and Sinha, R.M., 1995. Rb-Sr age of metaluminous granitiods of South Khasi batholith, Meghalaya: implication on its genesis and Pan-Africian activity in Northeastern India. *J. Geol. Soc. India*, **46**: 619-624.

Seth, B., Amstrong, R.A., Brandt, S.V., Igor, M., and Kramers, J.D., 2003. Mesoproterozoic U-Pb and Pb-Pb ages of granulites in NW Namibia: reconstructing a complete orogenic cycle. *Precamb. Res,* **126**: 147-168.

Shand, S. J., 1943. *Eruptive Rocks. Their Genesis, Composition, Classification, and Their Relation to Ore-Deposits with a Chapter on Meteorite.* New York: John Wiley & Sons.

Shaw, R.K., Arima, M., Kagami, H., Fanning, C.M., Shiraishi, K., and Motoyoshi,Y., 1997. Proterozoic events in the Eastern Ghats Granulite Belt, India: evidence from Rb–Sr, Sm–Nd systematics, and SHRIMP dating. *J. Geol*. 105, 645–656.

Sheraton, J.W., 1980. Geochemistry of Precambrian metapelites from east Antartica: Secular and metamorphic variations. *DRM J. Aust. Geol. and Geoph,* **5**: 279-288.

Spulber, D.S., and Rutherford. M.J., 1983. The origin of granite and plagiogranite in oceanic crusts: An experimental study. *Jour.Petrol,* **24**: 1.

Srinivasan, V., 2005. The Dauki Fault in northeast India; through remote sensing. *J. Geol. Soc. Ind*, **66 (4)**: 413–426.

Srivastava, R. K., 2006. Geochemistry and petrogenesis of Neoarchean high - mg low - Ti mafic igneous rocks in an intra cratonic setting, Central Indian craton: Evidence for boninite magmatism. *Geochem J*, **40**: 15 – 31.

Srivastava, R.K., and Sinha, A.K., 2004. Geochemistry of Early Cretaceous alkaline ultramafic–mafic complex from Jasra, Karbi Anglong, Shillong Plateau, Northeastern India; *Gond Res,* **7(2)**: 549–561.

Srivastava, R.K., and Sinha, A.K., 2007. Nd and Sr isotope systematics and geochemistry of plume related early Cretaceous alkaline-mafic-ultramafic igneous complex from Jasra, Shillong Plateau, Northeastern India; *Geol. Soc. Am. Spec. Paper,* 430, 815–830.

Sun, S.S., McDonough, W.F., 1989. Chemical and isotopic systematic of oceanic basalts: implication for mantle composition and processes. In: Saunders, A.D., Norry, M.J.(Eds), Magmatism in the Ocean Basins: *Geological Society of London Special Publications*, **42**: 313 – 345.

Tarney, J., 1977. Petrology, mineralogy and geochemistry of the Falkland Plateau basement rocks. Site 30, deep sea drilling project, *Initial Report*, **36**: 893–920.

Tatsumi, Y., Sakuyama, M., Fukuyama, H., and Kushiro, I., 1983. Generation of arc basalt magmas and thermal structure of the mantle wedge in subduction zones. *J Geophys Res*, **88**: 5815– 5825.

Tatsumi,Y., Hamilton, D. L. & Nesbitt, R.W., 1986. Chemical characteristics of fluid phase released from a subducted lithosphere and origin of arc magmas: Evidence from high-pressure experiments and natural rocks. *J Volcanol Geoth Res*, **29**: 293-309.

Taylor, S.R., McLennan, S.M., 1985. *The continental Crust: Its composition and evolution*. Oxford: Blackwell Scientific Publications.

Taylor, S.R., Rudnick, R.L.,McLennan, S.M., Erickson, K.A., 1986. Rare earth element patterns in Archean High Grade metasedimentsand their tectonic significance. *Geochim. Cosmochim. Acta,* **50**: 2267 – 2280.

Tsunogae, T., Osanai, Y., Owada, M., Toyoshima, T., Hokada, T. and Crowe, W.A., 2003. High fluorine pargasites in ultrahigh temperature granulites from Tonagh Island in the Archean Napier Complex, East Antarctica. *Lithos,* **70**: 21–38.

Veena, K., Pandey, B. K., Krishnamurthy, P., and Gupta, J.N., 1998. Pb, Sr and Nd isotope systematics of Sung Valley, Meghalaya, Northeast India: Implications for contemporary plume-related mantle source characteristics. *J. Petrol,* **39:** 1975–1984.

Von Platen, H., 1965. Kristallisation granitischer Schmelzen. *Contrib. Miner. Petrol*, **11**: 334-381.

Weaver , C. E., 1989. *Clays, muds and shales*. Amsterdam: Elsevier, 820.

Weaver, B.L., and Tarney, J., 1984. Empirical approach to estimating the composition of the continental crust. *Nature,* **310**: 575 – 577.

Wedepohl, K.H., 1995. The composition of the continental crust. *Geochim. Cosmochim. Acta,* **59**: 1217 – 1232.

Wheller, G. E., Varne, R., Foden, J. D., and Abbott, M. J., 1987. Geochemistry of Quaternary volcanism in the Sunda-Banda arc, Indonesia, and three-component genesis of island-arc basaltic magmas. *J Volcanol Geoth Res,* **32**: 137-160.

Yin, An., Dubey, C.S., Wedd, A.A.G., Kelty, T.K., Grove, M., Gehrels., G.E and Burge, W.P., 2010. Geologic correlation of the Himalayan orogen and Indian craton: Part I. Structural geology, U-Pb zircon geochronology, and tectonic evolution of the Shillong Plateau and its neighboring regions in NE India. *GSA Bulletin*, **122 (3/4)**: 336-359; doi: 10.1130/B26460.1.

Yu, J., Xu, X., O'reilly, S. Y., Griffin, W. L., and Zhang, M., 2003. Granulite xenoliths from Cenozoic basalts in SE China provide geochemical fingerprints to distinguish lower crust terrenes from the North and South China tectonic blocks. *Lithos,* **67**: 77–102.

Zhao, Y., Liu, X., Song, B., Zhang, Z., Li, J., Yao, Y., and Wang, Y., 1995. Constraints on the stratigraphic age of metasedimentary rocks from the Larsemann Hills, East Antarctica: possible implications for Neoproterozoic tectonics. *Precamb. Res*, **75**: 175–188.

APPENDICES

APPENDIX- I

Representative whole rock major and trace element analysis, CIPW norms and Niggli`s value of granite gneisses of Sonapahar area, Shillong Plateau

Sample No	S08-4	S08-8	S08-14	S08-26	S08-27	S08-28	S08-30	S08-32	S08-42	S08-44
Major Oxides (wt %)										
SiO_2	75.13	71.14	70.56	66.24	76.7	77.76	67.31	64.63	74.73	69.91
Al_2O_3	13.05	13.46	13.52	13.45	12.99	11.85	14.92	16.7	13.25	13.89
Fe_2O_3	1.77	3.85	4.47	6.56	0.84	1.35	5.58	7.25	1	4.5
MnO	0.02	0.04	0.03	0.08	0.01	0.02	0.06	0.11	0.01	0.03
MgO	0.43	1.11	1.21	2.17	0.08	0.73	2.09	3.31	0.44	1.48
CaO	1.32	1.78	1.83	2.89	0.7	1.37	1.87	0.72	0.36	2.04
Na_2O	3.59	3.21	3.25	2.57	3.83	3.73	2.42	1.59	2.89	3.19
K_2O	3.29	3.36	3.47	3.27	3.4	1.16	4.01	3.71	5.37	3.24
TiO_2	0.24	0.54	0.57	0.81	0.19	0.2	0.64	0.64	0.25	0.6
P_2O_5	0.02	0.08	0.09	0.19	0.01	0.04	0.07	0.04	0.02	0.11
TOTAL	98.86	98.57	99	98.23	98.75	98.21	98.97	98.7	98.32	98.99
A/CNK	1.1	1.11	1.09	1.03	1.15	1.2	1.27	2.1	1.18	1.11
CIPW Norms										
Q	42.34	33.72	15.56	44.55	44.22	15.63	41.93	34.52	33.48	41.06
C	10.53	8.38	0	18.48	11.2	1.93	9.14	9.33	8.17	13.26
Or	17.37	16.39	6.94	8.1	17.09	25.36	17.72	21.54	21.52	15.18
Ab	8.03	15.3	20.05	1.13	4.08	38.74	11.35	12.59	13.21	3.48
An	2.69	4.99	17.8	0.49	0.86	5.36	3.34	2.98	4.52	0.97
Hy(MS)	8.36	9.23	6.8	15.46	9.94	5.69	7.42	8.44	8.69	12.28
Hy(FS)	8.14	9.27	9.35	9.22	9.64	5.42	7.05	8.14	7.97	10.44
Mt	1.36	1.52	2.45	1.5	1.61	0.91	1.16	1.34	1.32	1.74
Il	1.11	1.15	2.27	0.99	1.29	0.86	0.82	1.01	1.01	1.52
Ap	0.07	0.07	0.79	0.1	0.07	0.12	0.1	0.12	0.12	0.07

Appendix- I Contd...

Sample No	S08-4	S08-8	S08-14	S08-26	S08-27	S08-28	S08-30	S08-32	S08-42	S08-44
Niggli values										
al	46.19	40.4	38.99	33.34	50.92	46.84	38.22	39.48	49.36	38.8
fm	11.82	23.12	25.16	34.37	4.96	14.1	31.75	41.75	8.84	26.39
c	8.49	9.71	9.6	13.03	4.99	9.85	8.71	3.09	2.44	10.36
alk	33.5	26.77	26.25	19.26	39.13	29.22	21.32	15.68	39.36	24.45
Si	451.24	362.38	345.35	278.69	510.28	521.61	292.65	259.29	472.46	331.39
Mg	0.33	0.36	0.35	0.4	0.16	0.52	0.43	0.47	0.47	0.4
Ti	1.08	2.07	2.1	2.56	0.95	1.01	2.09	1.93	1.19	2.14
K	0.38	0.41	0.41	0.46	0.37	0.17	0.52	0.61	0.55	0.4
P	0.05	0.17	0.19	0.34	0.03	0.11	0.13	0.07	0.05	0.22

Appendix- I Contd...

Sample No	S08-4	S08-8	S08-14	S08-26	S08-27	S08-28	S08-30	S08-32	S08-42	S08-44
Trace Elements (ppm)										
Sc	2.10	4.18	5.94	8.52	1.85	2.64	6.60	9.44	3.12	4.67
V	8.46	21.41	23.13	47.80	4.43	7.69	36.01	42.50	5.03	23.88
Cr	3.89	5.03	4.41	5.78	3.27	3.45	5.55	6.86	3.30	4.49
Co	2.40	23.63	7.66	15.00	0.70	1.64	12.18	15.88	0.96	7.78
Ni	0.76	1.17	1.17	1.66	0.65	1.12	1.65	2.56	0.63	1.17
Cu	0.27	0.34	0.30	0.55	0.24	0.25	0.54	1.15	0.25	0.54
Zn	60.95	12.43	17.87	58.88	46.57	33.56	32.86	34.48	22.22	14.19
Ga	19.12	20.08	20.47	22.07	18.05	17.04	22.58	24.18	17.55	20.27
Rb	95.42	150.51	140.31	150.56	69.44	53.48	196.64	230.94	157.06	158.66
Sr	68.45	91.02	60.28	100.39	54.76	94.19	106.55	72.46	58.55	80.06
Y	23.46	19.67	37.84	77.11	14.51	35.39	29.23	27.82	4.88	21.22
Zr	67.12	134.11	155.02	101.27	102.10	81.07	82.43	35.44	66.31	121.44
Nb	7.88	14.26	16.85	14.96	3.29	2.58	15.91	15.73	2.30	14.47
Cs	0.64	1.58	2.43	5.94	0.56	1.15	7.34	14.73	1.64	2.04
Ba	989.98	872.89	815.37	764.67	526.99	182.63	925.24	588.56	881.26	829.92
Hf	1.90	4.03	5.14	3.22	3.93	2.82	2.67	1.22	1.93	3.44
Ta	0.20	0.38	0.63	0.83	0.23	0.15	0.83	0.85	0.11	0.45
Pb	8.56	8.21	6.57	5.86	4.58	7.99	9.90	15.28	5.06	8.69
Th	18.14	26.91	18.15	12.41	35.21	60.89	23.73	26.13	17.50	17.63
U	3.32	1.61	2.05	2.05	3.60	7.31	3.91	2.65	1.09	1.79

Appendix- I Contd...

Sample No	S08-4	S08-8	S08-14	S08-26	S08-27	S08-28	S08-30	S08-32	S08-42	S08-44
Rare Earth Elements (ppm)										
La	59.63	40.69	50.62	40.84	90.85	85.12	58.14	61.54	30.15	46.13
Ce	123.59	133.37	99.52	90.43	242.79	170.40	122.10	129.83	50.45	95.12
Pr	13.48	8.18	11.15	10.30	28.96	17.52	13.34	13.80	4.47	10.10
Nd	53.19	30.00	44.31	43.46	111.43	65.07	53.17	53.96	15.06	39.72
Sm	10.33	4.75	8.75	9.78	19.45	12.79	10.47	10.01	2.22	7.61
Eu	1.28	1.33	1.22	1.66	1.20	0.89	1.54	1.22	0.67	1.28
Gd	8.29	4.37	7.59	8.73	14.07	10.38	8.32	8.25	2.00	6.47
Tb	1.14	0.57	1.19	1.63	1.62	1.47	1.25	1.15	0.23	0.90
Dy	5.67	3.57	7.28	12.05	5.52	7.62	6.66	5.98	1.10	4.73
Ho	0.48	0.38	0.74	1.38	0.35	0.70	0.59	0.55	0.10	0.43
Er	1.33	1.24	2.29	4.88	1.05	2.16	1.80	1.72	0.34	1.20
Tm	0.13	0.14	0.27	0.66	0.08	0.26	0.21	0.22	0.03	0.12
Yb	1.11	1.35	2.65	6.55	0.83	2.39	2.39	2.34	0.37	0.98
Lu	0.18	0.24	0.43	1.06	0.14	0.39	0.41	0.38	0.08	0.18
∑REE	279.84	230.19	237.99	233.41	518.34	377.15	280.38	290.96	107.24	214.96
Important ratios										
Eu/Eu*	0.41	0.88	0.45	0.54	0.21	0.23	0.49	0.40	0.95	0.54
(La/Sm)N	3.17	4.70	3.17	2.29	2.56	3.65	3.05	3.37	7.46	3.32
(La/Yb)N	32.49	18.26	11.57	3.78	66.41	21.61	14.71	15.91	48.98	28.56
Rb/Zr	11.96	28.10	11.37	9.24	12.48	13.32	11.67	12.97	22.78	12.49
Nb/Y	93.05	71.76	29.00	14.90	151.76	417.02	28.63	30.60	165.10	39.18
Th/Y	0.10	0.20	0.20	0.30	0.30	0.10	0.20	0.10	0.10	0.10

APPENDIX- II

Representative whole rock major and trace element analysis, CIPW norms, Niggli`s value and Indices of weathering and alterations etc. of metapelites of Sonapahar area, Shillong Plateau.

Sample No	S08-18	S08-21	S08-22	S08-33	S08-34	S08-37	S08-41	S08-9	S08-16	S08-6
Major Oxides (wt%)										
SiO_2	67.59	66.44	57.42	62.82	67.1	65.29	68.69	65.43	65.95	64.04
Al_2O_3	15.93	16.11	11.35	19.91	15.06	15.69	15.45	16.38	16.01	16.61
Fe_2O_3	6.8	7.74	12.2	7.45	8.02	4.55	5.77	6.66	6.59	8.69
MnO	0.07	0.11	0.18	0.12	0.07	0.07	0.07	0.1	0.08	0.11
MgO	3.29	3.69	4.13	6.07	3.89	2.23	2.91	3.3	3.42	4.8
CaO	0.57	1.04	8.13	0.15	0.21	1.12	0.71	0.65	0.96	0.23
Na_2O	0.93	1.8	2.3	0.13	0.47	4.47	1.31	1.45	1.53	0.4
K_2O	2.88	2.76	1.14	1.34	2.82	4.19	2.93	3.55	3.57	2.5
TiO_2	0.57	0.6	1.16	0.51	0.66	0.44	0.42	0.52	0.52	0.78
P_2O_5	0.03	0.03	0.33	0.04	0.03	0.05	0.04	0.05	0.05	0.03
TOTAL	98.66	100.32	98.34	98.54	98.33	98.1	98.3	98.09	98.68	98.19
A/CNK	2.8	2.05	0.57	10.3	3.58	1.13	2.33	2.21	1.97	4.37
CIPW Norms										
Q	42.34	33.72	15.56	44.55	44.22	15.63	41.93	34.52	33.48	41.06
C	10.53	8.38	0	18.48	11.2	1.93	9.14	9.33	8.17	13.26
Or	17.37	16.39	6.94	8.1	17.09	25.36	17.72	21.54	21.52	15.18
Ab	8.03	15.3	20.05	1.13	4.08	38.74	11.35	12.59	13.21	3.48
An	2.69	4.99	17.8	0.49	0.86	5.36	3.34	2.98	4.52	0.97
Hy(MS)	8.36	9.23	6.8	15.46	9.94	5.69	7.42	8.44	8.69	12.28
Hy(FS)	8.14	9.27	9.35	9.22	9.64	5.42	7.05	8.14	7.97	10.44
Mt	1.36	1.52	2.45	1.5	1.61	0.91	1.16	1.34	1.32	1.74
Il	1.11	1.15	2.27	0.99	1.29	0.86	0.82	1.01	1.01	1.52
Ap	0.07	0.07	0.79	0.1	0.07	0.12	0.1	0.12	0.12	0.07

Appendix- II Contd...

Sample No	**S08-18**	**S08-21**	**S08-22**	**S08-33**	**S08-34**	**S08-37**	**S08-41**	**S08-9**	**S08-16**	**S08-6**
Niggli Values										
al	38.07	41.28	42.58	42	40.29	37.32	38.33	38.87	19.86	38.2
fm	53.26	43.99	53.27	40.01	41.48	44.53	50.96	41.41	45.49	27.9
c	0.96	2.69	0.58	3.51	2.91	4.38	0.97	4.24	25.86	4.96
alk	7.71	12.04	3.56	14.48	15.32	13.78	9.74	15.49	8.78	28.94
Si	249.12	297.23	228.02	316.91	273.13	261.17	289.84	271.7	170.51	269.76
Mg	0.52	0.49	0.62	0.5	0.5	0.49	0.49	0.51	0.4	0.49
Ti	2.28	1.88	1.39	1.46	1.63	1.77	2.14	1.61	2.59	1.37
K	0.80	0.67	0.87	0.6	0.62	0.5	0.8	0.61	0.25	0.38
P	0.05	0.06	0.06	0.08	0.09	0.05	0.05	0.09	0.41	0.09

Appendix- II Contd...

Sample No	S08-18	S08-21	S08-22	S08-33	S08-34	S08-37	S08-41	S08-9	S08-16	S08-6
Trace Elements (ppm)										
Sc	8.11	8.05	9.01	5.65	9.08	6.06	4.42	7.26	7.44	8.26
V	39.89	41.41	34.51	35.15	41.58	30.32	26.12	38.94	42.44	50.45
Cr	6.69	6.78	6.73	7.86	5.82	3.58	5.85	7.52	6.24	7.35
Co	13.67	18.06	12.81	10.71	15.36	9.59	9.53	14.39	13.95	17.69
Ni	2.21	2.90	2.38	3.80	2.38	1.43	1.46	2.59	2.10	3.79
Cu	1.60	1.89	1.30	0.23	0.25	0.49	0.22	1.44	1.31	0.27
Zn	32.83	69.46	44.82	26.98	48.46	29.35	13.63	55.57	30.48	41.12
Ga	18.06	24.60	20.22	32.05	30.37	22.58	22.72	24.06	23.21	24.44
Rb	173.61	166.63	224.45	101.75	153.31	175.34	153.88	211.95	200.01	144.27
Sr	49.98	64.54	94.64	9.32	18.14	89.15	82.71	63.80	79.95	25.35
Y	16.46	22.32	18.80	29.63	17.37	16.95	27.27	18.66	17.58	20.65
Zr	23.94	28.78	50.68	45.50	12.46	96.66	31.63	31.52	35.82	12.78
Nb	10.64	15.03	13.76	8.01	17.15	12.45	10.66	13.61	11.12	12.40
Cs	7.13	7.06	4.87	5.24	5.06	6.97	6.45	11.26	7.43	5.56
Ba	358.47	484.94	586.19	156.26	450.38	550.25	505.30	418.70	455.57	505.29
Hf	0.80	0.93	1.66	1.59	0.45	3.06	0.99	1.07	1.21	0.46
Ta	0.36	0.63	0.81	0.58	0.60	0.72	0.60	0.97	0.51	0.65
Pb	8.70	15.71	17.80	6.50	6.38	16.71	6.29	23.08	14.77	8.37
Th	21.17	31.84	22.47	36.22	24.74	15.76	30.70	20.52	20.32	26.44
U	2.72	2.02	3.27	4.36	2.49	2.60	3.12	3.05	2.69	2.89

Appendix- II Contd...

Sample No	**S08-18**	**S08-21**	**S08-22**	**S08-33**	**S08-34**	**S08-37**	**S08-41**	**S08-9**	**S08-16**	**S08-6**
Rare Earth Elements (ppm)										
La	50.27	75.92	56.28	78.76	50.19	46.01	63.24	52.25	52.16	57.95
Ce	105.54	156.25	117.85	170.23	106.16	91.82	138.47	107.79	106.38	123.68
Pr	11.22	16.33	12.56	18.31	11.47	9.34	15.26	11.39	11.07	13.12
Nd	43.46	62.51	48.59	72.42	43.43	36.08	61.50	43.87	43.42	52.33
Sm	8.07	10.99	9.00	12.96	7.71	6.42	11.76	8.19	7.76	9.53
Eu	1.05	1.23	1.40	0.67	0.89	1.33	0.94	1.12	1.36	0.95
Gd	6.29	8.79	7.06	10.17	5.87	5.20	9.37	6.71	6.23	7.52
Tb	0.85	1.15	0.98	1.40	0.80	0.71	1.32	0.93	0.85	1.03
Dy	4.16	5.58	4.78	7.01	3.97	3.71	6.67	4.69	4.19	4.95
Ho	0.34	0.44	0.39	0.61	0.34	0.34	0.55	0.38	0.35	0.42
Er	0.94	1.16	1.05	1.71	0.95	1.06	1.43	1.00	1.00	1.09
Tm	0.07	0.09	0.09	0.01	0.09	0.14	0.12	0.10	0.08	0.09
Yb	0.57	0.67	0.74	1.15	0.72	1.67	0.85	0.94	0.69	0.71
Lu	0.08	0.10	0.11	0.17	0.12	0.29	0.12	0.16	0.11	0.09
Important ratios										
Eu/Eu*	0.44	0.37	0.52	0.17	0.39	0.68	0.27	0.45	0.58	0.33
$(La/Yb)_N$	62.82	81.65	54.40	48.95	49.87	19.73	53.24	39.78	54.16	58.30
K/Rb	137.73	137.52	42.17	109.34	152.72	198.40	158.09	139.06	148.19	143.87
Th/U	7.79	15.76	6.88	8.31	9.92	6.06	9.85	6.73	7.56	9.16
La/Th	2.38	2.38	2.50	2.17	2.03	2.92	2.06	2.55	2.57	2.19

Appendix- II Contd…

Sample No	S08-18	S08-21	S08-22	S08-33	S08-34	S08-37	S08-41	S08-9	S08-16	S08-6
CIA	78.43	74.21	49.52	92.48	81.14	61.60	75.74	74.35	72.54	84.14
CIW	91.39	85.01	52.11	98.61	95.68	73.73	88.44	88.64	86.54	96.35
PIA	89.69	82.46	49.47	98.52	94.74	67.29	86.11	85.93	83.32	95.73
ICV	0.72	0.81	1.36	0.61	0.81	0.88	0.70	0.76	0.79	0.80

CIA : Chemical index of alteration

CIW : Chemical index of weathering

PIA : Plagioclase of index of alteration

ICV : Idex of compositional variety

APPENDIX-III

Representative whole rock major and trace element analysis, CIPW norms and Niggli`s value of basic granulites of Sonapahar area, Shillong Plateau

Major oxides (wt%)

Samples	S08-7	S06-22	S08-29	S08-39	S08-40	S08-43
SiO_2	55.46	64.62	49.16	47.63	54.02	56.8
Al_2O_3	14.08	15.22	13.42	14.39	13.65	13.84
Fe_2O_3	11.25	7.74	15.06	15.81	13.35	11.95
MnO	0.16	0.13	0.19	0.2	0.19	0.15
MgO	5.64	4.53	7.89	5.8	5.35	4.67
CaO	8.14	0.11	7.64	8.5	7.51	5.6
Na_2O	2.48	1.58	1.98	2.57	2.47	2.65
K_2O	0.87	3.53	1.48	1.34	0.84	1.65
TiO_2	0.71	0.71	1.32	1.5	1.18	1.09
P_2O_5	0.12	0.06	0.25	0.33	0.25	0.19
Total	98.91	98.23	98.38	98.06	98.8	98.58
Mg#	53.88	57.7	54.97	46.09	48.29	47.66
FeOt/MgO	1.1	0.94	1.05	1.5	1.37	1.41
Na_2O/K_2O	2.85	0.45	1.34	1.92	2.94	1.61
A/CNK	2.11	6.38	1.69	1.74	2.18	2.76
CIPW norm						
Q	16.62	37.35	8.14	5.74	17.12	19.39
C	0	9.31	0	0	0	0
Or	5.54	22.2	9.71	8.86	5.43	10.6
Ab	22.64	14.22	18.6	24.34	22.86	24.37
An	26.66	0.16	25.92	26.6	25.89	22.82
Di(MS)	10.95	0	7.83	10.28	7.31	1.98
Hy(MS)	10.08	12.01	18.18	11.4	11.18	11.73
Il	0.37	0.3	0.45	0.48	0.45	0.35
Hm	5.46	3.7	7.51	7.96	6.56	5.84
Tn	1.4	0	3.01	3.5	2.59	2.46
Ap	0.3	0.15	0.64	0.86	0.63	0.48

Appendix- III Contd...

Sample No	S-7	S-39	S-22	S-40	S-29	S-43
al	24.68	22.98	38.59	24.23	20.98	26.94
fm	40.58	43.28	44.63	42.72	49.72	41.29
c	25.94	24.67	0.51	24.23	21.71	19.82
alk	8.8	9.07	16.28	8.83	7.59	11.96
Si	194.97	129.06	278.04	162.7	130.4	187.61
Mg	0.62	0.54	0.65	0.56	0.63	0.56
Ti	1.59	3.06	2.3	2.67	2.63	2.71
K	0.19	0.26	0.6	0.18	0.33	0.29
P	0.15	0.38	0.11	0.32	0.28	0.27

Appendix- III Contd...

Trace elements (ppm)

Sample No	**S08-7**	**S06-22**	**S08-29**	**S08-39**	**S08-40**	**S08-43**
Sc	31.39	33.81	23.67	36.84	33.6	25.64
V	185.99	225.27	192.31	265.73	213.8	171.9
Cr	71.77	44.41	135.76	48.68	49.27	44.46
Co	38.44	44.9	55.17	42.88	39.22	31.93
Ni	18.65	16.02	66.65	13.1	15.1	11.83
Cu	51.06	74.64	51.44	27.33	50.5	37.52
Zn	166.61	140.02	134.74	302.95	106.41	159.42
Ga	15.97	17.79	17.07	21.06	17.43	17.78
Rb	11.87	16.08	37.22	31.87	15.27	42.99
Sr	149.26	163.14	233.62	178.96	164.27	147.74
Y	33.97	45.91	33.1	54.52	41.01	50.97
Zr	48.59	58.2	60.37	66.96	46.93	57.86
Nb	8.85	31.52	10.94	23.02	17.45	17.68
Cs	0.24	0.61	2.78	1.33	1.07	1.08
Ba	144.95	288.25	474.64	451.05	330.96	422.14
Hf	1.43	1.78	1.56	2.07	1.36	1.75
Ta	1.6	8.27	2.28	5.41	4.76	4.14
Pb	1.42	1.98	1.72	2.2	2.92	2.29
Th	1.76	1.72	1.31	3.42	3.84	5.26
U	0.34	1.13	0.27	0.54	0.61	0.79

Appendix- III Contd...

Rare Earth Elements (ppm)

Sample No	**S08-7**	**S06-22**	**S08-29**	**S08-39**	**S08-40**	**S08-43**
La	15.61	27.22	19.71	31.71	24.71	31.62
Ce	35.85	62.51	44.83	73.18	55.31	70.71
Pr	3.85	6.67	4.78	7.91	5.82	7.4
Nd	20.24	35.04	24.92	42.31	30.71	38.47
Sm	4.43	7.64	5.43	8.81	6.62	8.12
Eu	1.04	2.13	1.68	2.46	1.77	1.98
Gd	5.62	8.97	6.48	10.66	8.02	9.73
Tb	0.91	1.34	0.98	1.62	1.19	1.46
Dy	4.9	7.09	5.21	8.27	6.3	7.73
Ho	1.09	1.56	1.08	1.78	1.36	1.65
Er	3.69	5.02	3.51	5.79	4.31	5.49
Tm	0.63	0.79	0.57	0.93	0.72	0.88
Yb	3.49	4.62	3.28	5.33	3.94	4.95
Lu	0.54	0.71	0.5	0.84	0.63	0.78
Important ratios						
(Ce/Yb)N	2.34	3.08	3.1	3.12	3.19	3.25
(La/Yb)N	3.21	4.23	4.3	4.27	4.5	4.58
Eu/Eu*	0.64	0.78	0.86	0.77	0.74	0.67
$\sum$REE	101.88	171.34	122.96	201.57	151.39	190.98
Rb/Sr	0.08	0.1	0.16	0.18	0.09	0.29
K/Rb	608.46	1822.47	330.14	349.07	456.62	318.65
Th/U	5.18	1.53	4.79	6.34	6.27	6.67
Ba/La	9.29	10.59	24.09	14.23	13.4	13.35
La/Nb	1.76	0.86	1.8	1.38	1.42	1.79
Ni/V	0.1	0.07	0.35	0.05	0.07	0.07
Ti/V	22.88	18.89	41.14	33.84	33.08	38.01
U/Th	0.19	0.65	0.21	0.16	0.16	0.15

APPENDIX-IV

Representative whole rock major and trace element analysis, CIPW norms, Niggli`s value and Indices chemical weathering and alteration etc. of quartz-sillimanite schists of Sonapahar area, Shillong Plateau

Sample No	**S08-8**	**S08-10**	**S08-17**	**S08-35**
SiO_2	74.9	67.65	76.82	60.59
Al_2O_3	22.3	29.23	20.5	36.85
TiO_2	0.68	0.56	0.5	0.8
Fe_2O_3	0.09	0.08	0.07	0.11
FeO	0.01	0.01	0.01	0.01
MnO	0.06	0.13	0.08	0.08
MgO	0.1	0.15	0.13	0.1
CaO	0.03	0.03	0.03	0.04
Na_2O	0.01	0.03	0.01	0.01
K_2O	0.22	0.29	0.13	0.35
P_2O_5	0.01	0.02	0.01	0.02
Total	98.25	98.05	98.17	98.77
CIPW Norm				
Q	97.86	97.41	98.15	96.86
Ac	0.29	0.33	0.26	0.49
Ks	0.02	0.07	0.02	0.03
Di(FS)	0.38	0.35	0.44	0.36
Di(MS)	0.11	0.39	0.20	0.15
Hy(MS)	0.15	0.29	0.17	0.25
Hy(FS)	0.59	0.29	0.42	0.71
Niggli Values				
al	94.72	95.4	96.14	94.65
fm	3.91	3.45	3.19	4.33
c	1.09	0.89	0.47	0.77
alk	0.28	0.27	0.2	0.26
Si	602.39	374.69	268.25	539.5
Mg	0.24	0.31	0.17	0.15
Ti	0.77	1.21	1.17	1.19
K	0.18	0.4	0.14	0.18
P	0.03	0.05	0.04	0.03

Appendix-IV Contd…

Trace elements (ppm)

Sample No	**S08-8**	**S08-10**	**S08-17**	**S08-35**
Sc	3.56	7.34	4.07	8.67
V	15.27	51.49	10.28	49.18
Cr	37.85	60.49	37.25	54.88
Co	0.45	0.37	0.21	0.29
Ni	8.12	11.01	8.10	14.03
Cu	7.90	8.59	8.36	7.39
Zn	95.15	36.37	62.11	72.02
Ga	5.37	14.88	2.81	10.40
Rb	2.38	2.52	0.84	1.68
Sr	5.78	14.33	4.88	25.14
Y	8.15	17.23	6.81	20.47
Zr	162.48	653.72	614.88	1036.98
Nb	1.47	1.30	1.33	5.97
Cs	0.26	0.08	0.06	0.13
Ba	11.74	18.88	16.93	28.55
Hf	3.09	19.29	18.60	30.49
Ta	0.10	0.15	0.13	0.44
Pb	3.69	5.40	3.03	2.93
Th	9.12	22.86	13.39	27.88
U	1.52	2.34	1.72	4.87

Rare Earth elements (ppm)				
Sample No	**S08-8**	**S08-10**	**S08-17**	**S08-35**
La	31.20	55.43	32.95	78.24
Ce	71.74	115.83	70.22	157.89
Pr	7.91	11.831	6.75	17.34
Nd	33.62	46.08	24.19	67.93
Sm	6.32	8.75	2.81	13.43
Eu	0.41	0.65	0.12	1.16
Gd	3.56	7.09	2.10	9.33
Tb	0.38	0.95	0.21	0.99
Dy	1.43	4.10	0.94	3.65
Ho	0.29	0.69	0.24	0.77
Er	0.91	1.58	0.80	2.36
Tm	0.11	0.17	0.10	0.34
Yb	0.66	0.91	0.75	2.05
Lu	0.08	0.12	0.11	0.26
∑REE	158.54	254.17	142.32	355.72
Important ratios				
Eu/Eu*	0.24	0.24	0.14	0.30
(La/Sm)N	2.70	3.47	6.44	3.19
(La/Yb)N	28.69	37.16	26.66	23.13
Weathering Indices				
CIW	99.42	99.38	99.22	99.62
CIA	99.376	99.28	99.17	99.59